

Effective Models for Confining Gauge Theories: Analytical and Numerical Tests

Dissertation

zur Erlangung des akademischen Grades
doctor rerum naturalium (Dr. rer. nat.)

vorgelegt dem Rat der Physikalisch–Astronomischen Fakultät
der Friedrich–Schiller–Universität Jena

von Dipl.–Phys. Leander Dittmann
geboren am 3. November 1974 in Weida

Gutachter

1. Prof. Dr. Andreas Wipf, Jena
2. Prof. Dr. Michael Müller-Preussker, Berlin
3. Prof. Dr. Hugo Reinhardt, Tübingen

Tag der letzten Rigorosumsprüfung: 29. Januar 2004

Tag der öffentlichen Verteidigung: 5. Februar 2004

Contents

1. Introduction	1
2. Lattice Gauge Theory	10
2.1. Discretization	10
2.2. Measuring Observables	12
2.3. Monte Carlo	13
2.4. Overrelaxation	15
2.5. Inverse Monte Carlo	17
2.6. Technical Pitfalls	19
3. Faddeev–Niemi Model	21
3.1. Introduction	21
3.2. Generating $SU(2)$ Lattice Configurations of n -Fields	23
3.3. Numerical Results	26
3.4. Effective Action and Schwinger–Dyson Equations	30
3.5. Comparing Yang–Mills and FN Configurations	33
3.5.1. Leading–Order Ansatz	33
3.5.2. FN Action with Symmetry–Breaking Term	37
3.6. Remarks I	44
4. Polyakov Loop Model	46
4.1. Introduction	46
4.2. Haar Measure and Schwinger–Dyson Identities	48
4.3. Single–Site Distributions of Polyakov Loops	52
4.3.1. Definitions	52
4.3.2. Determination of Single–Site Distributions	54
4.4. Determination of the Effective Action	62
4.5. The Constraint Effective Potential	66
4.6. Reproducing the Two–Point Function	72
4.7. Remarks II	79
5. Summary	80

Bibliography	84
A. Conventions	95
B. Relating LLG and MAG	96
C. Schwinger–Dyson Equations and Ward Identities	97
D. Histograms and Bins	99
E. Least Squares, Singular Value Decomposition and IMC	102
E.1. Least-Square Method and SVD	102
E.2. Avoiding Trouble with IMC	104
Zusammenfassung	106
Ehrenwörtliche Erklärung	111
Danksagung	112
Lebenslauf	113

1. Introduction

Once upon a time ancient Greeks came up with the idea that all matter consists of some fundamental entities. While Anaximenes assumed the element Air to be the fundamental origin [1], soon afterwards Democrit and Leukipp supposed that matter consists of elementary particles which they called atoms according to the Greek word for indivisible. Since then, more than twothousand years passed by during which no considerable progress in particle physics was made. Things, however, changed dramatically within the last hundred years due to the invention of quantum field theory and the development of particle accelerators. In addition, theoretical and experimental physics have been crucially affected by the evolution of computer technology. Thanks to those efforts, a theoretical framework of particle physics has emerged which is known as the Standard Model. This is a gauge theory with symmetry group $SU(3) \times SU(2) \times U(1)$ where the $SU(2) \times U(1)$ symmetry is associated with the electro-weak theory [2, 3, 4], a unified description of two fundamental forces corresponding to electromagnetic and weak interactions. The $SU(3)$ gauge group is associated with strong interactions between hadrons¹ described by Quantum Chromodynamics (QCD). Gravitation as the fourth fundamental force, however, is not captured by the Standard Model. As shown in Tab. 1.1, on the subatomic level it is many orders of magnitudes weaker than all the other forces. Thus it is expected to play no role in this regime. Nevertheless, theoretical physicists and mathematicians keep working hard on finding an even more fundamental theory that treats all four forces in a unified way and thus might even describe phenomena near the very beginning of the universe.

The strong interactions provide the forces acting between quarks and gluons which yield the binding of protons and neutrons in nuclei. Many fundamental questions in particle physics are related to this force. On the other hand, however, the study

¹Strongly interacting particles are called hadrons.

force	strong	electromagnetic	weak	gravitational
rel. strength	1	10^{-2}	10^{-5}	10^{-39}
range [m]	$\sim 10^{-15}$	∞	$\sim 10^{-18}$	∞
acts on	quarks, hadrons	electr. charges	leptons, quarks	all matter
mediator	gluons	photons	W^\pm/Z^0 -bosons	gravitons

Table 1.1.: Properties of fundamental interactions. The relative strengths are measured between two up-quarks at distance $3 \cdot 10^{-17}\text{m}$.

of QCD is a very demanding task. It is this field where the present work aims to contribute to the scientific understanding of Nature.

Phenomenology of Strong Intercation

In the early twentieth century, Rutherford concluded from his scattering experiments that the atom is mostly empty space except for a small and dense core containing positively charged particles, the protons. But if so, one would expect this nucleus to burst apart due to the electromagnetic repulsion between the equally charged protons. Chadwick's discovery of the neutron as a second constituent of the nucleus still did not answer the question why it is stable. Obviously, there had to be another, yet unknown, mechanism responsible for that.

In the middle of the last century cosmic ray experiments and, even more important, the availability of newly developed particle accelerators led to a plethora of known particles, the 'particle zoo', which called for an explanation to bring order into this chaos.

The great variety of hadrons, subdivided into baryons and mesons, has been classified by Gell-Mann [5] and Zweig [6]. They invented the quark model according to which hadrons can be grouped into multiplets of $SU(3)_f$ associated with the quantum number 'flavor'. However, particles in the fundamental triplet carry fractional electric charge, a property which has never been observed in any experiment.

Later on, electron-nucleon scattering experiments confirmed Bjorken's prediction of the scaling of structure functions [7, 8] which could be explained by Feynman's parton model [9], stating that hadrons consist of point-like sub-particles, called partons. In

1971 scattering experiments with neutrinos and nucleons indicated that the data could indeed be accounted for if the partons had exactly the properties of the particles in the fundamental triplet of $SU(3)_f$. Therefore, Feynman's partons got identified with the quarks and antiquarks. These particles are fermions and come in six flavors as listed in Tab. 1.2. For example, the proton with charge 1 is built up from two up-quarks and a down-quark, uud , whereas the charge-zero neutron is a udd -state.

quark	u (up)	d (down)	s (strange)	c (charme)	b (bottom)	t (top)
mass [GeV]	0.003(2)	0.007(2)	0.117(38)	1.2(2)	4.25(25)	174(5)
charge [e]	2/3	-1/3	-1/3	2/3	-1/3	2/3

Table 1.2.: Masses and electromagnetic charges of the six quark flavors [10].

However, implementing the quark scheme ran into trouble because the properties of the Δ^{++} -resonance, originally discovered by Fermi, forced one to combine three identical fermions u into a completely symmetric ground state, $\Delta^{++} = uuu$. This is, of course, forbidden by the Pauli principle. Another unsatisfactory issue was that a number of possible combinations like quark-quark, antiquark-antiquark or single quarks had never been observed. Both problems were solved by introducing a new quantum number of quarks, called color, with corresponding symmetry group $SU(N_c)$. Quarks are supposed to come in three colors, red, green and blue, which implies $N_c = 3$. Thus, the quarks in the Δ -ground state are now distinguishable and hence not forbidden anymore. But in contrast with observations, there seem to be different kinds of protons or neutrons if one thinks of all color combinations of the quarks u and d . For this reason one assumes all particles observed in Nature to be colorless, or equivalently, to be unchanged under rotations in color space. In other words, observable particles are represented as color singlets, i.e. states combining all three colors or color-anticolor states. Quite recently, several groups have announced the observation of colorless combinations of five quarks [11, 12, 13, 14]. The fact that *there are no isolated particles in Nature with non-vanishing color charge* [15] is known as ‘color confinement’². Due to the different quark masses the flavor symmetry is not exactly realized in Nature in contrast to the color symmetry which is unbroken.

²See, however, [16] where weak confinement, i.e. the absence of free quarks and gluons, is distinguished from strong confinement which refers to an indefinitely rising potential. See Fig. 1.1.

QCD

This last fact prepared the ground to formulate a theory for the strong interaction, known as Quantum Chromodynamics [17, 18, 19]. Being a gauge theory with the non-Abelian symmetry group $SU(N_c)$ it describes the interaction of quarks with $\dim SU(N_c) = N_c^2 - 1$ color charged gauge bosons, the gluons. It is a local theory like all other theories in the Standard Model.

The QCD-Lagrangian,

$$\mathcal{L}_{QCD} = \mathcal{L}_f + \mathcal{L}_g , \quad (1.1)$$

decomposes into a fermionic part including the quarks,

$$\mathcal{L}_f = \sum_{\alpha,\beta=1}^{N_c} \sum_{f,f'=1}^{N_f} \bar{\psi}_{f\alpha} (i\gamma^\mu D_\mu^{\alpha\beta} - m_{ff'}\delta^{\alpha\beta}) \psi_{f'\beta} , \quad (1.2)$$

and a purely gluonic part

$$\mathcal{L}_g = -\frac{1}{4g^2} \sum_{a=1}^{N_c^2-1} F_{\mu\nu}^a F^{\mu\nu a} , \quad (1.3)$$

which describes the kinematic of the gluons and by itself is a non-trivial Yang-Mills theory. The field strength tensor belongs to the adjoint representation, and in terms of the Lie algebra valued gauge field $A_\mu = A_\mu^a T^a$ it is given by

$$F_{\mu\nu}^a = \partial_\mu A_\nu^a - \partial_\nu A_\mu^a + f_{abc} A_\mu^b A_\nu^c , \quad (1.4)$$

where the f_{abc} are the structure constants. The T^a denote a complete set of generators of the gauge group normalized according to

$$\text{tr}(T^a T^b) = \frac{1}{2} \delta^{ab} , \quad [T^a, T^b] = i f_{abc} T^c . \quad (1.5)$$

The quark fields $\psi_{f\alpha}$ with masses m_f are labelled by their flavor and color quantum number, f and α respectively. g is the strong coupling constant, and the covariant derivative $D_\mu = \partial_\mu - iA_\mu$ ensures local gauge invariance.

Let us note that it is possible to add a ‘ θ -term’,

$$\mathcal{L}_\theta \propto \frac{\theta}{16\pi^2} \text{tr}(\epsilon_{\alpha\beta\mu\nu} F^{\alpha\beta} F^{\mu\nu}) , \quad (1.6)$$

to the Lagrangian as a source for CP violation. Usually, such a term is discarded because it can be expressed as a divergence of a current and thus appears as a surface term in the action. However, a term of this form survives in non-Abelian gauge field theories because there are non-trivial instanton configurations. We nevertheless discard this term in this thesis because of the very small experimental upper bound for the QCD θ parameter, $\theta < 10^{-9}$ [20].

Apart from the realistic $N_c = 3$ for QCD, of great theoretical interest is also the study of Yang-Mills theory with arbitrary $N_c \geq 2$. There are crucial effects like asymptotic freedom and confinement of color charges that are generally believed to be a consequence of the non-Abelian nature of the gauge group and thus should occur for all $SU(N_c)$. Of particular interest, on the one hand, is the large N_c limit, where typical leading corrections scale with the small parameter $1/N_c$. On the other hand, there is the $SU(2)$ -case which is the simplest for analytical and numerical investigations but nevertheless leads to reasonable results in understanding confinement.

Confinement

The most essential property of QCD is confinement [21] and its understanding is one of the most exciting challenges of modern physics [22].

Confinement and asymptotic freedom are closely related to the running coupling of QCD which has its origin in the non-Abelian nature of the theory. The gluons, also carrying color, not only interact with quarks but also among themselves. By turning into pairs of gluons they spread out the effective color charge of the quark and the closer one approaches the quark color charge, the more the measured charge decreases due to this anti-screening. This behavior shows up in the running coupling which decreases for high energy (short distance) and increases for low energy (large distance). The first fact leads to a vanishing interaction in the ultraviolet region at energy scale $Q^2 \rightarrow \infty$. Quarks become essentially free in this limit, and perturbation theory can be applied. The second fact signals the occurrence of nonperturbative effects in the infrared region of the theory. However, this is the regime where one

has to investigate issues like the hadron spectrum, the topological structure of the vacuum, the $U_A(1)$ -problem, chiral symmetry breaking and also confinement of color.

The latter denotes the fact that color charges have never been observed in free space, i.e. at distances of about 1 fm, though visible in deep-inelastic scattering experiments at scales $\ll 1$ fm. To get some intuition one may imagine to separate a quark q and an antiquark \bar{q} from each other. Inspired by superconductors where the electromagnetic field lines are expelled from the interior, Nambu proposed the QCD vacuum to behave like a dual superconductor where the chromoelectric field lines between quark and antiquark are squeezed into a thin flux tube with constant energy density per unit length, the string tension σ . Thus, the total energy of such a configuration is proportional to the $q\bar{q}$ -separation. If the increasing energy is sufficiently large, an energetically favorable new quark-antiquark pair is created from the vacuum and breaks the string into two short pieces. This procedure ends when their energy has degraded into clusters of quarks and gluons, each colorless, while the strong color coupling turns them into hadrons as the particles to be detected.

To some extent the effects are already present in the gluonic part of the theory and it is much easier to restrict to that and look for their remnants in pure Yang-Mills theory.

In pure Yang-Mills theory the phenomenon of confinement is described by introducing a static quark potential $V(R)$ for quarks in the fundamental representation which is of Coulomb type for small distances R and rises linearly for large distances [23]. Due to the emerging virtual quark-antiquark pairs in full QCD or color charges in higher representations the string breaks and the potential flattens off, see Fig. 1.1. In that case the linear behavior is valid only in an intermediate range. Comparing different representations of the sources one observes Casimir scaling of the string tension [24, 25], which means that potentials of sources in different representations are proportional to each other with ratios given by the corresponding ratios of eigenvalues of the quadratic Casimir operators. It should be mentioned that there is another approach. According to [26, 27], for $SU(N)$ with $N \geq 4$ typical sources may be thought of as k fundamental charges, and there are new stable confining strings, called k -strings. For $SU(N)$ there are non-trivial stable k -strings up to a k -value equal to the integer part of $N/2$ with string tensions σ_k depending on k and N . The different models (e.g. Casimir scaling, M-theory approach to QCD [28], bag model

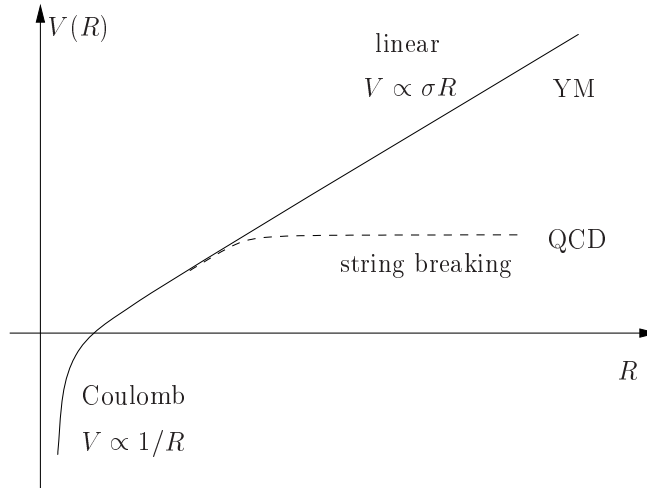


Figure 1.1.: Qualitative picture of the quark potential. At about 1 fm, which is approximately the size of a hadron, the string breaks in QCD.

[29]) predict different dependences of σ_k on N and k . Computations in respect thereof are under way.

Moreover, one expects glueballs in the pure glue sector of QCD at low energies. These are bound states of gluons the lowest masses of which are predicted by lattice simulations to be around 1.7 GeV [30]. Such a mass gap would lead to an exponential decay of any correlation function, thereby explaining the absence of long ranged fields. In experiments several candidates for glueballs have been found (see e.g. [31, 32]).

At sufficiently high temperature or density, QCD shows a phase transition. In Nature this is realized when hadrons start to overlap and the quarks and gluons therein are free to travel over larger distances which is assumed to happen in the early universe and neutron stars. This new state of matter, where color charges are not confined anymore, is referred to as quark-gluon plasma. Lattice simulations predict a critical temperature for this deconfinement phase transition of about 170 MeV³[34].

As physical problems have different scales, for practical reasons it is quite useful to restrict oneself to the scale of interest while effects outside of this scope are absorbed in an adequate manner. One of the most powerful such tools is the effective field theory approach [35, 36]. The phenomena we are interested in belong to the nonperturbative sector of QCD which amounts to the low energy regime.

³Here for zero baryonic chemical potential and 2+1 flavors. For a review see e.g. [33].

Effective Theories

The basic idea of this approach is to introduce an energy scale μ , or equivalently a distance μ^{-1} , separating the low and high energy regime of the theory. Short distance effects are put together into the coefficients or couplings of the effective field theory while low energy effects from distances longer than μ^{-1} are described by operators in the effective theory. The degrees of freedom are chosen to reproduce the features of the underlying theory when only processes of energy lower than μ are considered. Compared to the underlying theory, the number of effective degrees of freedom might be remarkably reduced. Thus the effective theory is expected to be much simpler and less complex.

There are several effective theories for QCD aiming towards different aspects. Well established approaches are, for example, the Nambu-Jona-Lasinio model [37], heavy-quark effective theory [38, 39] as well as non-relativistic QCD (NRQCD) [40, 41] and the dual Abelian Higgs model (DAHM) [42, 43, 44] where it is argued that glueballs correspond to closed vortices or flux-tube excitations [45]. Also a couple of effective string theories for Yang–Mills [46] have been derived.

Most interesting in the context of this thesis are, however, yet two other attempts. First, there is the Faddeev-Niemi action [47], the main ingredient of which is a unit vector in color space. It can be viewed as a generalization of the non-linear σ -model but is just as well obtained from the Skyrme model [48]. The action supports stable solitons [49], i.e. static solutions of minimal energy, and a rich variety of linked and knotted solitons has been revealed in recent years [50, 51]. The most remarkable point is that this model serves as a possible low energy effective action for pure $SU(2)$ Yang-Mills theory where the knot-like solitons are identified with glueballs.

A second class of models is inspired by the fact that the deconfinement phase transition in pure Yang-Mills theory [52, 53] is controlled by the dynamics of the Polyakov loop (see Chapter 4). The expectation value of the traced Polyakov loop serves as an order parameter associated with spontaneous breaking of the center symmetry, as it is nonzero above the critical temperature and vanishes below. There is a conjecture by Svetitsky and Yaffe who have argued that finite-temperature $SU(N)$ Yang–Mills theory in d dimensions lies in the universality class of a \mathbb{Z}_N spin model in dimension $d - 1$ [54, 55]. Mapping the microscopic theory (YM) onto a macroscopic one (Ising)

should thus provide an effective model describing the deconfinement phase transition. Instead of the (discrete) Ising spins one may establish an effective model for the (traced) Polyakov loop variable itself [56, 57, 58].

Both, the Faddeev-Niemi conjecture and the Svetitsky-Yaffe conjecture are subject to our investigation throughout this thesis. We test a possible relation of $SU(2)$ Yang-Mills theory to the proposed effective actions in a numerical and analytical manner. The method we use is the inverse Monte Carlo technique (see Section 2.5) based on Schwinger-Dyson equations and Ward Identities.

As already pointed out, the effective theories we consider are designed for low energies. At this scale perturbation theory fails, and obviously one has to apply some nonperturbative technique to access the structure of this regime. One of the most powerful nonperturbative approaches at present, and thus the method we use, is lattice gauge theory, originally invented by Wilson in his pioneering work [59].

The outline of this thesis is as follows. Chapter 2 summarizes some very basic facts about lattice gauge theory as the method we focus on. In particular, we briefly address the Inverse Monte Carlo (IMC) technique. Its application to the Faddeev-Niemi model including additional symmetry breaking terms is the content of Chapter 3. Chapter 4 deals with the Polyakov loop model where we also derive the constraint effective potential. We conclude with a summary in Chapter 5.

2. Lattice Gauge Theory

As already mentioned in the introduction, lattice gauge theory provides a systematic approach to the nonperturbative sector of quantum field theories, in the present case Yang-Mills theory. In this chapter we will briefly introduce some basic concepts of this approach. However, the wide variety of this subject calls for a restriction on the techniques which have been used in this thesis. Readers interested in additional details on field theory on the lattice are referred to the literature, e.g. [60, 61, 62, 63, 64, 65, 66, 67].

2.1. Discretization

The key feature of lattice gauge theory is that it provides an ultraviolet cutoff from the outset by replacing continuous spacetime with a discrete hypercubic lattice. Due to limited computer power the lattice volume in practical simulations is finite which provides also an infrared regulator. Choosing periodic boundary conditions turns the finite lattice into a torus. The computational methods are very similar to those in statistical mechanics.

Let us define a Euclidean lattice in d dimensions,

$$\Lambda = \{x = (x_0, x_1, \dots, x_{d-1}) \in a\mathbb{Z}^d \mid 0 \leq x_\mu \leq a(N_\mu - 1) \forall \mu = 0, \dots, d-1\} \quad (2.1)$$

which extends over N_μ lattice spacings a into direction $\hat{\mu}$. In this thesis we restrict ourselves to the case $d = 4$ with x_0 denoting the temporal coordinate and x_i , $i = 1, \dots, 3$, the spatial coordinates where $N_t \equiv N_0$ and $N_s \equiv N_1 = N_2 = N_3$. Two neighboring lattice sites in a particular direction $\hat{\mu}$ are separated by a distance of one lattice spacing, i.e. x and $x + a\hat{\mu} \equiv x + \mu$. The number of lattice points, or sites, is denoted by $V = N_s^3 N_t \equiv \Omega N_t$ describing a physical volume of $a^4 V$ in spacetime. The

temporal extension is proportional to the inverse temperature, $N_t \sim 1/aT$. Using anisotropic lattices where $N_t < N_s$ refers to finite temperature.

To set up quantum field theory on the lattice, first of all the physical fields defined in the continuum must be attached to the elements of the lattice. The natural choice is to assign a scalar field to a site of the lattice, ϕ_x , and a vector field, which is characterized by a site and a direction, to the link $U_l \equiv U_{x,\mu}$. Also plaquette variables $H_p \equiv H_{x,\mu\nu}$ can be defined corresponding to a tensor field in the continuum as shown in Fig. 2.1.

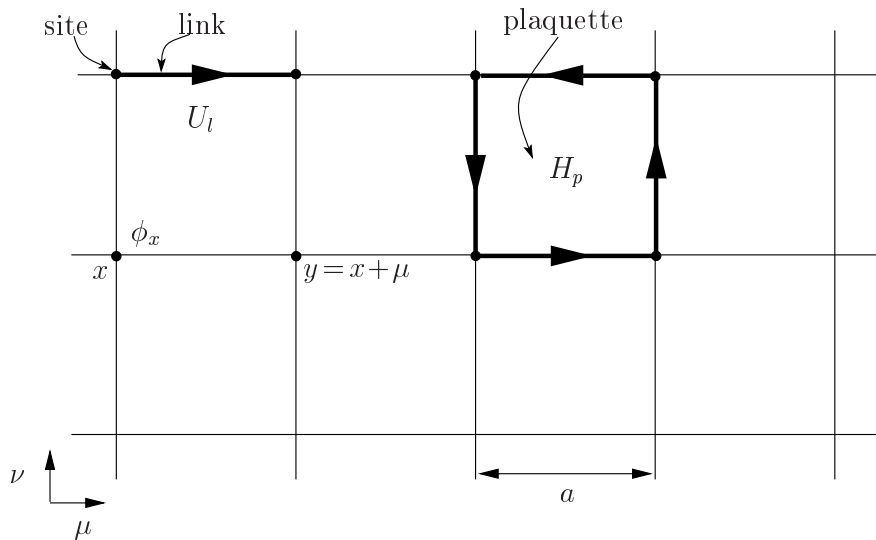


Figure 2.1.: Illustration of site, link and plaquette and corresponding variables on a two-dimensional lattice.

In the case of $SU(N_c)$ Yang-Mills theory the Lie-algebra valued gauge field $A_\mu(x)$ is reexpressed as a parallel transporter $U_{x,\mu}$ between two neighboring lattice sites x and $x + \mu$ which is defined as the path ordered exponential

$$U_{x,\mu} = \mathcal{P} \exp \left(i \int_x^{x+a\hat{\mu}} A_\mu(y) dy \right) \longrightarrow e^{iaA_\mu(x)} \quad \text{as } a \rightarrow 0. \quad (2.2)$$

Out of these link variables the lattice action is constructed in such a way that one recovers the continuum action in the limit $a \rightarrow 0$. As in the continuum case, the QCD-action splits up into a purely gluonic and a fermionic part, $S = S_g[U] + S_f[\bar{\Psi}, \Psi, U]$. Following Wilson [59], at each site x a plaquette variable U_p is constructed as a path

ordered product of links around an elementary plaquette located at x ,

$$U_p = U_{x,\mu} U_{x+\mu,\nu} U_{x+\nu,\mu}^\dagger U_{x,\nu}^\dagger, \quad (2.3)$$

to write the gluonic part of the action as

$$S_g[U] = \beta \sum_p \left(1 - \frac{1}{N_c} \Re \text{tr} U_p \right). \quad (2.4)$$

The usage of plaquettes (2.3) in this construction ensures local stress gauge invariance since a link transforms under gauge transformation g_x according to

$$U_{x,\mu} \longrightarrow g_x U_{x,\mu} g_{x+\mu}^\dagger.$$

The lattice Yang-Mills coupling is $\beta = 2N_c/g^2$. In the fermionic part the Dirac operator gets replaced by its discrete version, the lattice Dirac operator (for example the Wilson operator) $D(x, x')$, and the quark fields are rescaled by the appropriate power of the lattice spacing, $\psi(x) = a^{-3/2} \Psi_x$.

$$S_f[\bar{\Psi}, \Psi, U] = \sum_{x, x'} \bar{\Psi}_x D(x, x')[U] \Psi_{x'}. \quad (2.5)$$

2.2. Measuring Observables

The goal of lattice simulations is to estimate expectation values of observables $\mathcal{O}[\bar{\Psi}, \Psi, U]$ calculated from

$$\langle \mathcal{O} \rangle = \frac{1}{Z} \int \mathcal{D}U \mathcal{D}\Psi \mathcal{D}\bar{\Psi} \mathcal{O}[\bar{\Psi}, \Psi, U] e^{-S_g[U] - S_f[\bar{\Psi}, \Psi, U]}, \quad (2.6)$$

where the partition function is given by

$$Z = \int \mathcal{D}U \mathcal{D}\Psi \mathcal{D}\bar{\Psi} e^{-S_g[U] - S_f[\bar{\Psi}, \Psi, U]}. \quad (2.7)$$

For observables which do not contain fermions the quark field integration separates giving rise to a fermion determinant,

$$\int \mathcal{D}U \mathcal{D}\Psi \mathcal{D}\bar{\Psi} e^{-S_g[U] - S_f[\bar{\Psi}, \Psi, U]} = \int \mathcal{D}U \det D[U] e^{-S_g[U]} . \quad (2.8)$$

However, computing the fermion matrix is a very demanding task and one of the most computer-time consuming parts in lattice simulations. Therefore lots of simulations today, including those done in this work, used the quenched approximation [68, 69, 70] which amounts to replacing the determinant by a constant, say $\det D[U] = 1$. Of course, this does not mirror QCD correctly. However, neglecting the fermion determinant is just a reweighting of the gauge configurations in the Monte Carlo update. Quenched approximation allows for a rather precise determination of phenomena that are substantially independent of dynamical fermion contributions [71] and it is also supported by phenomenological arguments [72, 73, 6] suggesting that closed quark loops contribute only small effects.

In what follows we restrict to the pure gauge sector. As already mentioned in the introduction, it still covers many crucial properties of QCD, in particular confinement and its phase transition which are due to non-Abelian nature of the theory.

Due to the extremely high multidimensionality of the integrals in (2.6) and (2.7) the partition function can never be summed up exactly and a statistical treatment is in order. As a simple example let us consider a rather small 4^4 -lattice with link variables taking on just two different values ± 1 . Even in this case there are of order 10^{308} possible configurations. Hence, on the lattice the computation of $\langle \mathcal{O} \rangle$ is done by Monte Carlo integration.

2.3. Monte Carlo

The aim of Monte Carlo simulation is to generate a sample $\{U^{(n)}, n = 1, \dots, N\}$ containing a sufficiently large number N of field configurations which are typical of thermal equilibrium in the sense of statistical mechanics. These configurations will strongly dominate in the partition function. The sample average as a good estimator

for the expectation value is defined as

$$\langle \mathcal{O} \rangle = \frac{1}{N} \sum_{n=1}^N \mathcal{O}[U^{(n)}] . \quad (2.9)$$

For this to work, the distribution of configurations in the sample has to follow the Boltzmann weight $\exp(-S[U])$. This property, commonly referred to as importance sampling, is essential for an effective Monte Carlo simulation. The configurations in the sample are generated as a sequence

$$U^{[0]} \longrightarrow U^{[1]} \longrightarrow \dots \longrightarrow U^{[M]} \quad (2.10)$$

starting from a given initial configuration $U^{[0]}$. Not every configuration in the sequence belongs to the sample. The latter is rather an appropriate subset of the former (see Section 2.6). The step from $U^{[n]}$ to $U^{[n+1]}$, during which every single link $U_{x,\mu}$ on the lattice is updated once, is called a sweep. The updating is a stochastic process done by a specific algorithm depending on the theory under consideration. It has to be designed in such a way that every configuration, say U' , can be reached by any other one, U , with a nonzero transition probability, $P(U' \leftarrow U) > 0$. This property is called ergodicity and ensures that the whole configuration space is covered such that no particular configurations are excluded by the algorithm. A third important condition on the updating algorithm is that it takes any initial configuration within a sufficiently large but finite number of updating sweeps to equilibrium. This implies in particular that the equilibrium distribution is a (unique) fixed point of the Markov process. A sufficient condition for this to occur is detailed balance,

$$P(U' \leftarrow U)e^{-S[U']} = P(U \leftarrow U')e^{-S[U]} , \quad (2.11)$$

which most algorithms in practice satisfy.

All update algorithms, although they may differ very much in detail, have one basic feature in common namely the acceptance-rejection-step. It defines the update procedure in the following schematical way. Given a configuration of fields, e.g. link variables U , let us choose a particular link U_l to be updated. First, a new trial value U'_l for this particular link is suggested while all other links are left untouched. Systematically finding a reasonable value U'_l is a big challenge since speed and efficiency

of the algorithm crucially depend on it. The different approaches are reflected in different algorithms like Metropolis [74, 75] which has been widely used in statistical mechanics. Another famous algorithm which is particularly suited for $SU(2)$ gauge theory is the heatbath algorithm [76] invented by M. Creutz and its generalization to the so called pseudo-heatbath algorithm [77] for larger $SU(N)$ groups. There are also cluster algorithms [78, 79] available where not only a single site or link but whole regions of the lattice are updated. Unfortunately, to the best of my knowledge there is no cluster algorithm known for non-Abelian gauge theories.

The Metropolis algorithm is rather easy to explain. After picking up the trial U'_i one has to compute the change in the action $\delta S = S[U'_i] - S[U_i]$ to compare the Boltzmann weights. In the case that $\delta S \leq 0$, i.e. if the action decreases under replacing the value of U_i by U'_i which amounts to increasing the Boltzmann weight of the configuration, this change is accepted in terms of assigning the new value U'_i to the link while the old one is dismissed. On the other hand, if $\delta S > 0$ the pseudo-randomness of the Monte Carlo procedure comes into play. Choosing an equally distributed random number $R \in [0, 1]$ the value U'_i is also accepted if $\exp(-\delta S) > R$ whereas it is definitely rejected otherwise.

It is this last but important step where quantum fluctuations are taken into account. As one can imagine, only small fluctuations are allowed for. Huge jumps with large δS are exponentially suppressed. On the other hand, rejecting all updates with $\delta S > 0$ would just yield a minimization of the action leading to the classical limit.

In this thesis we used the Metropolis algorithm for the Polyakov loop fields, the cluster algorithm for the n field and the $SU(2)$ Yang–Mills ensembles were generated by the heatbath algorithm.

2.4. Overrelaxation

Let us briefly mention a tool the aim of which is to speed up the Monte Carlo process and which thus enjoys great popularity. It goes under the name of overrelaxation [80, 81, 82] and is used not only for updating but also for maximizing functionals as will be done for gauge fixing in Section 3.2. The concept is the same in both cases, namely to choose the new value of the variable as far as possible from the old one.

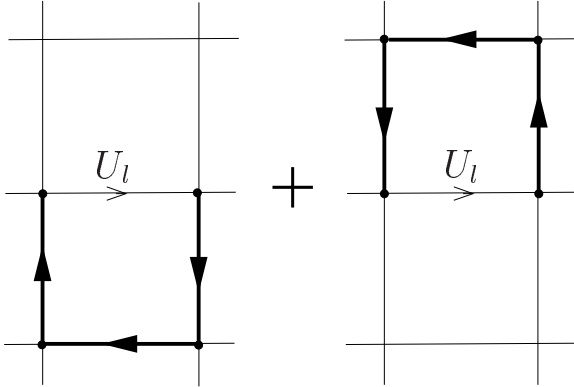


Figure 2.2.: The two contributions to a staple at link U_l in a hyperplane of the lattice.

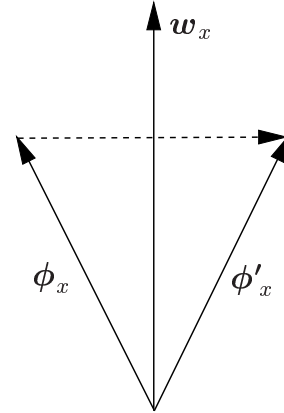


Figure 2.3.: Geometric illustration of (2.12).

For updating $SU(2)$ link variables this is achieved by setting the trial value to $U'_l = s^\dagger U_l^\dagger s^\dagger$. Here $s \in SU(2)$ is the sum over all staples at the link U_l projected onto the group. A staple, as shown in Fig. 2.2, is a plaquette with a missing link. This proposal U'_l is always accepted since the action is unchanged, which is special for $SU(2)$. Moreover, the constant action implies that this algorithm is not ergodic. One way out to get a reasonable updating is to mix overrelaxation with some ergodic steps, since a combination of ergodic and non-ergodic procedures is always ergodic. In this work we have mixed overrelaxation and heatbath at a ratio of about one to three for the gauge fields. The ratio has to be chosen appropriately by observing the effect on Monte Carlo time for different ratios.

On the other hand, an overrelaxation step for maximizing functionals may be implemented as follows. If the functional can be expressed as a sum over scalar products, $\sum_x \phi_x \cdot \mathbf{w}_x$, then the new scalar field is simply chosen to be

$$\phi'_x = 2\phi_x \cdot \mathbf{w}_x - \phi_x . \quad (2.12)$$

This amounts to a planar reflection of the field ϕ_x with respect to the direction \mathbf{w}_x , as depicted in Fig. 2.3. Obviously, the functional is unchanged since the projection onto \mathbf{w}_x is the same for both, ϕ_x and ϕ'_x . The amount of acceleration due to overrelaxation depends on the process under consideration and can be quite remarkable as shown in Fig. 3.4 for the gauge fixing procedure.

2.5. Inverse Monte Carlo

Given an action, a Monte Carlo simulation provides a set of field configurations distributed according to the corresponding Boltzmann weight as described above. This allows for a computation of expectation values, for instance n -point functions, out of which one can extract intrinsic parameters of the theory like masses, critical exponents, magnetization or energies.

On the other hand, Inverse Monte Carlo, as the name implies, solves the inverse problem of statistical mechanics. It reconstructs the interactions if the distribution is known. More precisely, within the scope of this thesis, we want to learn something about the action according to which a given sample of field configurations is distributed. The direct approach would be to explicitly solve the expectation value (2.6) or even (2.9) for the action, but, of course, this is not possible at all. However, according to Wightman's reconstruction theorem [83], the knowledge of all (infinitely many) n -point functions is equivalent to solving the underlying theory. Therefore, there must be a way to extract at least some basic details of the action from the configurations. Due to the finite extension of the lattice, the number of accessible n -point functions is restricted, which, however, is not a serious handicap since, in practice, a finite but characteristic subset suffices.

In addition to numerical investigations also analytical arguments based e.g. on symmetries turn out to be very powerful because they allow to constrain the structure of the action. This fact is of great advantage since it provides the opportunity to make an ansatz for the action where only a number of coupling constants are left to be evaluated. Possible models for instance are a gradient expansion in powers of derivatives while the potential term may be given as a polynomial or power series in the field. Varying the number of terms taken into account one can study how the couplings of leading operators are affected by truncation. The latter makes sense if there are only minor deviations and potentially a stabilisation within the error bars.

A similar technique has already successfully been used in studying the flow of couplings [84, 85] in the context of renormalization group transformations [86, 87]. Applied to a scalar theory, critical exponents, the fixed point and truncation effects were discussed [88]. However, these investigations have started with a definite action to generate configurations which are then subjected to a block spin transformation with

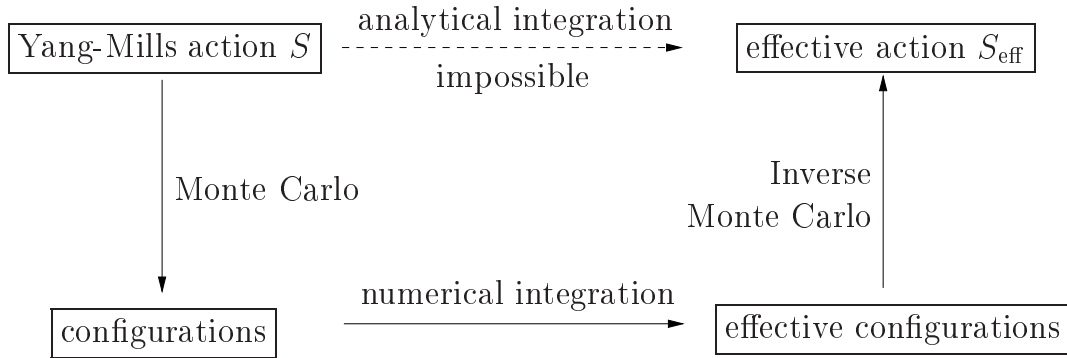


Figure 2.4.: Monte Carlo and Inverse Monte Carlo technique. In this thesis we follow the way indicated by the solid arrows.

tunable parameter to see how the initial couplings change under coarse graining.

This is different from what is done in this thesis. Here we are interested in determining effective actions describing the low energy sector of QCD. To do so we numerically integrate out degrees of freedom in Yang-Mills theory with the exception of those which are supposed to be relevant for physics at low energies. What is left are 'effective configurations' of field variables distributed with respect to the *effective* action S_{eff} (see Fig. 2.4). Our goal now is to verify to which extent the proposed effective action is actually able to describe physical phenomena at the desired energy scale. As stated above, the effective action can be written as a sum of operators, each of which attached with a coupling constant.

A naive method to calculate the latter would be to scan iteratively all the parameter space by Monte Carlo simulation, adjusting the input couplings by guess and comparing the result to the effective configurations. Certainly this is a very consumptive and clumsy procedure since a single Monte Carlo simulation still requires much time and computer resources. As one can imagine, even for only two parameters to be fixed dozens of simulations have to be performed which is a hopeless venture.

Therefore, in this work we develop a much more efficient and transparent way to determine the effective action from expectation values taken in the effective sample of configurations. Basic ingredients are the Schwinger-Dyson equations following from the invariance of the functional measure. In general this provides an overdetermined system of equations for the couplings to be solved by least square method [89] (see also

App. E). The fact that there are more equations than unknowns makes it possible to check truncation effects which may appear due to the finite number of terms in the ansatz for the action.

Once a sensible ansatz is established a cross check is in order to verify whether the effective ensemble obtained from the full theory is indeed recovered. The most natural way is to generate configurations by Monte Carlo using the obtained action for which a set of expectation values of characteristic observables is computed. These can be compared to the values taken in the effective configurations to check for coincidence. Another test is already contained in the method itself, since Schwinger-Dyson equations involve both, the ansatz for the action and the expectation values within the effective sample. Supposed they do not mainly match up the Schwinger-Dyson equations would not be valid and solving the overdetermined system would barely result in a stable solution for the couplings.

2.6. Technical Pitfalls

As a Monte Carlo simulation can be viewed as an experiment measuring specific data, there are of course certain sources of errors present. Reasonable results are nevertheless obtained by sticking to the following rules.

Due to the statistical nature of the procedure there are first of all statistical fluctuations which decrease with the square root of computer time as the sample is enlarged. Additionally, there is a couple of systematic errors. A serious one is made if measurements are taken before equilibrium is reached in the updating sequence (2.10). Though measuring observables on a sample which is not yet in equilibrium produces some numbers, they are completely meaningless with respect to the action under consideration. Apart from the algorithm used, how fast a configuration is brought to equilibrium also depends on the lattice volume and the initial conditions. In the present work we ran several hundred up to a few thousand thermalization sweeps before the measurement was started.

Quite a similar problem are autocorrelations in subsequent configurations. A single sweep in the updating (2.10) may change only a small fraction of variables and therefore these two configurations would be almost identical. A measurement over

highly correlated configurations typically results in small error bars but the mean value is unphysical. This problem is avoided when the configurations in the sample are each separated by a sufficiently large number of sweeps. A few hundred did it in our simulations.

Another important point to be aware of is the finite and discrete structure of the lattice. Discretization of the continuum theory yields lattice artifacts which grow as the lattice spacing a is increased away from the continuum value, $a = 0$. Important quantities are often related to the decay of correlation functions. Thus the lattice spacing has to be small enough to trace the signal over several slices before it goes down in the noise. It should be mentioned that there is the concept of improved actions [90, 91, 92] where lattice artifacts are suppressed by adding additional operators. Moreover, there are global symmetries of the original theory, like Poincaré invariance, which are partially or even completely lost on the lattice. However, the construction of a lattice theory is done in such a way that the most important symmetry, namely gauge invariance, remains intact.

Another technical point is that the lattice size is very much restricted by computer power. Therefore, in a reasonable simulation the extension of the lattice is at most a few Fermi. This has consequences for what is accessible to measurement, since only objects or distances smaller than the lattice size can be observed. It is also known that spontaneous symmetry breaking does not occur in finite volume. However, tunneling effects among degenerate states are exponentially suppressed with increasing volume. In general, one requires $a \ll \xi \ll N$, where ξ is the correlation length defined by the exponential decay of the correlation functions.

3. Faddeev–Niemi Model

3.1. Introduction

Confinement in pure Yang–Mills theory is still a theoretical challenge. The problem actually has two faces. On the one hand, there is confinement of static external sources in the fundamental representation which manifests itself through the appearance of a linear potential (nonzero string tension). On the other hand, there should be gluon confinement implying a finite range of the gluonic interactions, i.e. a mass gap. How the two faces are related is largely unclear at the moment.

Recently, Faddeev and Niemi (FN) have suggested that the infrared dynamics of glue might be described by the following low–energy effective action [47],

$$S_{\text{FN}} = \int d^4x \left[m^2 (\partial_\mu \mathbf{n})^2 + \frac{1}{e^2} H_{\mu\nu} H^{\mu\nu} \right]. \quad (3.1)$$

Here, \mathbf{n} is a unit vector field with values on S^2 , $\mathbf{n}^2 \equiv n^a n^a = 1$, $a = 1, 2, 3$; m is a dimensionful and e a dimensionless coupling constant. The FN ‘field strength’ is defined as

$$H_{\mu\nu} \equiv \mathbf{n} \cdot \partial_\mu \mathbf{n} \times \partial_\nu \mathbf{n}. \quad (3.2)$$

Faddeev and Niemi argued that (3.1) “is the *unique* local and Lorentz–invariant action for the unit vector \mathbf{n} which is at most quadratic in time derivatives so that it admits a Hamiltonian interpretation and involves *all* such terms that are either relevant or marginal in the infrared limit” [47].

It has been shown that S_{FN} supports string–like knot solitons [49, 50, 93], characterized by a topological charge which equals the Hopf index of the map $\mathbf{n} : S^3 \rightarrow S^2$. Here, \mathbf{n} is supposed to be static and approaches a uniform limit at spatial infinity, $\mathbf{n}_\infty = \mathbf{e}_z$. In analogy with the Skyrme model, the H^2 term is needed for stabilization.

The knot solitons can possibly be identified with closed gluonic flux tubes and are thus conjectured to correspond to glueballs. For a rewriting in terms of curvature-free $SU(2)$ gauge fields and the corresponding reinterpretation of S_{FN} we refer to [94].

In order for the model to really make sense, however, the following problems have to be solved. First of all, neither the interpretation of \mathbf{n} nor its relation to Yang–Mills theory have been fully clarified. An analytic derivation of the FN action requires

- an appropriate change of variables, $A \rightarrow (\mathbf{n}, X)$, relating the Yang–Mills potential A to \mathbf{n} and some remainder X
- the functional integration over X to arrive at an effective action S_{eff} for the \mathbf{n} -field.

Some progress in this direction has been made [95, 96, 97, 98, 99, 100] on the basis of the Manton–Cho decomposition [101, 102],

$$\mathbf{A}_\mu = C_\mu \mathbf{n} - \mathbf{n} \times \partial_\mu \mathbf{n} + \mathbf{W}_\mu, \quad (3.3)$$

where C is an Abelian connection and $\mathbf{n} \cdot \mathbf{W}_\mu = 0$.

Second, there is no reason why in a low-energy effective action for the \mathbf{n} -fields both operators in the FN ‘Skyrme term’, which can be rewritten as

$$H^2 = (\partial_\mu \mathbf{n} \cdot \partial_\mu \mathbf{n})^2 - (\partial_\mu \mathbf{n} \cdot \partial_\nu \mathbf{n})^2, \quad (3.4)$$

should have the same coupling. Third, and conceptually most important, S_{FN} has the same spontaneous symmetry breaking pattern as the nonlinear σ -model, $SU(2) \rightarrow U(1)$. Hence, it should admit two Goldstone bosons and one expects to find *no* mass gap. In order to exclude these unwanted massless modes we have suggested to break the global $SU(2)$ *explicitly* [LRD1], an idea that has subsequently also been adopted by Faddeev and Niemi [103].

In what follows the FN hypothesis will be tested on the lattice. To avoid the appearance of Goldstone bosons we allow for explicit symmetry-breaking terms. The main part of this chapter is based on [LRD2].

3.2. Generating $SU(2)$ lattice configurations of \mathbf{n} -fields

The conceptual problem to be solved in the first place is to obtain a reasonable ensemble of \mathbf{n} -fields. The (lattice version of the) decomposition (3.3) is of no help: it *assumes* some particular choice of \mathbf{n} on which the decomposition is then based. One way of defining an \mathbf{n} -field is via Abelian gauge fixing, originally introduced by 't Hooft [104]. A prominent example in this class of gauges is the maximally Abelian gauge (MAG) which is obtained via maximizing the functional [105]

$$F_{\text{MAG}}[U; g] \equiv \sum_{x,\mu} \text{tr} (\tau_3 {}^g U_{x,\mu} \tau_3 {}^g U_{x,\mu}^\dagger) \equiv \sum_{x,\mu} \text{tr} (n_x U_{x,\mu} n_{x+\mu} U_{x,\mu}^\dagger) \equiv \tilde{F}_{\text{MAG}}[U; n] , \quad (3.5)$$

with respect to the gauge transformation g . The maximizing g then defines the \mathbf{n} -field according to

$$n_x \equiv g_x^\dagger \tau_3 g_x \equiv \mathbf{n}_x \cdot \boldsymbol{\tau} . \quad (3.6)$$

Instead of maximizing F_{MAG} with respect to g one can equivalently maximize \tilde{F}_{MAG} with respect to n [106] which results in the condition

$$\Delta[U] n_x \equiv \lambda_x n_x . \quad (3.7)$$

Here, $\Delta[U]$ denotes the covariant Laplacian in the adjoint representation (see App. A), while λ_x is a Lagrange multiplier imposing that \mathbf{n}_x is normalized to unity, locally at each lattice site x . In principle, (3.7) can be solved for the field \mathbf{n} associated with the background U . However, as this background is distributed randomly along its orbit we will in turn obtain a random ensemble of \mathbf{n} -fields characterized by the two-point function

$$G_{xy}^{ab} \equiv \langle n_x^a n_y^b \rangle = \frac{1}{3} \delta^{ab} \delta_{xy} . \quad (3.8)$$

Thus, nontrivial correlations are absent. Fig. 3.1 shows that this is indeed what one gets in a typical Monte Carlo run. One way out of this problem is to follow the continuum approach of [97] which starts out with a covariant gauge fixing. After having generated $SU(2)$ lattice configurations using the standard Wilson action we therefore fix to lattice Landau gauge (LLG). The latter is defined by maximizing the

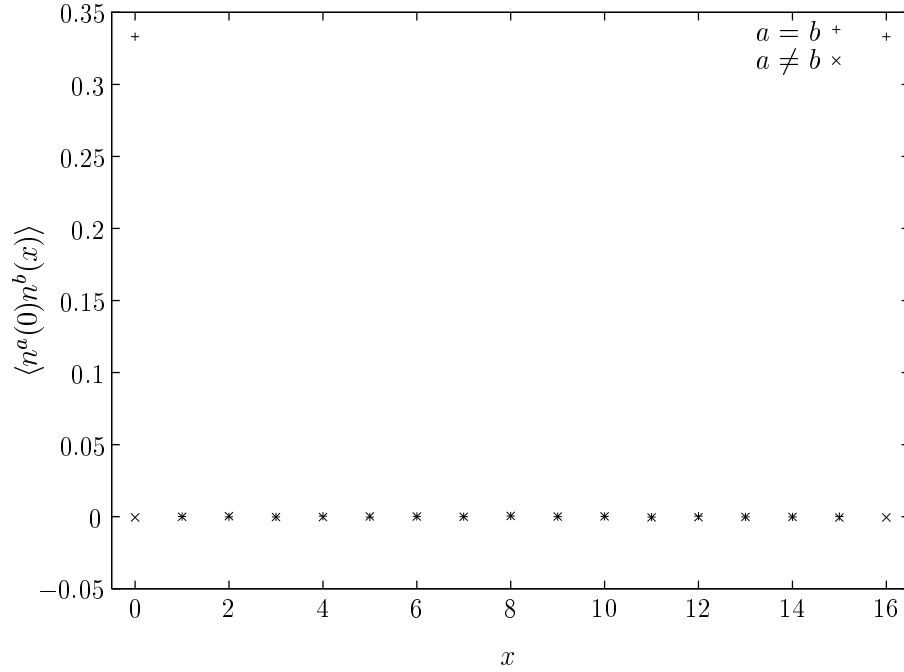


Figure 3.1.: Behavior of the two–point function G_{xy}^{ab} along a lattice axis for a random ensemble of \mathbf{n} –fields, obtained via MAG and (3.6). Note that also the value $1/3$ for $a = b$, $x = 0$ and $x = N_s$ is correctly reproduced.

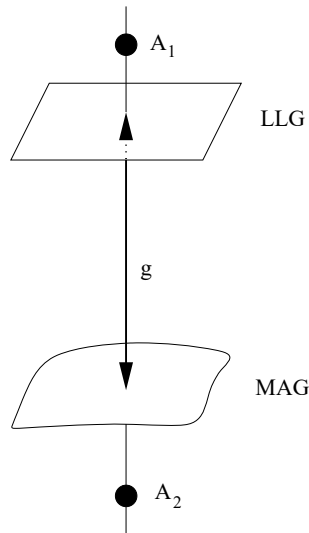


Figure 3.2.: Gauge invariant definition of $n \equiv g^\dagger \tau_3 g$. The gauge equivalent configurations A_1 and A_2 are both mapped onto the same ‘representatives’ on the LLG or MAG slices (ignoring Gribov copies). Thus, they are both associated with the *same* gauge transformation g defining n .

functional

$$F_{\text{LLG}} \equiv \sum_{x,\mu} \text{tr} \Omega U_{x,\mu}, \quad (3.9)$$

with respect to the gauge transformation Ω . In this way we impose some ‘preconditioning’ [107] which (i) eliminates the randomness in our Yang–Mills configurations and (ii) leaves a residual global $SU(2)$ –symmetry. The Landau gauge configurations are then plugged into the MAG functional (3.5) which subsequently is maximized with respect to g . The gauge transformation g obtained this way determines \mathbf{n} according to (3.6). One may say that g (and hence \mathbf{n}) measure the gauge–invariant (!) distance between the LLG and MAG gauge slices (see Fig. 3.2). In App. B we show that LLG and MAG are ‘close’ to each other. Therefore, the maximizing g is on average close to unity, hence, on average, \mathbf{n} will be aligned in the positive 3–direction. In this way we have explicitly broken the global $SU(2)$ down to a global $U(1)$.

All computations have been done on a N^4 –lattice with $N = N_s = N_t = 16$ and Wilson coupling $\beta = 2.35$, lattice spacing 0.13 fm and periodic boundary conditions. For the LLG we used Fourier accelerated steepest descent [108] (see Fig. 3.3). The MAG was

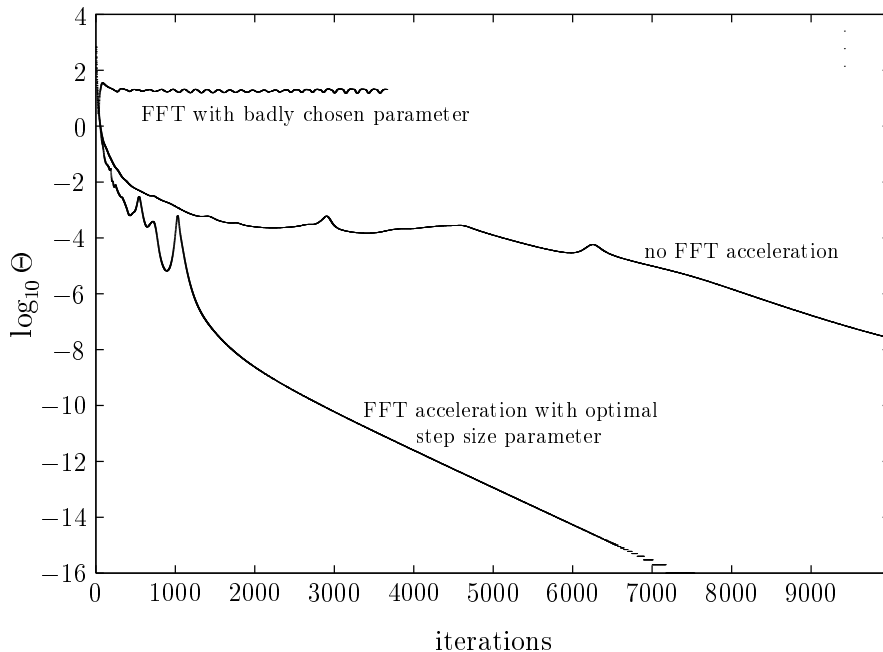


Figure 3.3.: Behavior of the LLG–functional using different algorithms. The parameter Θ measures the ‘distance’ from the LLG, i.e. for $\Theta = 0$ the LLG is achieved.

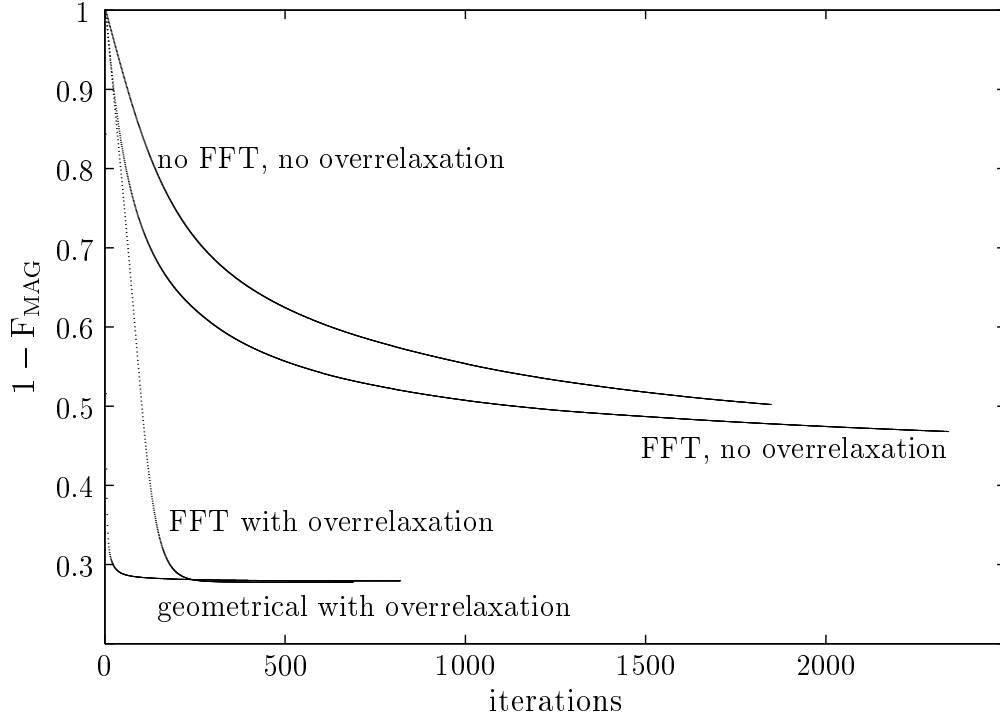


Figure 3.4.: Behavior of the MAG–functional using different algorithms.

achieved using two independent algorithms, one (AI) using iterations based on elementary geometric manipulations (including overrelaxation steps), the other (AII) being analogous to LLG fixing (see Fig. 3.4).

3.3. Numerical Results

As expected, we observe a non-vanishing expectation value of the field in the 3–direction, a ‘magnetization’ \mathfrak{M} defined through $\langle n^a \rangle = \mathfrak{M} \delta^{a3}$. Thus, the global symmetry is indeed broken explicitly according to the pattern $SU(2) \rightarrow U(1)$. We demonstrate this by exhibiting the angular distribution of the \mathbf{n} –field on its target space S^2 in Fig. 3.5. The azimuthal angle ϕ is equally distributed, while the distribution of the polar angle θ has a maximum near $\pi/2$ corresponding to the north pole, $\mathbf{n} = (0, 0, 1)$. Explicit symmetry breaking also shows up in the behavior of the two–point functions as depicted in Fig. 3.6. The longitudinal correlator, $G_x^{\parallel} \equiv \langle n_x^3 n_0^3 \rangle \sim \langle n^3 \rangle \langle n^3 \rangle = \mathfrak{M}^2$, exhibits clustering for large distances, the plateau being given by the magnetization

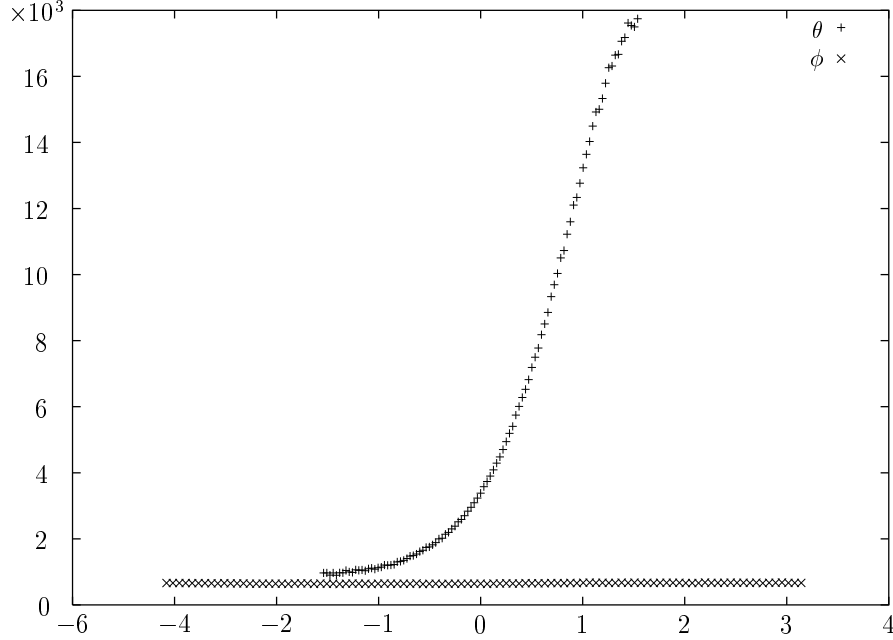


Figure 3.5.: Distribution of polar and azimuthal angles (θ and ϕ) associated with the unit vector \mathbf{n} on S^2 . The uniform distribution for ϕ and the maximum for $\theta = \pi/2$ shows that \mathbf{n} is located near the north pole, $\mathbf{n} = (0, 0, 1)$.

(squared). The transverse correlation function (of the would-be Goldstone bosons)

$$G_x^\perp \equiv G_{x0}^\perp \equiv \frac{1}{2} \sum_{i=1}^2 \langle n_x^i n_0^i \rangle, \quad (3.10)$$

decays exponentially as shown in Fig. 3.7. This means that there is a nonvanishing mass gap M whose value can be obtained by a fit to a cosh-function (see Fig. 3.7). The numerical values of the observables, \mathfrak{M} , M and the transverse susceptibility,

$$\chi^\perp \equiv \sum_x G_x^\perp, \quad (3.11)$$

which all can be derived from the two-point functions, are summarized in Tab. 3.1 for both algorithms.

The disagreement between AI and AII is statistically significant. We attribute it to the ubiquitous Gribov problem [109] (for Abelian gauges, see [110, 111]). On the lattice, this is the statement that maximizing gauge fixing functions like F_{MAG} or

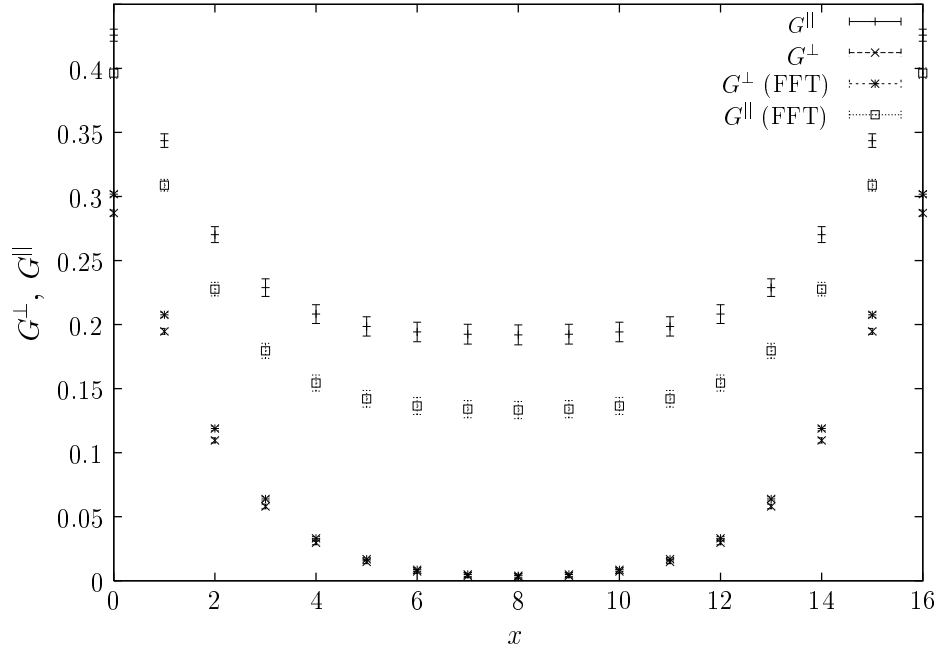


Figure 3.6.: Behavior of the two–point correlators of the \mathbf{n} –field along a lattice axis (labelled by coordinate x). Note the difference between algorithms AI and AII (FFT). Error bars exhibit the statistical error of the Monte Carlo simulation.

F_{LLG} is equivalent to a spin–glass problem with an enormous number of degenerate extrema. This implies that the algorithms AI and AII will almost certainly end up in different local maxima, which explains the difference between rows one and two in Tab. 3.1.

As shown in the last column of Tab. 3.1, the numerical results for the mass gap M lead to a value of about 1 GeV in physical units.

n^3 is a local functional of the n^i , $n^3 = (1 - n^i n^i)^{1/2}$. Thus, one expects the same exponential decay for the longitudinal correlator G^{\parallel} . This can be confirmed with a numerical value for the mass gap of $M = 0.66 a^{-1}$.

To improve statistics, we have calculated the time–slice correlator,

$$C^{\perp}(t) \equiv N_s^{-3} \sum_{\mathbf{x}} G_{\mathbf{x},t}^{\perp}. \quad (3.12)$$

In the continuum, for purely exponential decay of G^{\perp} , this would become proportional

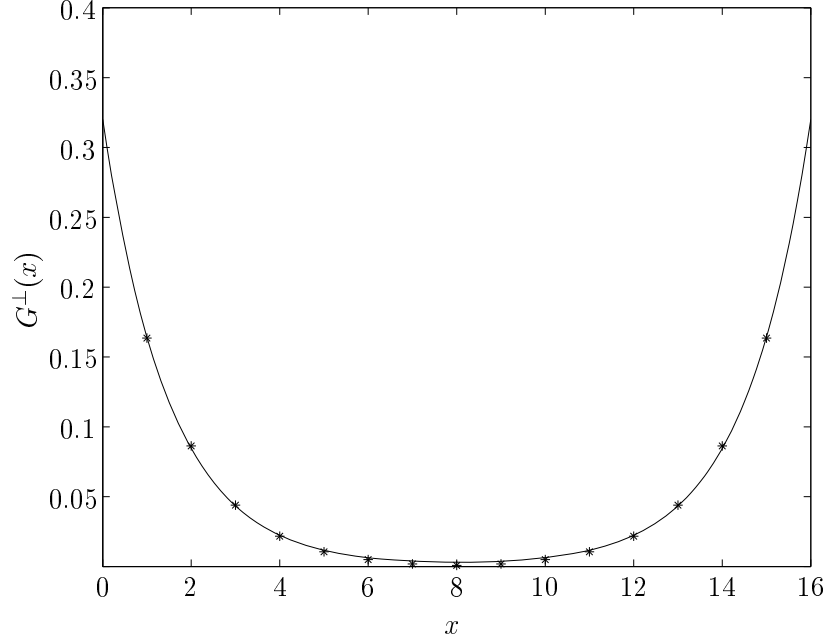


Figure 3.7.: The transverse correlation function along an arbitrary lattice axis, fitted as $G^\perp(x) = a_1 \cosh(M(x - N_s/2)) + a_2$ with $a_1 = 0.0048$, $a_2 = -0.0053$, $M = 0.6084$. Data points are obtained with algorithm AI.

algorithm	\mathfrak{M}	$a^{-4}\chi^\perp$	aM	M [GeV]
AI	0.438	92.57	0.61	0.95
AII	0.366	79.66	0.67	1.03

Table 3.1.: Numerical results for some observables as obtained from the longitudinal and transverse two–point functions, G^\parallel and G^\perp , respectively.

to a modified Bessel function K_2 . An associated fit works very well as is shown in Fig. 3.8. Fitting the time–slice correlator according to Fig. 3.8, we obtain for the mass gap

$$aM = 0.642 \quad \text{i.e.} \quad M = 0.97 \text{ GeV} . \quad (3.13)$$

This is the value with the smallest statistical errors.

The mass gap obtained differs significantly from the $SU(2)$ mass gap, $M_{SU(2)} \simeq 1.5$ GeV, obtained directly from Wilson configurations with $\beta = 2.4$ [30]. We believe that the difference is due to the highly nonlocal relation between the original Yang–Mills degrees of freedom (the link variables) and the color spin \mathbf{n} . After all, we

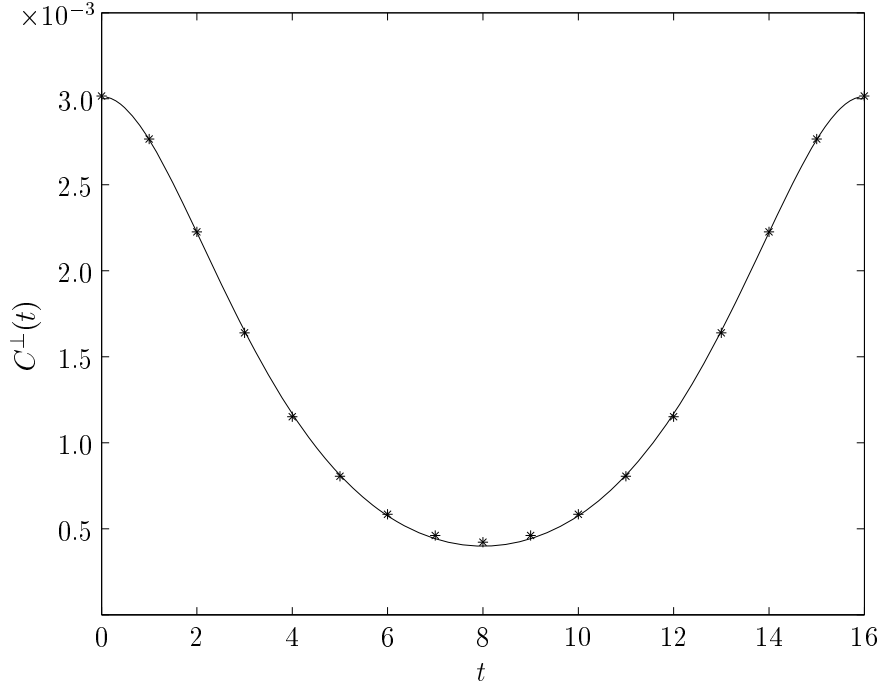


Figure 3.8.: The time–slice correlator fitted to a (properly symmetrized) Bessel function, $C^\perp(t) = c_1[t^2 K_2(Mt) + (t - N_t)^2 K_2(M(N_t - t))] + c_2$, where $c_1 = 0.0006$, $c_2 = 0.0001$ and $M = 0.6423$. Data points are obtained with algorithm AI.

have implicitly solved the partial differential equation (3.7) with link variables U in Landau gauge entering the adjoint Laplacian. The solution \mathbf{n} will clearly be a nonlocal functional of these U 's. Consequently, we cannot expect that the exponential decay of $G^\perp[n]$ will be governed by the lowest excitation of the U -ensemble.

3.4. Effective Action and Schwinger–Dyson Equations

At this point it is natural to ask whether there is an effective action $S_{\text{eff}}[n]$ that reproduces the distribution of \mathbf{n} -fields leading to the results of the previous section.

At low energies, it should make sense to employ an ansatz in terms of a derivative expansion,

$$S_{\text{eff}} = \sum_j \lambda_j S_j[\mathbf{n}] + \sum_j \lambda'_j S'_j[\mathbf{n}, \mathbf{h}], \quad (3.14)$$

with $O(3)$ invariant operators S_j and noninvariant operators S'_j , which are ordered by increasing mass dimension. Up to dimension four, one has the symmetric terms,

$$\begin{aligned} S_1 &= (\mathbf{n}, \Delta \mathbf{n}) , & S_2 &= (\mathbf{n}, \Delta^2 \mathbf{n}) , \\ S_3 &= (\mathbf{n} \cdot \Delta \mathbf{n}, \mathbf{n} \cdot \Delta \mathbf{n}) , & S_4 &= (\mathbf{n} \cdot \partial_\mu^\dagger \partial_\nu \mathbf{n}, \mathbf{n} \cdot \partial_\mu^\dagger \partial_\nu \mathbf{n}) , \end{aligned} \quad (3.15)$$

and the symmetry–breaking terms including a unit vector ‘source field’ \mathbf{h} [LRD1] (which can be thought of as the direction of an external magnetic field),

$$S'_1 = (\mathbf{n}, \mathbf{h}) , \quad S'_2 = (\mathbf{n} \cdot \mathbf{h}, \mathbf{n} \cdot \mathbf{h}) , \quad S'_3 = (\mathbf{n} \cdot \Delta \mathbf{n}, \mathbf{n} \cdot \mathbf{h}) . \quad (3.16)$$

In the above, we have introduced the scalar products

$$(f, g) \equiv \sum_x f_x g_x , \quad \mathbf{u} \cdot \mathbf{v} \equiv u^a v^a , \quad (3.17)$$

and the usual lattice Laplacian Δ (see App. A).

Note that the \mathbf{n} –field configurations are classified by the Hopf invariant irrespective of the particular form of the (effective) action. This, together with the usual scaling arguments, shows that the action (3.14) with the operators (3.15) and (3.16) should still support classical knot soliton solutions. Our ansatz thus does not exclude this important feature.

The couplings in (3.14) can be determined by inverse Monte Carlo techniques. The notion is suggestive: instead of creating an ensemble from a given action, one wants to compute a (truncated) action which gives rise to the given ensemble of \mathbf{n} –fields. A particular approach uses the Schwinger–Dyson equations [112, 88]. These represent an overdetermined linear system which can be used to solve for the couplings in terms of correlation functions. The latter are nothing but the coefficients of the linear system.

For an unconstrained scalar field ϕ , the Schwinger–Dyson equations follow from translational invariance of the functional measure, implying

$$0 = \int \mathcal{D}\phi \mathbb{P}_x \left\{ F[\phi] \exp(-S[\phi]) \right\} , \quad (3.18)$$

where $\mathbb{P}_x \equiv -i\delta/\delta\phi_x$ is the (functional) momentum operator, and F an arbitrary

functional of the field ϕ . Usually one chooses $F[\phi] = \phi(x_1) \dots \phi(x_k)$. For a constrained field like \mathbf{n} with a curved target space things are slightly more subtle [112]. There is, however, a rather elegant way to derive the Schwinger–Dyson equations if one exploits the isometries of the target space S^2 [113]. The target space measure,

$$\mathcal{D}\mathbf{n} = \prod_x d\mathbf{n}_x \delta(\mathbf{n}_x^2 - 1) , \quad (3.19)$$

is obviously rotationally invariant, i.e. under $\mathbf{n} \rightarrow R\mathbf{n}$, $R \in O(3)$. This implies the modified Schwinger–Dyson identity

$$\int \mathcal{D}\mathbf{n} \mathbf{L}_x \left\{ F[\mathbf{n}] \exp(-S_{\text{eff}}[\mathbf{n}, \mathbf{h}]) \right\} = 0 , \quad (3.20)$$

where \mathbf{L}_x denotes the angular momentum operator (at lattice site x),

$$i\mathbf{L}_x = \mathbf{n}_x \times \frac{\partial}{\partial \mathbf{n}_x} \quad \text{or} \quad iL_x^a \equiv \epsilon^{abc} n_x^b \frac{\delta}{\delta n_x^c} . \quad (3.21)$$

In shorthand-notation, (3.20) can be rewritten as

$$\langle \mathbf{L}_x F[\mathbf{n}] - F[\mathbf{n}] \mathbf{L}_x S_{\text{eff}}[\mathbf{n}] \rangle = 0 . \quad (3.22)$$

These exact identities can be used to determine the unknown couplings λ_j . To this end one chooses a set of field monomials $F_i[\mathbf{n}]$ and plugs them into (3.22) together with the form (3.14) of the action. This yields the *local* linear system

$$\sum_j \langle F_i \mathbf{L}_x S_j \rangle \lambda_j + \sum_k \langle F_i \mathbf{L}_x S'_k \rangle \lambda'_k = \langle \mathbf{L}_x F_i \rangle , \quad (3.23)$$

which, in principle, can be solved numerically, for instance by least-square methods. The identities obtained so far hold for arbitrary actions $S_{\text{eff}}[\mathbf{n}]$. In particular, we have not made use of any symmetries. Taking the latter into account will lead to Ward identities.

Let us specialize to our lattice effective action (3.14). It is a sum of a symmetric part S containing the terms (3.15) and an asymmetric part S' containing the terms (3.16),

$$S_{\text{eff}} = S[\mathbf{n}] + S'[\mathbf{n}, \mathbf{h}] . \quad (3.24)$$

Due to the invariance of S under global $O(3)$ rotations it is an $O(3)$ –singlet and hence annihilated by the total angular momentum,

$$\mathbf{L}S = 0, \quad \mathbf{L} = \sum_x \mathbf{L}_x, \quad (3.25)$$

such that $\mathbf{L}S_{\text{eff}} = \mathbf{L}S'$. Thus, summing over all lattice sites x in (3.22) yields the (broken) Ward identity,

$$\langle \mathbf{L}F[\mathbf{n}] - F[\mathbf{n}] \mathbf{L}S'[\mathbf{n}, \mathbf{h}] \rangle = 0, \quad (3.26)$$

where the second term contains the infinitesimal change of the non-invariant part S' of the effective action under rotations of \mathbf{n} . Note that the coupling constants λ_j of the $O(3)$ –symmetric operators S_j have disappeared in the Ward identity (3.26) so that only the symmetry–breaking couplings λ'_j are present. We have collected the explicit lattice Schwinger–Dyson and Ward identities used in our simulations in App. C. As the former are local relations, they naturally contain more information than the global Ward identities. In particular, one does have access to length scales.

3.5. Comparing Yang–Mills and FN Configurations

3.5.1. Leading–Order Ansatz

To leading order (LO) in the derivative expansion we have a standard nonlinear sigma model with symmetry–breaking term,

$$S_{\text{eff}} = \sum_x (\lambda \mathbf{n}_x \cdot \Delta \mathbf{n}_x + \lambda' \mathbf{n}_x \cdot \mathbf{h}), \quad \mathbf{h} \equiv \mathbf{e}_z. \quad (3.27)$$

Inverse Monte Carlo amounts to determining the couplings λ and λ' such that the probability distribution associated with the LO action (3.27) fits the observables of the Yang–Mills ensemble of \mathbf{n} –fields¹. The associated Schwinger–Dyson equation (3.23), with $F[\mathbf{n}] = n_x^a$, can be written as

$$\lambda H_{xy} + \lambda' G_{xy}^\perp = -\mathfrak{M} \delta_{xy}, \quad (3.28)$$

¹Throughout this section, we refer to algorithm AI.

where H denotes the (antisymmetrized) two–point function of n^i and the operator $n^i \Delta n^3$,

$$H_{xy} \equiv \langle n_x^i n_y^i \Delta n_y^3 \rangle - \langle n_x^i n_y^3 \Delta n_y^i \rangle \equiv \langle n_x^i n_y^{[i} \Delta n_y^{3]} \rangle . \quad (3.29)$$

To analyse (3.28) we define a ‘reduced’ two–point function h_{xy} and magnetization μ ,

$$h_{xy} \equiv H_{xy}/G_{xy}^\perp , \quad (3.30)$$

$$\mu \equiv \mathfrak{M}/G_{xx}^\perp , \quad (3.31)$$

and rewrite (3.28) as the inhomogeneous system (using translational invariance to replace $x - y \rightarrow x$),

$$\lambda h_x + \lambda' = 0 , \quad x = 1, \dots, 8 , \quad (3.32)$$

$$\lambda h_0 + \lambda' = -\mu . \quad (3.33)$$

The solution is found to be

$$\lambda = \frac{1}{h_x - h_0} \mu , \quad (3.34)$$

$$\lambda' = -\frac{h_x}{h_x - h_0} \mu , \quad (3.35)$$

with the numerical boundary value given by $h_0 = 0.1410$ (cf. Fig. 3.9). Clearly, the system (3.32) with (3.33) is overdetermined since there are nine equations for two unknowns. This is reflected in the fact that λ and λ' in (3.34) and (3.35) depend on the lattice *distance* x via h_x . If the Yang–Mills ensemble were exactly described by the LO action (3.27), there would be no such x –dependence. Rather, for any $x = 1, \dots, 8$, we would have the same values for λ and λ' , respectively. Thus, to test the quality of the LO ansatz, we divide (3.35) by (3.34) showing explicitly that h_x should be constant,

$$h_x = -\frac{\lambda'}{\lambda} \equiv -\kappa' = \text{const.} , \quad x \neq 0 . \quad (3.36)$$

Fig. 3.9 shows that this is not the case. Therefore, a minimal sigma model with symmetry–breaking term does not yield a good representation of our Yang–Mills ensemble of \mathbf{n} –fields. If we nevertheless insist on the LO description, we have to ‘fit’ h_x by a horizontal line so that the numerical determination of the couplings via (3.34)

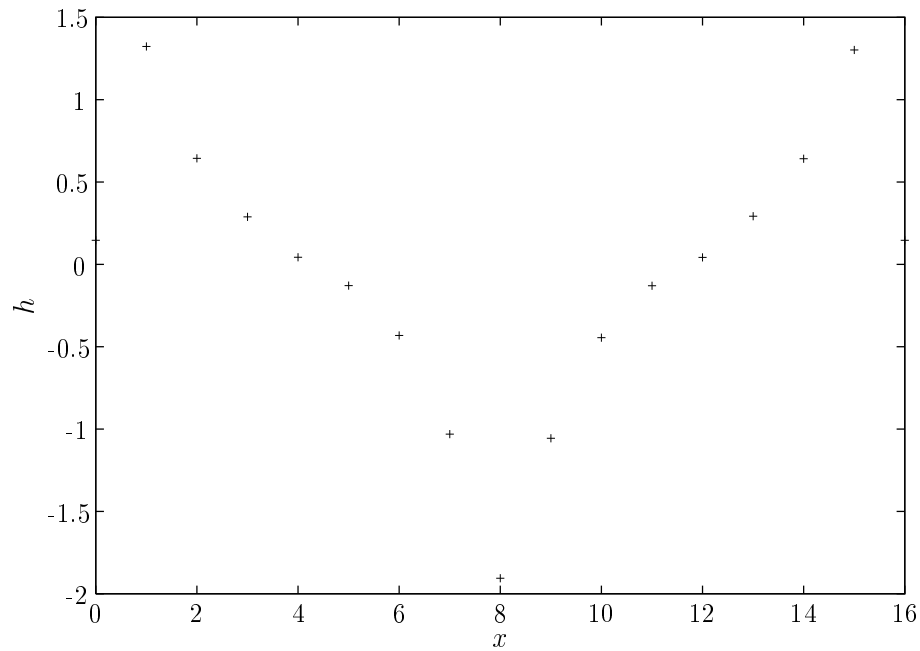


Figure 3.9.: h_x for the Yang–Mills ensemble. The boundary value is $h_0 = 0.1410$.

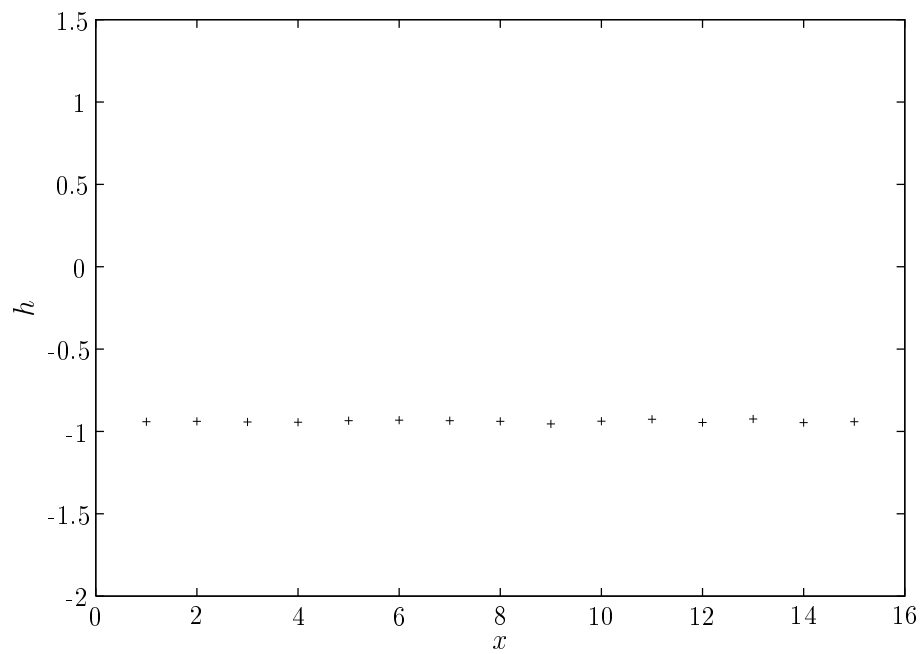


Figure 3.10.: h_x for the LO ensemble. Fitting the data points yields $h_x = -\kappa' = -0.938 \pm 0.002$.

and (3.35) is beset by large errors,

$$\lambda = -1.41 \pm 5.25 , \quad (3.37)$$

$$\lambda' = -1.33 \pm 0.74 . \quad (3.38)$$

Obviously, λ (including its sign) remains essentially undetermined. For λ' the situation is slightly better.

In order to assess the errors it is worthwhile to check whether our numerical accuracy is sufficient to really validate the Schwinger–Dyson identity (3.28) for the LO action (3.27) on the lattice. To this end we have simulated (3.27) with a combination of Metropolis and cluster algorithms producing configurations using the central values (3.37) and (3.38) as the input couplings. The result for h_x in the LO ensemble is presented in Fig. 3.10.

It is reassuring to note that the simulation of the minimal sigma model reproduces the input value $\kappa' = 0.943$ very well (for $x \neq 0$), the error being of the order of one percent. The prediction (3.36) thus can be verified with high accuracy for the LO action (3.27). We conclude that inverse Monte Carlo works quite well when applied to the minimal σ -model.

The discrepancy between the LO and Yang–Mills ensemble can be further visualized by looking at the susceptibility. For the action (3.27) and the choice $F[\mathbf{n}] = n_x^a$, the Ward identity (3.26) assumes the simple form

$$\chi^\perp = -\mathfrak{M}/\lambda' . \quad (3.39)$$

A consistency check is provided by noting that this can directly be obtained by summing (3.28) over x . Plugging in the magnetization from Tab. 3.1 and λ' from (3.38) we find

$$\chi^\perp = 0.33 \pm 0.18 , \quad (3.40)$$

This is way off the Yang–Mills value of 92.57 displayed in Tab. 3.1. For magnetization and mass gap the simulation of the LO ensemble yields the values

$$\mathfrak{M} = 0.93 , \quad M = 1.5 , \quad (3.41)$$

which are both larger than the Yang–Mills values of Tab. 3.1.

The discussion of this subsection thus shows quite clearly that more operators will have to be included in order to possibly make inverse Monte Carlo work reasonably well.

3.5.2. FN Action with Symmetry–Breaking Term

In this subsection we consider the FN action (3.1) with a LO symmetry–breaking term,

$$S_{\text{eff}} = \sum_x \{ \lambda \mathbf{n}_x \cdot \Delta \mathbf{n}_x + \lambda_{\text{FN}} [(\mathbf{n} \cdot \Delta \mathbf{n})^2 - (\mathbf{n} \cdot \partial_\mu^\dagger \partial_\nu \mathbf{n})^2] + \lambda' \mathbf{n}_x \cdot \mathbf{h} \} . \quad (3.42)$$

This ansatz does not include all terms of next–to–leading order (NLO) in the derivative expansion. It should be viewed as a minimal modification of the original FN action by adding an explicit symmetry–breaking term to obtain a mass gap.

The Schwinger–Dyson equation generalizing (3.28) becomes

$$\lambda H_{xy} + \lambda_{\text{FN}} H_{xy}^{\text{FN}} + \lambda' G_{xy}^\perp = -\mathfrak{M} \delta_{xy} . \quad (3.43)$$

The new two–point function H^{FN} is given by (C.19). The local identities (3.43) are to be solved for the three unknown couplings λ , λ' and λ_{FN} . Introducing another reduced two–point function,

$$h_{xy}^{\text{FN}} \equiv H_{xy}^{\text{FN}} / G_{xy}^\perp , \quad (3.44)$$

which is plotted in Fig. 3.11, we obtain, instead of (3.32) and (3.33), the (overdetermined) system,

$$\lambda h_x + \lambda_{\text{FN}} h_x^{\text{FN}} + \lambda' = 0 , \quad x = 1, \dots, 8 ; \quad (3.45)$$

$$\lambda h_y + \lambda_{\text{FN}} h_y^{\text{FN}} + \lambda' = 0 , \quad y > x ; \quad (3.46)$$

$$\lambda h_0 + \lambda_{\text{FN}} h_0^{\text{FN}} + \lambda' = -\mu , \quad (3.47)$$

to be solved for each pair of lattice *distances* (x, y) , $y > x$. The number of independent pairs is $7(7+1)/2 = 28$ for lattice extension $L = 16$. Defining the determinant

$$d_{xy} \equiv h_0(h_x^{\text{FN}} - h_y^{\text{FN}}) - h_0^{\text{FN}}(h_x - h_y) + h_x h_y^{\text{FN}} - h_y h_x^{\text{FN}} , \quad (3.48)$$

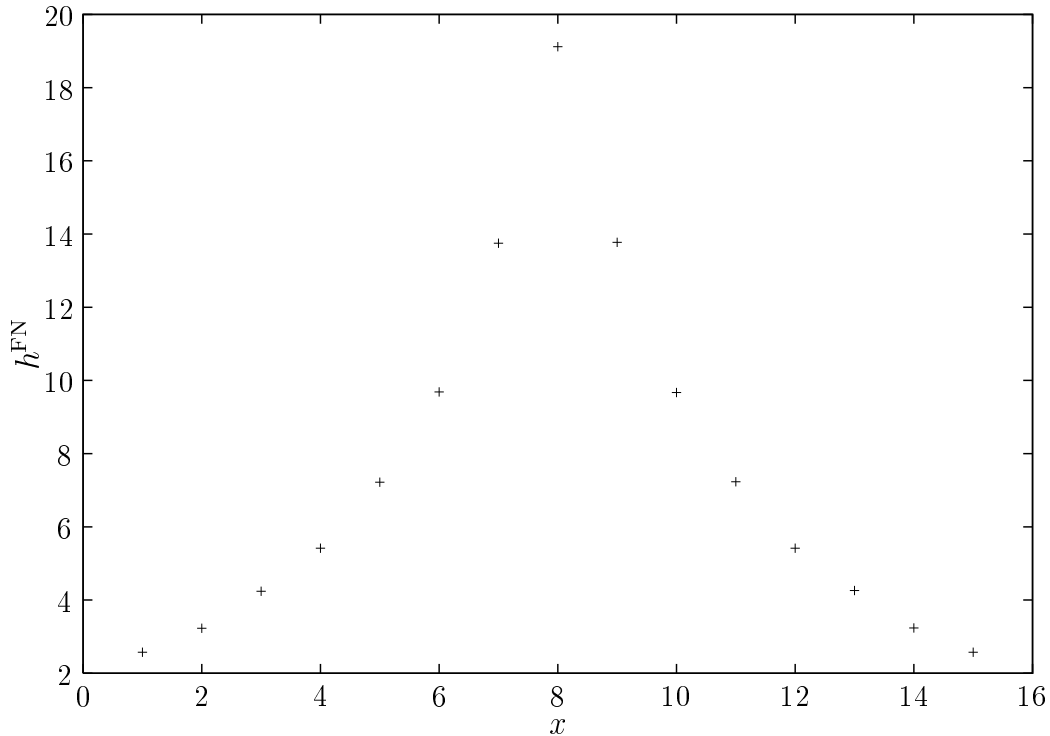


Figure 3.11.: h_x^{FN} for the Yang–Mills ensemble. The boundary value $h_0^{\text{FN}} = -31.24$ is not displayed.

the solutions, labelled by x and y , are

$$\lambda = \frac{h_x^{\text{FN}} - h_y^{\text{FN}}}{d_{xy}} \mu, \quad (3.49)$$

$$\lambda' = \frac{h_x h_y^{\text{FN}} - h_y h_x^{\text{FN}}}{d_{xy}} \mu, \quad (3.50)$$

$$\lambda_{\text{FN}} = -\frac{h_x - h_y}{d_{xy}} \mu. \quad (3.51)$$

We have checked that the numerical values for d_{xy} are not close to zero so that there is no problem with small denominators in the solutions. For each pair of lattice distances (x, y) we thus have a certain value for any of the three couplings (3.49–3.51). For each particular coupling those would all agree (within statistical errors) if the NLO action (3.42) would exactly describe the Yang–Mills ensemble. Again, however, analogous to the LO case, the couplings do vary with lattice distances x and y . For larger distances, however, the data seem to deviate less from the central

values. Numerically, one finds,

$$\lambda = -0.232 \pm 0.035 , \quad (3.52)$$

$$\lambda' = 0.257 \pm 0.014 , \quad (3.53)$$

$$\lambda_{\text{FN}} = -0.0402 \pm 0.0004 . \quad (3.54)$$

Several remarks are in order. First of all, the relative errors, given by the standard deviation from the mean, are small compared to the LO ansatz. In particular, the signs of all couplings are fixed. Interestingly, the addition of the FN coupling λ_{FN} , although small numerically, has a large effect: it reverts the sign of λ' as compared to (3.38), implying a *negative* magnetization. This follows, for instance, from the Ward identity (3.39), which still holds for the action (3.42), and the positivity of the susceptibility, hence

$$\mathfrak{M} = -\lambda' \chi^\perp < 0 , \quad (3.55)$$

in contradistinction with the positive Yang–Mills value of Tab. 3.1.

To further analyse the result for the couplings, we divide (3.45) by λ , leading to a linear relation between h and h^{FN} (for $x \neq 0$),

$$h_x = -\kappa' - \kappa_{\text{FN}} h_x^{\text{FN}} , \quad \kappa_{\text{FN}} \equiv \lambda_{\text{FN}}/\lambda . \quad (3.56)$$

Thus, plotting h_x against h_x^{FN} should yield a straight line with intercept $-\kappa'$ and slope $-\kappa_{\text{FN}}$. The numerical values (3.52–3.54) yield

$$\kappa' = -1.108 \pm 0.228 , \quad \kappa_{\text{FN}} = 0.173 \pm 0.024 . \quad (3.57)$$

In analogy with the LO case, we have numerically checked the prediction (3.56) for the NLO action (3.42) by a Monte Carlo simulation using the input couplings (3.52–3.54). Fig. 3.12 clearly demonstrates the expected linear behavior. A corresponding fit results in

$$\kappa' = -1.120 , \quad \kappa_{\text{FN}} = 0.171 , \quad (3.58)$$

being consistent with the central values of (3.57) to within one percent. We thus conclude that inverse Monte Carlo also works quite well for the NLO ensemble. For the sake of explicit comparison with Figs 3.9 and 3.11 we display the reduced two-point functions obtained by simulating the NLO action in Figs 3.13 and 3.14. As

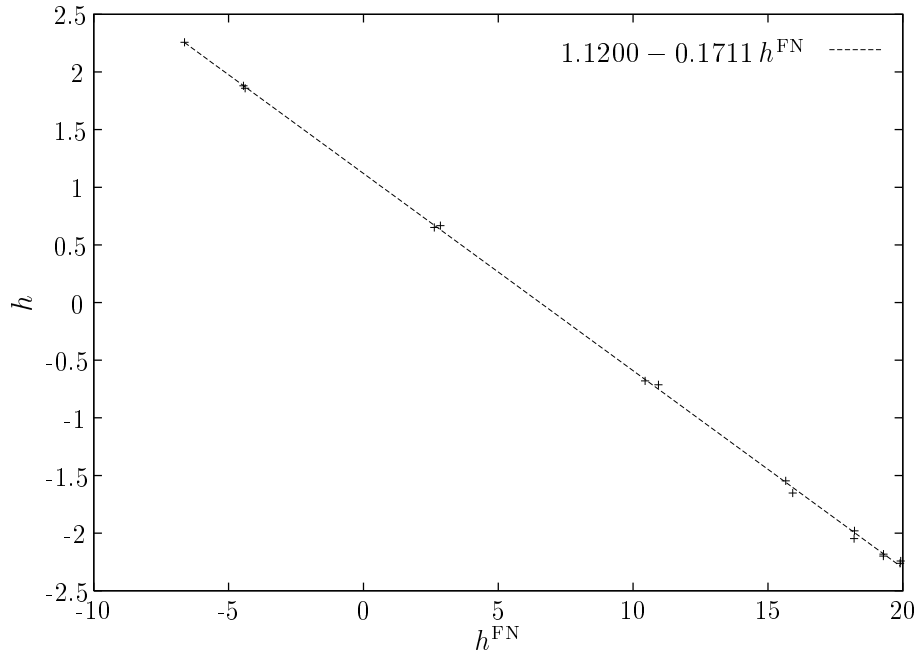


Figure 3.12.: h vs. h^{FN} for the NLO action (3.42).

expected, the NLO simulation yields a negative magnetization,

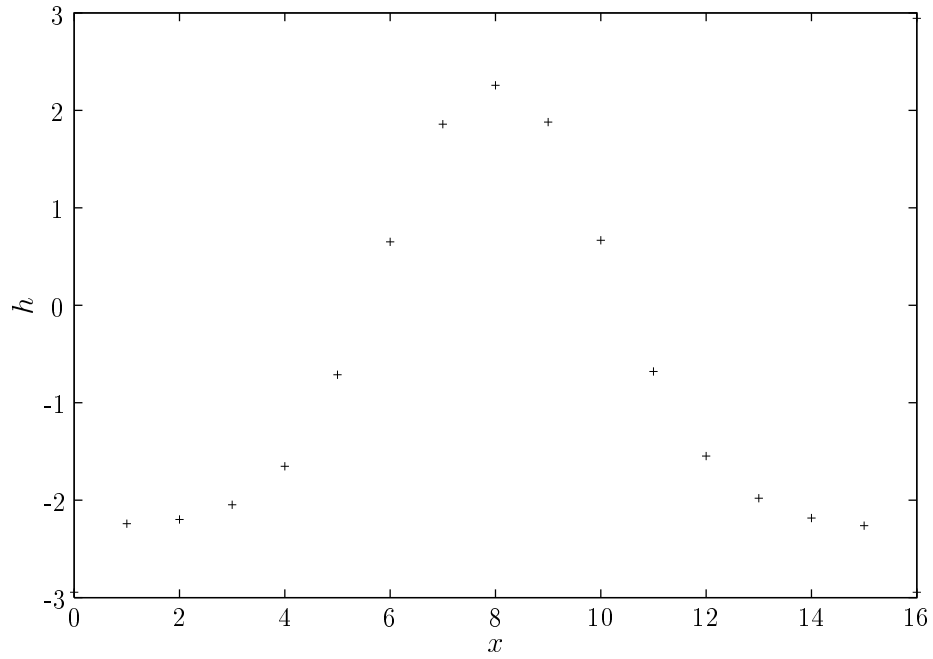
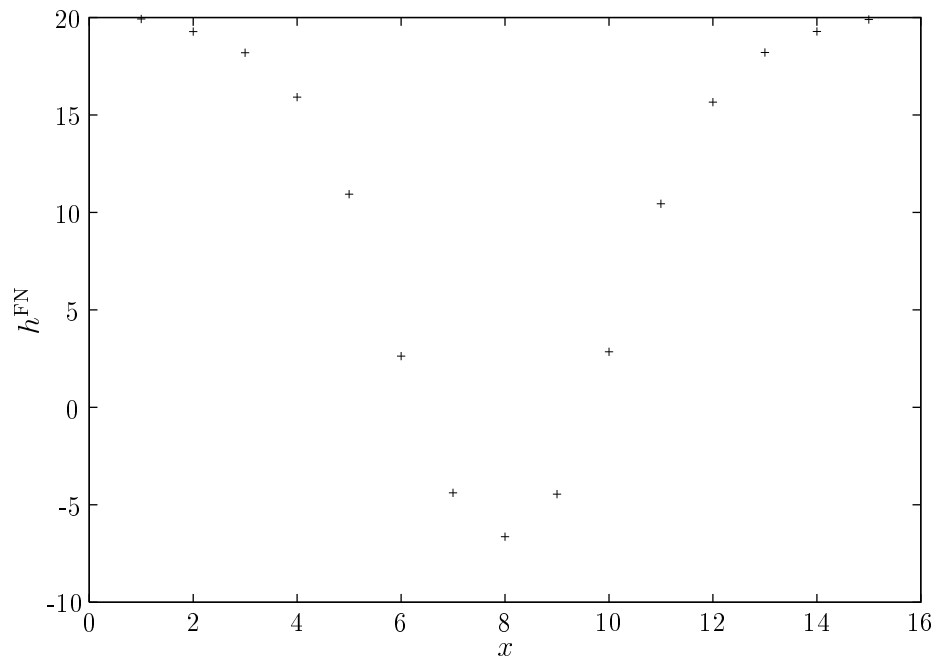
$$\mathfrak{M} = -0.49 , \quad (3.59)$$

while the mass gap becomes $M = 1.2$, i.e. slightly larger than the value listed in Tab. 3.1.

If the Yang–Mills ensemble has anything to do with the FN one, then plotting h vs. h^{FN} (as obtained from Yang–Mills) should also show straight–line behavior, at least approximately. Fig. 3.15 displays a linear fit to the Yang–Mills data with parameters

$$\kappa' = -1.232 , \quad \kappa_{\text{FN}} = 0.170 . \quad (3.60)$$

Again, within error bars, these values are consistent with the preceding analysis (3.57). Note that reverting the sign of λ' amounts to reverting the sign of the intercept in Fig. 3.15. The data points clearly do not support anything like that. On the contrary, it seems that, for small h^{FN} (corresponding to small distances x , see Fig. 3.11), the data points deviate from a straight line. Playing around with different fits indicates

Figure 3.13.: h_x for the NLO ensemble.Figure 3.14.: h_x^{FN} for the NLO ensemble.

that h rises with a *negative* power of h^{FN} for small h^{FN} so that in reality there may be no intercept at all.

The behavior of κ' as a function of lattice distances x and y may also be investigated. Dividing (3.50) by (3.49) we find

$$\kappa' = \lambda'/\lambda = \frac{h_x h_y^{\text{FN}} - h_y h_x^{\text{FN}}}{h_x^{\text{FN}} - h_y^{\text{FN}}} = -1.38 \pm 0.29 , \quad (3.61)$$

where, in the analytic expression, the determinant d_{xy} has dropped out. Fig. 3.16 shows the variation of κ' with x and y . Again, a different sign for κ' is completely out of reach.

Following the logic of gradient expansions, one may argue that the effective action (3.42) is supposed to represent the Yang–Mills ensemble only for large distances. Fig. 3.15, for instance, seems to indicate that the straight–line fit works particularly well for the last three points to the right which correspond to $x = 6, 7, 8$, respectively. In physical units, this amounts to distances R larger than six lattice units, i.e. $R \gtrsim 0.8$ fm. Restricting to the analogous data points, we obtain for the couplings in (3.42),

$$\lambda = -0.2775 \pm 0.026 , \quad (3.62)$$

$$\lambda' = 0.2661 \pm 0.012 , \quad (3.63)$$

$$\lambda^{\text{FN}} = -0.040 \pm 0.0005 , \quad (3.64)$$

and for the ‘reduced’ ones,

$$\kappa' = -0.97 \pm 0.13 , \quad \kappa^{\text{FN}} = 0.15 \pm 0.01 . \quad (3.65)$$

All these do not differ significantly from the values (3.52–3.54) and (3.57) obtained by using the unrestricted data set. In particular, the sign of λ' remains positive. We therefore conclude that, also at large distances, the minimally modified FN action (3.42) fails to describe the Yang–Mills ensemble of \mathbf{n} -fields.

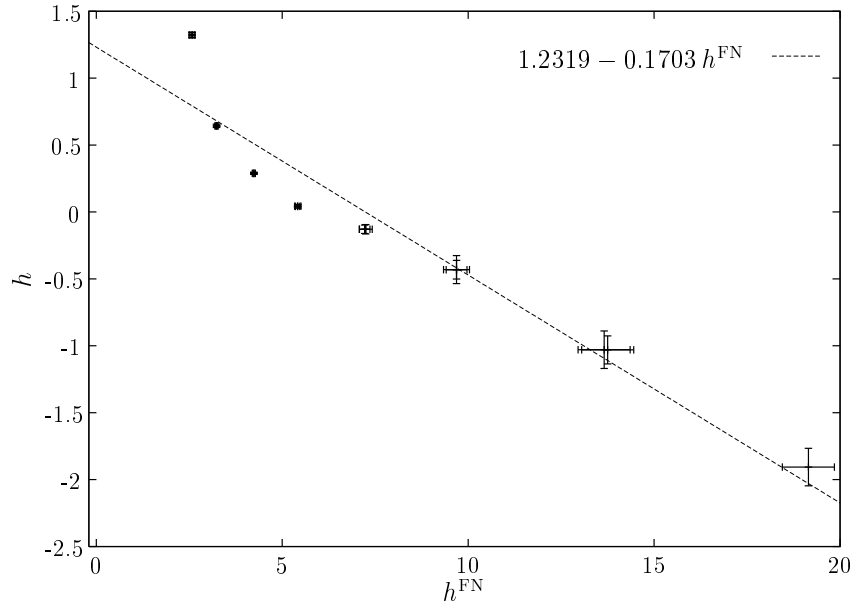


Figure 3.15.: h vs. h^{FN} for the Yang–Mills ensemble. The error bars reflect the fact that, for large distances x (i.e. $x \simeq N_s/2 = 8$ for the lattice size used), h and h^{FN} are obtained by dividing two small numbers (from the tails of the two–point functions G^\perp , H and H^{FN}).

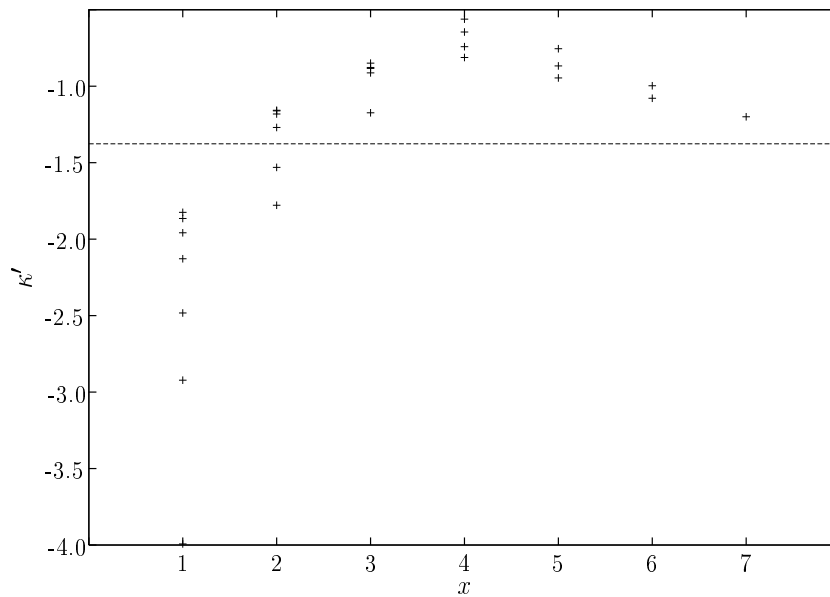


Figure 3.16.: Variation of κ' with lattice distances x and y . The central value is $\kappa' = -1.38$.

3.6. Remarks I

We have found strong evidence that the ensemble of unit color vector fields \mathbf{n} generated from $SU(2)$ Yang–Mills theory *cannot* be described by the FN action plus a minimal symmetry–breaking term, introduced to allow for a mass gap. This follows from a number of discrepancies between the two ensembles. First, and most prominent, the sign of λ' is positive, implying *negative* magnetization \mathfrak{M} , at variance with the value from the Yang–Mills ensemble. Second, the reduced two–point function h (h^{FN}) from the NLO ensemble *increases* (*decreases*) with lattice distance x , while for Yang–Mills the behavior is just the opposite. Third, the size of the mass gap is larger than for the Yang–Mills ensemble of \mathbf{n} –fields.

It is quite conceivable that magnetization (and susceptibility) can be recovered correctly by adding more (symmetry–breaking) terms to the NLO action (work in this direction is under way). The same remark applies to the mass gap. Note, however, that one cannot naturally expect the Yang–Mills and σ –model mass gaps to coincide due to the nonlocal relation between \mathbf{n} and the link variables U . Whether this represents a problem is a question of scales. If the effective σ –model were valid only for distances of, say, $R \gtrsim 0.8$ fm corresponding to energies $E \lesssim 0.25$ GeV, as suggested by the discussion of Section 3.5, then it would make no sense to address questions like the glueball spectrum. An analogous situation holds for the Fermi theory of weak interactions which also is only effective much below the W and Z scales.

One should also say that we have only ruled out the Faddeev–Niemi conjecture for one particular choice of an \mathbf{n} –field. As there is no unique or natural definition for \mathbf{n} , one may try alternative prescriptions for $\mathbf{n} = \mathbf{n}[U]$. A fairly local one is the following. Write the (gauge fixed) links as $U_{x,\mu} = u_{x,\mu}^0 + iu_{x,\mu}$. Then define $\bar{n}_x \equiv \bar{u}_x/|\bar{u}_x|$ with the link average $\bar{u}_x \equiv \sum_{\mu} u_{x,\mu}$. Under global gauge transformations this transforms properly such that $\bar{\mathbf{n}}$ is another color unit vector.

To check the Faddeev–Niemi conjecture in the most general way possible is clearly beyond the scope of this work. The following caveat, however, holds irrespective of the choice made for the \mathbf{n} –field in the effective σ –model. Allowing for finite temperature, the latter is in the universality class of the $4d$ Heisenberg model, while $SU(2)$ Yang–Mills theory is in the $3d$ Ising class [54]. This issue has been discussed recently in the context of constructing effective actions via Abelian projections [114, 115, 116].

Again, if the σ -model scale were below the critical temperature, the effective theory would only be valid in the confined phase and would have nothing to say about the behavior of Yang–Mills theory close to the phase transition. Otherwise, an infinite number of operators would be required which, of course, is anything else but an ‘effective’ description. Summarizing, we conclude that, while a reasonable effective model generalizing the FN action may exist in principle, it will be of little practical use.

4. Polyakov Loop Model

4.1. Introduction

The deconfinement phase transition in pure Yang–Mills theory [52, 53] is controlled by the dynamics of the Polyakov loop variable $\mathfrak{P}_{\mathbf{x}}$. Above a critical temperature T_c , the singlet part $L_{\mathbf{x}} \equiv \text{tr } \mathfrak{P}_{\mathbf{x}}/2$ develops a nonvanishing vacuum expectation value (VEV). In this high–temperature phase one expects to find a plasma of liberated gluons (and, in QCD, also quarks). The VEV of $L_{\mathbf{x}}$ thus represents an order parameter associated with spontaneous symmetry breaking. The symmetry in question is a global \mathbb{Z}_N symmetry, \mathbb{Z}_N being the center of the gauge group $SU(N)$. While the Yang–Mills action is center symmetric, $L_{\mathbf{x}}$, although gauge invariant, transforms nontrivially, $L_{\mathbf{x}} \rightarrow zL_{\mathbf{x}}$, $z \in \mathbb{Z}_N$. Combining renormalization group ideas and dimensional reduction, Svetitsky and Yaffe have conjectured that finite–temperature $SU(N)$ Yang–Mills theory in d dimensions is in the universality class of a \mathbb{Z}_N spin model in dimension $d - 1$ [54, 55]. For some recent and rather sophisticated confirmations of the statement on the lattice the reader is referred to [117, 118, 119, 120].

The universality argument implies that effective field theory methods may be put to use. It should make sense to map the microscopic theory, here Yang–Mills, onto a macroscopic one, described by an effective action with \mathbb{Z}_N symmetry. For gauge group $SU(2)$, for instance, one can try to coarse–grain the gauge fields all the way down to \mathbb{Z}_2 Ising spins [121, 122, 123]. An intermediate procedure is to establish an effective action for the Polyakov loop variable itself [56, 57, 58]. This may be achieved analytically using strong–coupling or, equivalently, high–temperature expansions [57, 124, 125]. Doing so for $SU(2)$, one obtains a local effective action depending on all characters $\chi_j(\mathfrak{P}_{\mathbf{x}})$ [124, 125]. The index $j \in \mathbb{N}/2$ labels the irreducible representations of $SU(2)$. In this most elementary case, χ_j can be expressed in terms of powers of $L_{\mathbf{x}}$ (the character of the fundamental representation, $j = 1/2$). For larger gauge groups,

however, more and more characters/representations become relevant. This fact has recently been employed for model building, regarding the untraced holonomy \mathfrak{P}_x [126] or, equivalently, its eigenvalues [127] as the fundamental degrees of freedom.

Generalizing old ideas for the traced Polyakov loop [58] we parametrize the (lattice) effective action as

$$S_{\text{eff}} = \sum_a \lambda_a S_a \quad (4.1)$$

where the operators $S_a[L]$ are symmetric under center symmetry and the couplings λ_a are to be determined. As stated above, for $SU(2)$ it is sufficient to work with only L_x and the \mathbb{Z}_2 center symmetric ($L_x \rightarrow -L_x$) effective action may be written as

$$S_{\text{eff}}[L_x] = \sum_x V[L_x^2] + \sum_{xy} L_x K_{xy}^{(2)} L_y + \sum_{xyuv} L_x L_y K_{xyuv}^{(4)} L_u L_v + \dots, \quad (4.2)$$

where the couplings λ_a are absorbed into the kernels $K^{(a)}$ and potential V . This representation is rather general and incorporates a multitude of operators composed of the compact dimensionless and unconstrained variable L . In respect of determining an effective action we will have to choose an appropriate subset of all possible operators to capture essential physics. On that score it turns out useful to follow [126] and view the effective action (4.1) as being embedded into a 'sigma-model' depending on \mathfrak{P}_x , $S_{\text{eff}}[L] \equiv S_{\text{eff}}[\mathfrak{P}_x]$. This yields an additional global $SU(2)$ symmetry,

$$\mathfrak{P}_x \rightarrow g \mathfrak{P}_x g^{-1}, \quad g \in SU(2), \quad (4.3)$$

which is a remnant of the underlying $SU(2)$ gauge invariance. The Haar measure $\mathcal{D}\mathfrak{P}_x$ has an even larger symmetry, namely $SU(2) \times SU(2)$, corresponding to the transformation law

$$\mathfrak{P}_x \rightarrow g \mathfrak{P}_x h, \quad g, h \in SU(2). \quad (4.4)$$

The invariance of the measure leads to novel Schwinger–Dyson identities which will be an important ingredient in our derivation of the effective couplings λ_a inherent in (4.1).

4.2. Haar Measure and Schwinger–Dyson Identities

The Polyakov loop variable on the lattice is given by a holonomy or parallel transport connecting the (periodic) boundaries in temporal direction,

$$\mathfrak{P}_{\mathbf{x}} \equiv \prod_{t=1}^{N_t} U_{t,\mathbf{x};0} , \quad (4.5)$$

where the U 's are the standard link variables on a lattice of size $N_t \times N_s^3$. The effective action for the Polyakov loops is obtained by inserting unity into the Yang–Mills partition function, such that (the trace of) (4.5) is imposed as a constraint,

$$\begin{aligned} Z_{\text{YM}} &= \int \mathcal{D}U \exp(-S_W[U]) \\ &= \int \mathcal{D}U \mathcal{D}\mathfrak{P} \delta\left(\text{tr } \mathfrak{P}_{\mathbf{x}} - \text{tr} \prod_{t=1}^{N_t} U_{t,\mathbf{x};0}\right) \exp(-S_W[U]) \\ &\equiv \int \mathcal{D}\mathfrak{P} \exp(-S_{\text{eff}}[\mathfrak{P}]) , \end{aligned} \quad (4.6)$$

with $\mathcal{D}U$ and $\mathcal{D}\mathfrak{P}$ the appropriate Haar measures (see below) and S_W the standard Wilson action. Of course, the integration over link variables U in the last step cannot be performed exactly. For this reason one has to resort to effective actions as given by (4.1) and (4.2), for instance [54, 55, 58]. Using inverse Monte–Carlo (IMC) techniques one should be able to determine a reasonable effective action from Yang–Mills configurations. In what follows, we will derive the Schwinger–Dyson equations for the action (4.1) corresponding to the symmetry (4.4). To do so we choose the parametrization

$$\mathfrak{P}_{\mathbf{x}} \equiv P_{\mathbf{x}}^0 \mathbb{1} + i\tau^a P_{\mathbf{x}}^a \equiv P_{\mathbf{x}}^\mu \sigma^\mu , \quad (4.7)$$

which is in $SU(2)$, $\mathfrak{P}_{\mathbf{x}}^\dagger \mathfrak{P}_{\mathbf{x}} = \mathbb{1}$, if the components $P_{\mathbf{x}}^\mu$ define a three–sphere S^3 according to

$$P_{\mathbf{x}}^\mu P_{\mathbf{x}}^\mu = (P_{\mathbf{x}}^0)^2 + P_{\mathbf{x}}^a P_{\mathbf{x}}^a = 1 . \quad (4.8)$$

We mention in passing that the points \mathbf{x} where the Polyakov loop is given by center elements, $\mathfrak{P}_{\mathbf{x}} = \pm \mathbb{1}$, correspond to the positions of monopoles in the Polyakov gauge [128, 129, 130], a particular realization of ‘t Hooft’s Abelian projections [131].

In terms of the coordinates (4.7), the traced Polyakov loop becomes $L_{\mathbf{x}} = P_{\mathbf{x}}^0$, while

the functional Haar measure can be written as

$$\mathcal{D}\mathfrak{P} \equiv \prod_{\mathbf{x}} d^4 P_{\mathbf{x}} \delta(P_{\mathbf{x}}^{\mu} P_{\mathbf{x}}^{\mu} - 1) . \quad (4.9)$$

Obviously, this is invariant under rotations $R \in SO(4)$ generated by the angular momenta

$$L_{\mathbf{x}}^{\mu\nu} \equiv -i \left(P_{\mathbf{x}}^{\mu} \frac{\partial}{\partial P_{\mathbf{x}}^{\nu}} - P_{\mathbf{x}}^{\nu} \frac{\partial}{\partial P_{\mathbf{x}}^{\mu}} \right) . \quad (4.10)$$

These can be split up into ‘electric’ and ‘magnetic’ components (or ‘boosts’ and $3d$ ‘rotations’),

$$iL_{\mathbf{x}}^{0a} \equiv P_{\mathbf{x}}^0 \frac{\partial}{\partial P_{\mathbf{x}}^a} - P_{\mathbf{x}}^a \frac{\partial}{\partial P_{\mathbf{x}}^0} \equiv iK_{\mathbf{x}}^a , \quad (4.11)$$

$$iL_{\mathbf{x}}^{ab} \equiv P_{\mathbf{x}}^a \frac{\partial}{\partial P_{\mathbf{x}}^b} - P_{\mathbf{x}}^b \frac{\partial}{\partial P_{\mathbf{x}}^a} \equiv i\epsilon^{abc} L_{\mathbf{x}}^c , \quad L_{\mathbf{x}}^a \equiv \frac{1}{2} \epsilon^{abc} L_{\mathbf{x}}^{bc} . \quad (4.12)$$

Summarizing, the $SO(4)$ generators $L_{\mathbf{x}}^{\mu\nu}$ rotate the four-vector $P_{\mathbf{x}}^{\mu}$, while the $SO(3)$ generators $L_{\mathbf{x}}^a$ rotate the three-vector $P_{\mathbf{x}}^a$. The self- and anti-selfdual combinations

$$M_{\mathbf{x}}^a \equiv \frac{1}{2} (L_{\mathbf{x}}^a - K_{\mathbf{x}}^a) , \quad (4.13)$$

$$N_{\mathbf{x}}^a \equiv \frac{1}{2} (L_{\mathbf{x}}^a + K_{\mathbf{x}}^a) , \quad (4.14)$$

generate left and right multiplication, respectively,

$$\mathfrak{P}_{\mathbf{x}} \rightarrow g \mathfrak{P}_{\mathbf{x}} , \quad \mathfrak{P}_{\mathbf{x}} \rightarrow \mathfrak{P}_{\mathbf{x}} h , \quad g, h \in SU(2) . \quad (4.15)$$

Global $SU(2)$ (gauge) transformations of the Polyakov loop as given by (4.3) are generated by $L_{\mathbf{x}}^{ab}$ (or $L_{\mathbf{x}}^a$) which do not differentiate with respect to the trace $P_{\mathbf{x}}^0$ and thus leave any functional of $P_{\mathbf{x}}^0 = L_{\mathbf{x}}$ invariant. Typical such invariants are

$$P_{\mathbf{x}}^0 , \quad P_{\mathbf{x}}^a P_{\mathbf{x}}^a \equiv 1 - P_{\mathbf{x}}^0 P_{\mathbf{x}}^0 , \dots . \quad (4.16)$$

The Schwinger–Dyson equations that follow from the $SO(4)$ invariance of the Haar measure (4.9) are given by

$$\int \mathcal{D}\mathfrak{P} L_{\mathbf{x}}^{\mu\nu} \{ F[\mathfrak{P}] \exp(-S_{\text{eff}}[\mathfrak{P}]) \} = 0 , \quad (4.17)$$

where $F[\mathfrak{P}]$ is an arbitrary functional of \mathfrak{P}_x . As the effective action depends on \mathfrak{P}_x solely through the $SU(2)$ invariant P_x^0 , $S_{\text{eff}}[\mathfrak{P}] \equiv S_{\text{eff}}[P^0]$, only the generators $L_x^{0a} \equiv K_x^a$ lead to nontrivial relations which can be written as

$$\langle K_x^a F[\mathfrak{P}] - F[\mathfrak{P}] K_x^a S_{\text{eff}}[\mathfrak{P}] \rangle = 0 , \quad (4.18)$$

using the expectation value notation,

$$\langle O \rangle \equiv Z^{-1} \int \mathcal{D}\mathfrak{P} O[\mathfrak{P}] \exp(-S_{\text{eff}}[\mathfrak{P}]) . \quad (4.19)$$

Because K_x^a transforms like a vector under gauge rotations, (4.18) in general will not be gauge invariant. However, we are still free to choose the functional $F[\mathfrak{P}]$ at our will. If we pick

$$F_x^a[\mathfrak{P}] \equiv P_x^a G[P^0] , \quad (4.20)$$

with an arbitrary functional $G[P^0]$, we have the action of K_x^a ,

$$K_x^a F_y^b = -i(\delta^{ab} \delta_{xy} P_x^0 G - P_x^a P_y^b G'_x) , \quad (4.21)$$

where we have denoted $G'_x \equiv \partial G / \partial P_x^0$. Plugging this into the Schwinger–Dyson equation (4.18), setting $\mathbf{x} = \mathbf{y}$ and taking the trace one finds,

$$\langle 3P_x^0 G - P_x^a P_x^a (G'_x - G S'_{\text{eff},x}) \rangle = 0 . \quad (4.22)$$

The same result is obtained using $F_x^a[\mathfrak{P}] \equiv K_x^a H[P^0]$ instead of (4.20) and identifying $H'_x \equiv -G_x$. Let us rewrite (4.22) as a functional integral,

$$\int \mathcal{D}\mathfrak{P} [3P_x^0 G - P_x^a P_x^a (G'_x - G S'_{\text{eff},x})] \exp(-S_{\text{eff}}) = 0 , \quad (4.23)$$

and parametrize \mathfrak{P}_x according to

$$\mathfrak{P}_x = \exp i\tau^a \theta_x^a = \mathbb{1} \cos \theta_x + i\tau^a n_x^a \sin \theta_x , \quad n_x^a \equiv P_x^a / (P_x^b P_x^b)^{1/2} . \quad (4.24)$$

Then, the traced Polyakov loop is $L_x \equiv \cos \theta_x$ while the Haar measure (4.9) becomes

$$\mathcal{D}\mathfrak{P} = \prod_x \sin^2 \theta_x \frac{d\theta_x d^2 n_x}{4\pi^2} . \quad (4.25)$$

As the functional integral (4.23) only depends on invariants we can integrate over the directions n (yielding an irrelevant volume factor) so that we are left with an integral involving only the *reduced* Haar measure,

$$\mathcal{D}L \equiv \prod_{\mathbf{x}} DL_{\mathbf{x}} \equiv \prod_{\mathbf{x}} d\theta_{\mathbf{x}} \sin^2 \theta_{\mathbf{x}} = \prod_{\mathbf{x}} d(\cos \theta_{\mathbf{x}}) \sin \theta_{\mathbf{x}} \equiv \prod_{\mathbf{x}} dL_{\mathbf{x}} \sqrt{1 - L_{\mathbf{x}}^2}, \quad (4.26)$$

namely,

$$\int \prod_{\mathbf{y}} d\theta_{\mathbf{y}} \sin^2 \theta_{\mathbf{y}} [3 \cos \theta_{\mathbf{x}} G - \sin^2 \theta_{\mathbf{x}} (G'_{\mathbf{x}} - GS'_{\text{eff},\mathbf{x}})] \exp(-S_{\text{eff}}) = 0. \quad (4.27)$$

A more compact notation is achieved in terms of total derivatives,

$$\begin{aligned} 0 &= \int \prod_{\mathbf{y} \neq \mathbf{x}} d\theta_{\mathbf{y}} \sin^2 \theta_{\mathbf{y}} \int d\theta_{\mathbf{x}} \frac{\delta}{\delta \theta_{\mathbf{x}}} \{ \sin^3 \theta_{\mathbf{x}} G \exp(-S_{\text{eff}}) \} \\ &= \int \prod_{\mathbf{y} \neq \mathbf{x}} d\theta_{\mathbf{y}} \sin^2 \theta_{\mathbf{y}} \int d(\cos \theta_{\mathbf{x}}) \frac{\delta}{\delta(\cos \theta_{\mathbf{x}})} \{ \sin^3 \theta_{\mathbf{x}} G \exp(-S_{\text{eff}}) \}. \end{aligned} \quad (4.28)$$

Note that the $\sin^3 \theta$ term ensures the absence of surface terms. As already stated in [LRD3], with (4.28) we have found the Schwinger–Dyson relations of the *reduced* theory involving only the invariant $L = \cos \theta$. We do not have a simple geometrical explanation for the invariance of the reduced Haar measure $\mathcal{D}L$ leading to (4.28). The $SO(4)$ symmetry of the measure $\mathcal{D}\mathfrak{P}$, however, is very natural.

In terms of the Polyakov loop $L_{\mathbf{x}}$, (4.27) is the expectation value

$$\langle 3L_{\mathbf{x}}G - (1 - L_{\mathbf{x}}^2)(G'_{\mathbf{x}} - GS'_{\text{eff},\mathbf{x}}) \rangle = 0. \quad (4.29)$$

Comparing with (4.22) we notice that it does not matter whether the expectation value is taken with the full or reduced Haar measure as long as $G = G[L]$. Plugging in the ansatz (4.1) the Schwinger-Dyson equations (4.29) become a linear system for the couplings λ_a ,

$$\sum_a \langle (1 - L_{\mathbf{x}}^2) GS'_{a,\mathbf{x}} \rangle \lambda_a = \langle (1 - L_{\mathbf{x}}^2) G'_{\mathbf{x}} - 3L_{\mathbf{x}}G \rangle. \quad (4.30)$$

To solve this unambiguously we need at least as many choices for the operator G as there are couplings λ_a . A particularly natural procedure which also turns out to

be rather stable numerically is to choose $G_y \equiv S'_{b,\mathbf{y}}$. This operator contains an odd number of $L_{\mathbf{x}}$'s so that the minimal set of Schwinger–Dyson equations relates only nontrivial expectation values. In matrix notation this is

$$\sum_a H_{ba} \lambda_a = u_b , \quad (4.31)$$

$$H_{ba} \equiv \langle (1 - L_{\mathbf{x}}^2) S'_{b,\mathbf{y}} S'_{a,\mathbf{x}} \rangle , \quad (4.32)$$

$$u_b \equiv \langle (1 - L_{\mathbf{x}}^2) S''_{b,\mathbf{y}\mathbf{x}} \rangle - 3 \langle L_{\mathbf{x}} S'_{b,\mathbf{y}} \rangle , \quad (4.33)$$

with a symmetric matrix H_{ba} and inhomogeneity u_b . At this stage, keeping \mathbf{x} and \mathbf{y} fixed, the problem of determining the couplings λ_a is well posed mathematically. Numerically, of course, it is better to use all the information one can get, for instance by scanning through all possible distances $x \equiv |\mathbf{x} - \mathbf{y}|$, $x < N_s/2$. The resulting overdetermined system is then solved by least-square methods. Another possibility is to add new equations to (4.31) by choosing some appropriate monomials or polynomials in $L_{\mathbf{x}}$ for the operator G . This philosophy will be extensively adopted in Section 4.6. Before that, however, we will try to proceed in a (semi-)analytical fashion.

4.3. Single-Site Distributions of Polyakov Loops

4.3.1. Definitions

From the effective action of Polyakov loops $S_{\text{eff}}[L]$ one can derive new probability densities by integrating over (part of) the loop variables L . Of course, this amounts to some kind of course-graining so that via the new densities one will only have access to gross properties of the effective action. Nevertheless, these densities, if chosen properly, exactly reproduce certain expectation values calculated within the full effective ensemble. Consider, for instance, the local moments,

$$\ell_p = \langle L_{\mathbf{x}}^p \rangle \equiv Z^{-1} \int \prod_{\mathbf{y}} DL_{\mathbf{y}} L_{\mathbf{x}}^p \exp(-S_{\text{eff}}[L]) , \quad (4.34)$$

where, as usual, the partition function Z is the integral over $\exp(-S_{\text{eff}})$. Splitting off the $L_{\mathbf{x}}$ -integration, (4.34) can be rewritten as

$$\ell_p = \langle L_{\mathbf{x}}^p \rangle \equiv \int_{-1}^1 DL_{\mathbf{x}} L_{\mathbf{x}}^p p_W[L_{\mathbf{x}}] \equiv \langle L_{\mathbf{x}}^p \rangle_W , \quad (4.35)$$

with the probability density p_W obtained via integrating over all $L_{\mathbf{y}} \neq L_{\mathbf{x}}$,

$$p_W[L_{\mathbf{x}}] \equiv Z^{-1} \int \prod_{\mathbf{y} \neq \mathbf{x}} DL_{\mathbf{y}} \exp(-S_{\text{eff}}[L_{\mathbf{x}}, L_{\mathbf{y}}]) \equiv Z^{-1} \exp(-W[L_{\mathbf{x}}]) . \quad (4.36)$$

Due to translational invariance, p_W (like ℓ_p) does not depend on the site \mathbf{x} . Thus, $DL p_W[L]$ is the probability to find the value of the Polyakov loop in the interval $[L, L + dL]$. The \mathbb{Z}_2 -symmetry of the effective action implies that the power p in (4.34) and (4.35) has to be even, $p = 2q$, at least for finite volume (no spontaneous symmetry breaking). Therefore, knowing p_W gives access to all local moments ℓ_{2q} and (by taking the logarithm) to all local cumulants c_{2q} as well. A particularly important quantity is the Binder cumulant [132, 133], defined as the quotient

$$b_4 \equiv \frac{c_4}{c_2^2} = \frac{\ell_4}{\ell_2^2} - 3 , \quad (4.37)$$

which measures the deviation from a Gaussian distribution. This will be analysed in some detail later on.

From the definition (4.36) it is obvious that p_W is blind against spatial correlations of Polyakov loops. In other words, one cannot calculate two-point functions like $G_{\mathbf{x}\mathbf{y}} \equiv \langle L_{\mathbf{x}} L_{\mathbf{y}} \rangle$. In principle, this can be remedied by a slight generalization of (4.36). To this end we define a new probability density depending on $L_{\mathbf{x}}$ and $L_{\mathbf{y}}$,

$$p_{W_2}[L_{\mathbf{x}}, L_{\mathbf{y}}] \equiv Z^{-1} \int \prod_{z \neq \mathbf{x}, \mathbf{y}} DL_z \exp(-S_{\text{eff}}[L]) \equiv Z^{-1} \exp(-W_2[L_{\mathbf{x}}, L_{\mathbf{y}}]) . \quad (4.38)$$

Then, one can calculate the following two-point correlators,

$$\langle L_{\mathbf{x}}^p L_{\mathbf{y}}^q \rangle = \int DL_{\mathbf{x}} DL_{\mathbf{y}} L_{\mathbf{x}}^p L_{\mathbf{y}}^q p_{W_2}[L_{\mathbf{x}}, L_{\mathbf{y}}] . \quad (4.39)$$

Obviously, p_W and p_{W_2} are related according to

$$p_W[L_{\mathbf{x}}] = \int DL_{\mathbf{y}} p_{W_2}[L_{\mathbf{x}}, L_{\mathbf{y}}] , \quad (4.40)$$

and one would have factorization, $p_{W_2}[L_{\mathbf{x}}, L_{\mathbf{y}}] = p_W[L_{\mathbf{x}}]p_W[L_{\mathbf{y}}]$, if there were no correlations.

4.3.2. Determination of Single-Site Distributions

At first glance, there seems to be not much of a gain by introducing densities like the single-site distribution p_W . Note, however, that $p_W[L]$ is much simpler than our original density $p_S \equiv Z^{-1} \exp(-S_{\text{eff}})$ which depends on N_s^3 variables rather than just one. In addition, p_W can rather easily be obtained from our Monte Carlo data. The results are fairly smooth histograms which are displayed in Fig. 4.1 (for details see App. D). The most important observation, however, is the finding that p_W is *flat* below T_c , that is, one has an *equipartition* for $L_{\mathbf{x}}$. Apparently, this is a remnant of the $SO(4)$ symmetry discussed in Section 4.2. Taking the (negative) logarithm of p_W we obtain the single-site potential $W[L]$ shown in Fig. 4.2.

We are thus led to employ the following ansatz for the potential W below (–) and above (+) the critical temperature T_c ,

$$W_-[L] = \text{const} , \quad (4.41)$$

$$W_+[L] = \text{const}' + \sum_k \frac{\kappa_{2k}}{2^k} L_{\mathbf{x}}^{2k} . \quad (4.42)$$

Demanding $\langle 1 \rangle = 1$ these imply for the density p_W ,

$$p_W^-[L] = \exp(-W_-)/Z_- = 2/\pi , \quad (4.43)$$

$$p_W^+[L] = \exp(-W_+[L])/Z_+ . \quad (4.44)$$

Things are particularly straightforward below T_c , so let us discuss this case first. The result (4.43) shows that, after normalization, the single-site distribution of Polyakov loops below T_c is known exactly. Furthermore, it is simple enough so that the asso-

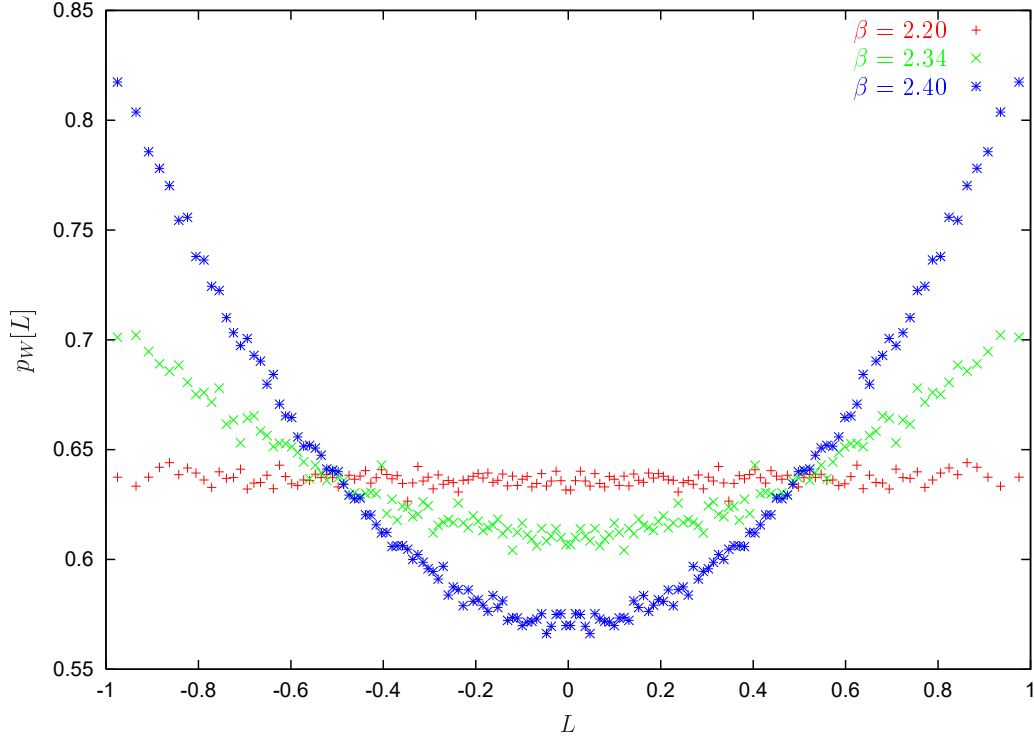


Figure 4.1.: Single-site density $p_W[L]$ for temperatures above ($\times, *$) and below T_c ($+$). For $T < T_c$ ($\beta < \beta_c \simeq 2.299$), the density is flat, $p_W = 2/\pi$. $N_s = 20$, $N_t = 4$.

ciated (local) moments can be determined analytically,

$$\ell_{2q}^- \equiv \langle L^{2q} \rangle_{W_-} = \frac{2}{\pi} \int_{-1}^1 dL \sqrt{1-L^2} L^{2q} = \frac{1}{\sqrt{\pi}} \frac{\Gamma(q+1/2)}{\Gamma(q+2)} = 2^{-q} \frac{(2q-1)!!}{(q+1)!}. \quad (4.45)$$

The generating function for these moments can also be calculated explicitly,

$$Z_-(t) \equiv \langle e^{tL} \rangle_{W_-} = \frac{2}{\pi} \int DL e^{tL} = \sum_{l \geq 0} \frac{\ell_{2l}^-}{(2l)!} t^{2l} = \frac{2}{t} I_1(t), \quad (4.46)$$

I_1 being the standard modified Bessel function. For the Binder cumulant (4.37) we thus find the result

$$b_4^- = \frac{\ell_4^-}{(\ell_2^-)^2} - 3 = \frac{1/8}{(1/4)^2} - 3 = -1. \quad (4.47)$$

We have checked that (4.45) and (4.47) hold numerically both for the histograms

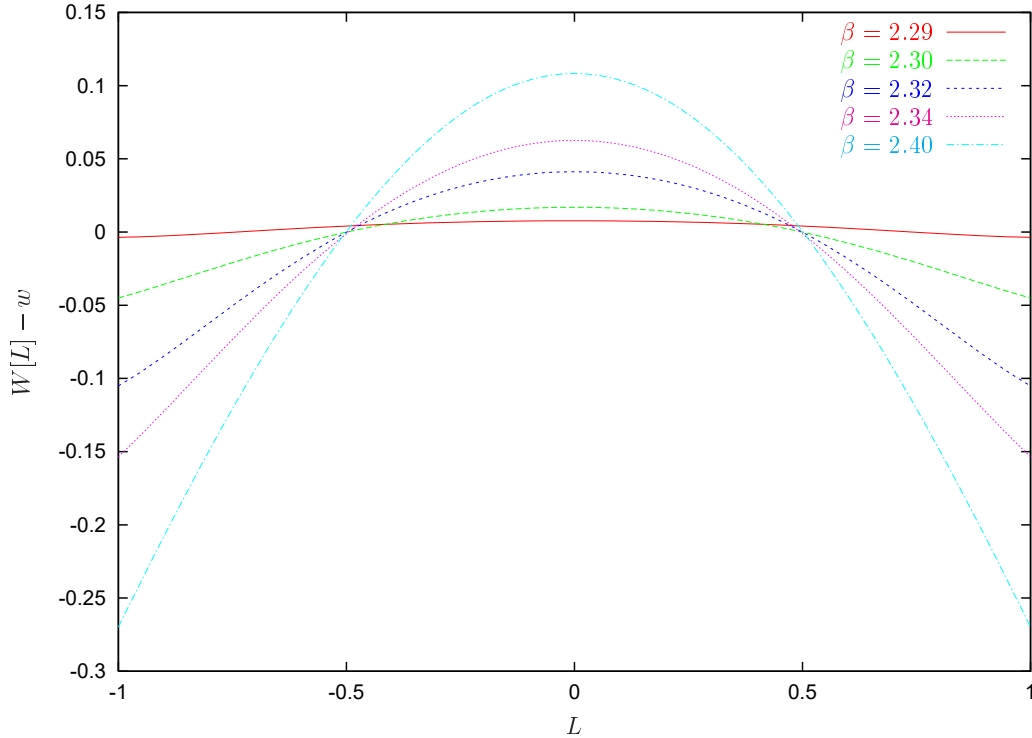


Figure 4.2.: The single-site potential $W[L]$ shifted by the offset w . For $T < T_c$ ($\beta < \beta_c \simeq 2.299$) it is constant. $N_s = 20$, $N_t = 4$.

p_W and the effective Yang–Mills probability density p_S . The results for the Binder cumulant are displayed in Fig. 4.3.

It may seem strange that we get a flat distribution p_W below T_c . However, this does not imply that the effective potential, which defines the distribution of the *mean field* \bar{L} , becomes trivial (see Section 4.5).

To proceed further, we have to specify our ansatz for the effective action beyond (4.1) and (4.2). Svetitsky and Yaffe have argued [54, 55, 58] that, close to the phase transition, the effective interactions should be short ranged so that S_{eff} is of Ginzburg–Landau type,

$$S_{\text{eff}} = \lambda_0 \sum_{\mathbf{x}, i} L_{\mathbf{x}} L_{\mathbf{x}+i} + \sum_{\mathbf{x}} \sum_{k>0} \frac{\lambda_{2k}}{2k} (L_{\mathbf{x}})^{2k} \equiv \lambda_0 S_0 + \lambda_2 S_2 + \dots \quad (4.48)$$

Note that the high-temperature character expansion mentioned in the introduction

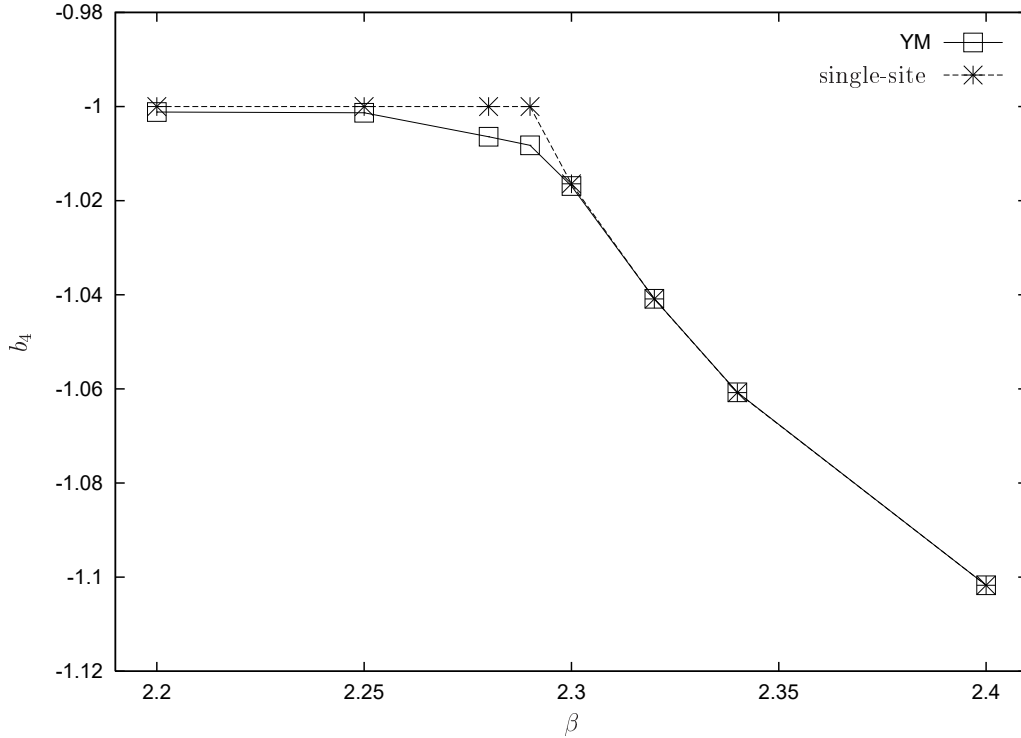


Figure 4.3.: The Binder cumulant b_4 as obtained from the simulated Yang–Mills configurations (\square) with $N_s = 20$, $N_t = 4$ compared to the single–site distribution p_W (*). Below $\beta_c \simeq 2.30$, the exact result (4.47) for p_W (i.e. $W = \text{const}$) has been used. The small deviation near the critical coupling is due to finite size effects. Above β_c , W has been fitted to a polynomial (see below).

yields additional hopping terms of the form $L_x^p L_y^q$ [124, 125, 134]. The relevance of these operators will be discussed in Section 4.6.

Let us investigate the consequences of the ansatz (4.48) for the single site distribution. Plugging (4.48) into the definition (4.36) and using (4.43) we obtain

$$\begin{aligned}
 e^{-W_-} &= \int_{-1}^1 \prod_{\mathbf{y} \neq \mathbf{x}} DL_{\mathbf{y}} \exp \left(-\lambda_0 \sum_{\mathbf{y}, i} L_{\mathbf{y}} L_{\mathbf{y}+i} - \sum_{\mathbf{y}, k > 0} \frac{\lambda_{2k}}{2k} L_{\mathbf{y}}^{2k} \right) \\
 &= \exp \left(-\sum_{k > 0} \frac{\lambda_{2k}}{2k} L_{\mathbf{x}}^{2k} \right) \int_{-1}^1 \prod_{\mathbf{y} \neq \mathbf{x}} DL_{\mathbf{y}} \exp \left(-\lambda_0 L_{\mathbf{x}} M_{\mathbf{x}} \right) \exp(-S'_{\text{eff}}[L_{\mathbf{y}}]), \quad (4.49)
 \end{aligned}$$

where, in the last line, we have introduced a new field representing the sum of nearest

neighbors of $L_{\mathbf{x}}$,

$$M_{\mathbf{x}} \equiv \frac{\partial S_0}{\partial L_{\mathbf{x}}} = \sum_i (L_{\mathbf{x}+i} + L_{\mathbf{x}-i}) . \quad (4.50)$$

Additionally, a modified action¹ S'_{eff} has been defined which is obtained from S_{eff} by setting $L_{\mathbf{x}} = 0$ at one particular single site \mathbf{x} ,

$$S'_{\text{eff}}[L] \equiv S_{\text{eff}}[L] \Big|_{L_{\mathbf{x}}=0} . \quad (4.51)$$

Now, the left-hand side of (4.49) is independent of $L_{\mathbf{x}}$. Thus we may put $L_{\mathbf{x}} = 0$ everywhere on the right-hand side yielding the identity,

$$e^{-W_-} = \int_{-1}^1 \prod_{\mathbf{y} \neq \mathbf{x}} DL_{\mathbf{y}} \exp(-S'_{\text{eff}}[L_{\mathbf{y}}]) \equiv Z' . \quad (4.52)$$

Accordingly, e^{-W_-} is the partition function associated with action S'_{eff} . We can go one step further and expand the exponential containing the nearest-neighbor field $M_{\mathbf{x}}$ on the right-hand side of (4.49). This is actually a hopping-parameter expansion in λ_0 which, upon using (4.52), implies

$$1 = \exp \left(- \sum_{k>0} \frac{\lambda_{2k}}{2k} L_{\mathbf{x}}^{2k} \right) \sum_{n \geq 0} \frac{(-\lambda_0)^n}{n!} L_{\mathbf{x}}^n \langle M_{\mathbf{x}}^n \rangle' . \quad (4.53)$$

Here, we have defined modified expectation values associated with S'_{eff} and Z' ,

$$\langle O[L] \rangle' \equiv \int \prod_{\mathbf{y} \neq \mathbf{x}} DL_{\mathbf{y}} O[L] \exp(-S'_{\text{eff}}[L]) / Z' . \quad (4.54)$$

The \mathbb{Z}_2 -symmetry of the effective action requires n to be even, $n = 2m$. Denoting $\langle M_{\mathbf{x}}^{2m} \rangle' \equiv \mu_{2m}$, we finally have

$$\sum_{m=0}^{\infty} \frac{\lambda_0^{2m} \mu_{2m}}{(2m)!} L_{\mathbf{x}}^{2m} = \exp \left(\sum_{k=1}^{\infty} \frac{\lambda_{2k}}{2k} L_{\mathbf{x}}^{2k} \right) . \quad (4.55)$$

To lowest order in $L_{\mathbf{x}}$ ($m = 0$) this consistently reproduces the normalization (4.52),

¹In contrast to the previous section the prime does not refer to any derivative here and from now on.

$\langle 1 \rangle' = 1 = e^{-W_-} / Z'$. A general interpretation can be given as follows. To have equipartition requires a delicate balance between the hopping term (λ_0) and the ‘potential’ terms (λ_{2k}). Setting $\lambda_0 = 0$ (so that the effective action leads to a product measure) implies that all λ_{2k} have to vanish and *vice versa*: $\lambda_{2k} = 0$ implies $\lambda_0 = 0$.

To further evaluate the identity (4.55) we note that it can be viewed as a particular example of a linked–cluster or Mayer expansion [135, 136, 137] expressing the moments $\lambda_0^{2m} \mu_{2m}$ in terms of the cumulants

$$\lambda'_{2k} \equiv (2k - 1)! \lambda_{2k} . \quad (4.56)$$

The relation between moments and cumulants can actually be solved for arbitrary m (see e.g. [138]),

$$\lambda_0^{2m} \mu_{2m} = \sum_{n=1}^m \frac{1}{n!} \sum_{\substack{k_1, \dots, k_n=1 \\ k_1 + \dots + k_n = m}} \frac{(2m)!}{(2k_1)! \dots (2k_n)!} \prod_{i=1}^n \lambda'_{2k_i} . \quad (4.57)$$

This somewhat clumsy formula yields for the first few orders

$$\lambda_0^2 \mu_2 = \lambda'_2 , \quad (4.58)$$

$$\lambda_0^4 \mu_4 = \lambda'_4 + 3 \lambda_2'^2 , \quad (4.59)$$

$$\lambda_0^6 \mu_6 = \lambda'_6 + 15 \lambda_2' \lambda_4' + 15 \lambda_2'^3 , \quad (4.60)$$

$$\lambda_0^8 \mu_8 = \lambda'_8 + 28 \lambda_2' \lambda_6' + 35 \lambda_4'^2 + 210 \lambda_4' \lambda_2'^2 + 105 \lambda_2'^4 . \quad (4.61)$$

It is quite obvious that by inverting (4.57) we can express the couplings λ_{2k} (or cumulants λ'_{2k}) in terms of the moments μ_{2m} . Alternatively, one may take the logarithm of (4.55) and compare coefficients. In any case, the first few cumulants are

$$\lambda'_2 = \lambda_0^2 \mu_2 , \quad (4.62)$$

$$\lambda'_4 = \lambda_0^4 (\mu_4 - 3 \mu_2^2) , \quad (4.63)$$

$$\lambda'_6 = \lambda_0^6 (\mu_6 - 15 \mu_4 \mu_2 + 30 \mu_2^3) , \quad (4.64)$$

$$\lambda'_8 = \lambda_0^8 (\mu_8 - 28 \mu_6 \mu_2 + 420 \mu_4 \mu_2^2 - 630 \mu_2^4 - 35 \mu_4^2) . \quad (4.65)$$

These identities almost solve our problem of determining S_{eff} as they express the unknown couplings λ_{2k} in terms of λ_0 (unknown as yet) and the modified expectation

values μ_{2m} .

Things become simple if one allows for only a finite number (say K) of couplings λ_{2k} . Then, there is only a finite number of independent moments μ_{2k} , $k = 1, \dots, K$. This is quite obvious from e.g. (4.65). Setting $\lambda_8 = 0 = \lambda'_8$ determines the moment μ_8 and all higher ones in terms of μ_2 , μ_4 and μ_6 .

For $K = 1$, (4.55) yields the general expression

$$\mu_{2m} = (2m - 1)!! \left(\frac{\lambda_2}{\lambda_0^2} \right)^m \equiv (2m - 1)!! \mu_2^m, \quad m = 1, 2, \dots \quad (4.66)$$

We thus have found factorization: all higher moments μ_{2m} , $m > 1$ can be expressed in terms of the lowest one, $\mu_2 \equiv \lambda_2/\lambda_0^2$. Of course, this is consistent with S_{eff} being quadratic in $L_{\mathbf{x}}$ (vanishing of quartic and higher cumulants λ'_{2k}).

For $K = 2$, we have three couplings, λ_0 , λ_2 and λ_4 . In this case, (4.55) implies the following generalization of (4.66),

$$\mu_{2m} = (2m - 1)!! \mu_2^m \sum_{k=0}^{[m/2]} \binom{m}{2k} (2k - 1)!! \left(\frac{\mu_4}{3\mu_2^2} - 1 \right)^k, \quad (4.67)$$

which shows that all moments μ_{2m} can be expressed in terms of μ_2 and μ_4 . The first two factors in the sum count the number of ways in which one can form k pairs out of m elements. The term raised to power k is actually (one third of) the Binder cumulant associated with the moments μ_{2m} . If it were zero we would get back at (4.66).

Clearly, in order to determine the couplings λ_{2k} one does not want to calculate the moments μ_{2k} by performing a new and costly Monte Carlo simulation with the action S'_{eff} , setting $L_{\mathbf{x}} = 0$ at a particular site \mathbf{x} . One expects, however, that, for large lattices and high dimensionality, one will have the approximate identity

$$\langle M^{2m} \rangle' \simeq \langle M^{2m} \rangle, \quad m > 0, \quad (4.68)$$

where the latter expectation is taken in the full Yang–Mills ensemble. This can be appreciated as follows. The particular site \mathbf{x} is just one among several thousand others in the lattice. Even locally there are $2d$ nearest neighbors of \mathbf{x} , i.e. 6 in case of $d = 3$. These are in turn affected by 18 other nearest neighbors different from \mathbf{x} .

Λ	0	1	10	100	1000	10000
$\langle M_{\mathbf{x}}^2 \rangle_{\Lambda}$	1.951	1.947	1.962	1.954	1.939	1.961
	18.79	18.87	18.83	18.78	18.80	18.78

Table 4.1.: The expectation value $\langle M_{\mathbf{x}}^2 \rangle_{\Lambda}$ as a function of the parameter Λ suppressing the single-site variable $L_{\mathbf{x}}$. Input parameters are $N_s = 16$, $\lambda_0 = -0.3$ (symmetric phase, upper line) and $\lambda_0 = -1$ (broken phase, lower line).

Furthermore L is anyhow restricted to $[-1, 1]$ so that the effect of changing one single $L_{\mathbf{x}}$ to zero is probably smaller than the statistical error. For our numerical evaluation we have tested assumption (4.68) as follows. Define the expectation values

$$\langle M_{\mathbf{x}}^{2m} \rangle_{\Lambda} \equiv Z_{\Lambda}^{-1} \int \prod_{\mathbf{y}} DL_{\mathbf{y}} M_{\mathbf{x}}^{2m} \exp(-S_{\text{eff}}[L_{\mathbf{y}}] - \Lambda L_{\mathbf{x}}^2), \quad (4.69)$$

so that one has

$$\langle M_{\mathbf{x}}^{2m} \rangle = \langle M_{\mathbf{x}}^{2m} \rangle_0, \quad \langle M_{\mathbf{x}}^{2m} \rangle' = \langle M_{\mathbf{x}}^{2m} \rangle_{\infty}. \quad (4.70)$$

If (4.68) is to hold then $\langle M_{\mathbf{x}}^{2m} \rangle_{\Lambda}$ must be approximately independent of Λ . We have checked this by simulating the leading-order action,

$$S_{\Lambda} \equiv \frac{\lambda_0}{2} \sum_{\langle \mathbf{x}\mathbf{y} \rangle} L_{\mathbf{x}} L_{\mathbf{y}} + \Lambda L_{\mathbf{x}}^2 \equiv \lambda_0 \sum_{\mathbf{x}, i} L_{\mathbf{x}} L_{\mathbf{x}+i} + \Lambda L_{\mathbf{x}}^2, \quad (4.71)$$

for different values of Λ on a lattice of size 16^3 with $\lambda_0 = -0.3$ (symmetric phase). The calculated expectation values $\langle M_{\mathbf{x}}^2 \rangle_{\Lambda}$ displayed in Tab. 4.1 show that $\langle M_{\mathbf{x}}^2 \rangle_{\Lambda}$ is indeed independent of Λ to an accuracy of about 0.5 %.

For $T > T_c$, we use the ansatz (4.42). This implies that formulae (4.53–4.65) still hold, however, with λ_{2k} now replaced by $\lambda_{2k} - \kappa_{2k}$. We have checked that the identification (4.68) also holds in the broken phase (choosing $\lambda_0 = -1$, see Tab. 4.1).

The couplings κ_{2k} can be obtained by fitting $W_+[L]$ (see Fig. 4.2) according to (4.42). The fit values are displayed in Tab. 4.2. Summarizing we note that we have good analytical and numerical control of the single-site distribution p_W or, equivalently, the histograms displayed in Fig. 4.1. Below T_c , the histogram is flat, $p_W^- = \text{const}$, above T_c , $W^+ \sim \log p_W$ is a simple polynomial in L^2 with coefficients given in Tab. 4.2.

β	$\kappa_2/2$	$\kappa_4/4$	$\kappa_2/2$	$\kappa_4/4$	$\kappa_6/6$
2.40	-0.4468	0.0703	-0.4531	0.0901	-0.0152
2.34	-0.2712	0.0526	-0.2626	0.0249	0.0216
2.32	-0.1772	0.0261	-0.1612	-0.0259	0.0408
2.30	-0.0717	0.0120	-0.0666	-0.0087	0.0133

Table 4.2.: Two- and three-parameter fit to $W_+[L]$.

β	2.20	2.25	2.28	2.29	2.30	2.32	2.34	2.40
μ_2	1.938	2.086	2.242	2.327	2.466	2.946	3.336	4.173
μ_4	10.16	11.55	13.07	13.89	15.27	20.16	24.22	33.60
μ_6	80.88	96.06	113.0	121.7	137.6	194.1	241.5	357.6
μ_8	8293	1019	1237	1341	1551	2297	2922	4536

Table 4.3.: The moments μ_{2m} for different values of the Wilson coupling β ($N_s = 20$, $N_t = 4$).

4.4. Determination of the Effective Action

The calculation of the couplings λ_{2k} , $k \geq 0$, in the effective action proceeds in three steps. First we determine the moments μ_{2m} from the Polyakov loop ensemble using the approximate identity (4.68). Second, from (4.62–4.65), we obtain the couplings $\lambda_{2k} = \lambda'_{2k}/(2k-1)!$, $k > 0$, in terms of the moments μ_{2k} and λ_0 . Third, we determine λ_0 .

The first step consists of straightforward numerics based on our Wilson ensembles obtained for several values of β near β_c . The results for the μ_{2m} are displayed in Tab. 4.3. With the moments μ_{2m} at hand we find the couplings

$$\lambda_{2k} = \lambda_0^{2k} \alpha_{2k}, \quad k > 0, \quad (4.72)$$

where the α_{2k} can be expressed in terms of the μ_{2k} according to (4.62–4.65). The final step consists in the determination of λ_0 . To this end we make use of the Schwinger–

Dyson relations (4.30) choosing the operators $G \equiv L_{\mathbf{x}}^{2l-1}$ which results in

$$\langle (1 - L_{\mathbf{x}}^2) M_{\mathbf{x}} L_{\mathbf{x}}^{2l-1} \rangle \lambda_0 + \sum_{k>0} \langle (1 - L_{\mathbf{x}}^2) L_{\mathbf{x}}^{2k+2l-2} \rangle \lambda_{2k} = (2l - 1) \langle (1 - L_{\mathbf{x}}^2) L_{\mathbf{x}}^{2l-2} \rangle - 3 \langle L_{\mathbf{x}}^{2l} \rangle. \quad (4.73)$$

We begin with $T < T_c$ where the single-site distribution is known exactly. In this case the right-hand side of (4.73) vanishes. This can either be inferred from the exact result (4.45) or by noting that the term in question is a total derivative,

$$(2l - 1) \langle (1 - L_{\mathbf{x}}^2) L_{\mathbf{x}}^{2l-2} \rangle - 3 \langle L_{\mathbf{x}}^{2l} \rangle = -\frac{2}{\pi} \int_{-1}^1 dL \frac{\partial}{\partial L} [(1 - L^2)^{3/2} L^{2l-1}] = 0. \quad (4.74)$$

Upon inserting (4.72), all λ_{2k} in (4.73) can be reexpressed in terms of λ_0 and α_{2k} . Dividing the resulting equation by λ_0 (assumed to be nonzero), the Schwinger–Dyson equation (4.30) becomes nonlinear of degree $2k - 1$ in λ_0 ,

$$\sum_{k \geq 1} \lambda_0^{2k-1} \frac{\alpha_{2k}}{2^{k+l+1}} \frac{(2k + 2l - 3)!!}{(k + l)!} = \langle (1 - L_{\mathbf{x}}^2) M_{\mathbf{x}} L_{\mathbf{x}}^{2l-1} \rangle. \quad (4.75)$$

With the coefficients α and all (nonlocal) expectation values determined numerically this finally yields the coupling λ_0 . As there are $2k - 1$ solutions we take the one which is approximately independent of the number K of couplings λ_{2k} . The resulting values of all couplings (for $K = 2$ and $K = 3$) are displayed in Tables 4.4 and 4.5.

With the effective couplings determined we are in the position to check our results by simulating the effective action. For both $\beta = 2.20$ and $\beta = 2.40$ we have produced 10000 configurations distributed according to S_{eff} using the couplings from Tab. 4.5 ($K = 3$, $N_s = 20$, $N_t = 4$). In Figs 4.4 and 4.5 we compare the single-site distributions obtained from the effective theory with those of Yang–Mills. The outcome is quite satisfactory. In particular, one notes that the inclusion of a L^6 -term ($K = 3$) still improves the matching of the histograms compared to the case $K = 2$. A further important check is provided by reproducing the input couplings of Tab. 4.5 via our IMC procedure. The results displayed in Tab. 4.6 show quite convincingly that the method works. If we allow for additional operators in the numerics (which are not present in the effective action) the numbers of Tab. 4.6 remain unchanged while the couplings of the new operators are consistently of order 10^{-5} , i.e. compatible with zero.

β	2.20	2.25	2.28	2.29	2.30	2.32	2.34	2.40
λ_0	-0.438	-0.473	-0.500	-0.509	-0.630	-0.685	-0.697	-0.725
$\lambda_2/2$	0.186	0.233	0.280	0.301	0.453	0.603	0.675	0.873
$\lambda_4/4$	-0.002	-0.003	-0.005	-0.007	-0.019	-0.053	-0.088	-0.212

Table 4.4.: Numerical values for the couplings λ_0 and $\lambda_{2k}/2k$, $k \leq K = 2$. The critical Wilson coupling is $\beta_c = 2.299$ ($N_s = 20$, $N_t = 4$).

β	2.20	2.25	2.28	2.29	2.30	2.32	2.34	2.40
λ_0	-0.438	-0.476	-0.507	-0.510	-0.628	-0.690	-0.705	-0.760
$\lambda_2/2$	0.186	0.237	0.288	0.303	0.453	0.621	0.698	0.979
$\lambda_4/4$	-0.002	-0.003	-0.006	-0.007	-0.020	-0.057	-0.093	-0.256
$\lambda_6/6$	0.000039	0.00011	0.00027	0.00037	0.0020	0.0106	0.0244	0.116

Table 4.5.: Numerical values for the couplings λ_0 and $\lambda_{2k}/2k$, $k \leq K = 3$. The critical Wilson coupling is $\beta_c = 2.299$ ($N_s = 20$, $N_t = 4$).

β		λ_0	λ_2	λ_4	λ_6
2.20	input	-0.43803	0.37182	-0.00681	0.00024
2.20	output	-0.43824	0.37351	-0.00621	0.00020
2.40	input	-0.76000	1.9572	-1.0216	0.69761
2.40	output	-0.76027	1.9605	-1.0222	0.69039

Table 4.6.: Comparison of couplings used as input of simulation with couplings obtained as output of inverse Monte Carlo applied to the effective action.

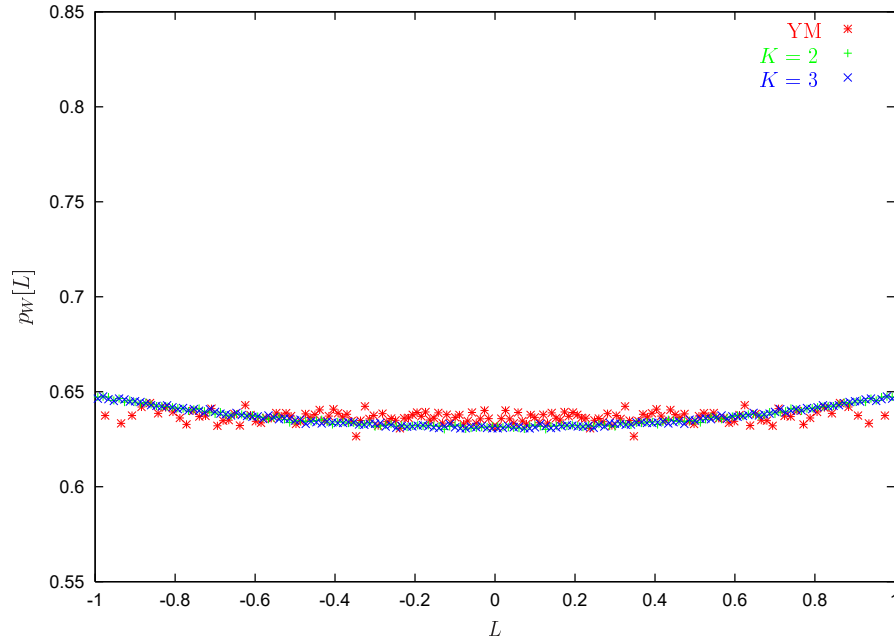


Figure 4.4.: Comparison of single-site histograms based on simulating Yang–Mills (*) vs. the effective action for $T < T_c$. The curves for two and three couplings λ_{2k} , i.e. $K = 2$ (+) and $K = 3$ (x), respectively, fall on top of each other. Input: $\beta = 2.20$, $N_s = 20$, $N_t = 4$.

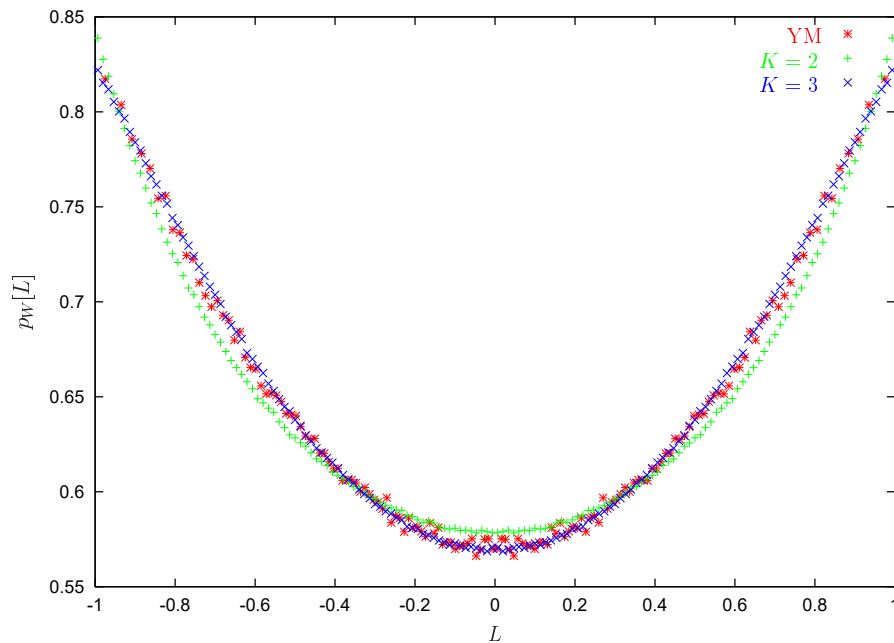


Figure 4.5.: Same as in Fig. 4.4 for $T > T_c$; $\beta = 2.40$, $N_s = 20$, $N_t = 4$.

4.5. The Constraint Effective Potential

With the effective action being found, one could go on and calculate the constraint effective potential [139] which defines the distribution of the constant *mean* field,

$$\bar{L} \equiv \frac{1}{\Omega} \sum_{\mathbf{x}} L_{\mathbf{x}} , \quad \Omega = N_s^3 . \quad (4.76)$$

In perturbation theory, the effective potential has been evaluated long ago [140, 141]. It describes a ‘gas’ of gluons at high temperature, i.e. deep in the deconfined phase. Recent models for the effective potential which also describe the confined phase are based on the eigenvalues of the Polyakov loop $\mathfrak{P}_{\mathbf{x}}$ [127] and not just their sum $L_{\mathbf{x}}$. As stated in the introduction, this difference becomes obsolete for $SU(2)$.

It thus seems of interest to investigate the effective potential on the lattice. This apparently requires further Monte–Carlo simulations of the effective action $S_{\text{eff}}[L]$ with the mean field \bar{L} held fixed, following the approach adopted in [139, 142]. It turns out, however, that these additional efforts can be avoided by making use of some statistical properties of the single–site distribution p_W discussed in Section 4.3.2.

The constraint effective potential V is defined in terms of the probability density of the mean field (4.76),

$$p_V[\bar{L}] \equiv Z_V^{-1} e^{-\Omega V[\bar{L}]} \equiv Z^{-1} \int \mathcal{D}L \delta\left(\bar{L} - \Omega^{-1} \sum_{\mathbf{x}} L_{\mathbf{x}}\right) \exp(-S_{\text{eff}}[L]) , \quad (4.77)$$

with the normalization Z_V given by the partition function

$$Z_V \equiv Z_V(0) \equiv \int_{-1}^1 d\bar{L} e^{-\Omega V[\bar{L}]} . \quad (4.78)$$

In what follows, we will try to obtain the mean–field distribution p_V from the single–site distribution p_W . We note, first of all, that, due to translational invariance, the first moments coincide,

$$\langle \bar{L} \rangle_V \equiv \int d\bar{L} \bar{L} p_V[\bar{L}] = \Omega^{-1} \sum_{\mathbf{x}} Z^{-1} \int \prod_{\mathbf{y}} DL_{\mathbf{y}} L_{\mathbf{x}} e^{-S_{\text{eff}}[L]} \equiv \langle L \rangle_W \equiv \langle L \rangle . \quad (4.79)$$

The higher moments, on the other hand, are different,

$$\langle L^p \rangle_W = \int \prod_{\mathbf{y}} DL_{\mathbf{y}} L_{\mathbf{x}}^p e^{-S_{\text{eff}}[L]} = \langle L^p \rangle \quad (4.80)$$

$$\langle \bar{L}^p \rangle_V = \Omega^{-p} \sum_{\mathbf{x}_1, \dots, \mathbf{x}_p} \langle L_{\mathbf{x}_1} \dots L_{\mathbf{x}_p} \rangle \equiv \chi^{(p)}. \quad (4.81)$$

For the mean-field distribution we thus get generalized susceptibilities $\chi^{(p)}$, while p_W yields expectation values of arbitrary powers of L at a single spatial site, taken in the ensemble of Polyakov loops extracted from Yang-Mills. This has been discussed at length in Section 4.3.2.

To obtain a connection between arbitrary moments we assume that the generating functions associated with p_V and p_W are related according to

$$Z_V(t) \equiv \langle \exp t\bar{L} \rangle_V = \langle \prod_{\mathbf{x}} \exp(tL_{\mathbf{x}}/\Omega) \rangle_V \stackrel{!}{\simeq} \prod_{\mathbf{x}} \langle \exp(tL/\Omega) \rangle_W \equiv [Z_W(t/\Omega)]^\Omega. \quad (4.82)$$

Here, we have made the assumption that only a small fraction of the random variables $\{L_{\mathbf{x}} : \mathbf{x} \in \Omega\}$ are statistically dependent. This is justified for large volumes and short-range correlations. According to the Law of Large Numbers we expect the collective random variable $\bar{L} = \sum_{\mathbf{x}} L_{\mathbf{x}}/\Omega$ to have a Gaussian distribution if the $L_{\mathbf{x}}$ are randomly distributed². Let us check to which extent this is realized.

Below T_c , $Z_W \equiv Z_-$ is exactly known from (4.46) so that

$$Z_V(t) \simeq \left[\frac{2\Omega}{t} I_1(t/\Omega) \right]^\Omega = \sum_k \frac{t^{2k}}{(2k)!} \langle \bar{L}^{2k} \rangle, \quad Z_V(0) = 1. \quad (4.83)$$

Thus, by expanding the Bessel function (to power Ω) we know all moments or susceptibilities of p_V . Explicitly, one finds

$$\langle \bar{L}^2 \rangle_V = \frac{1}{4\Omega}, \quad (4.84)$$

$$\langle \bar{L}^4 \rangle_V = \frac{1}{8\Omega^3} + \frac{3(\Omega-1)}{16\Omega^3}, \quad (4.85)$$

$$\langle \bar{L}^6 \rangle_V = \frac{5}{64\Omega^5} + \frac{15(\Omega-1)}{32\Omega^5} + \frac{15(\Omega-1)(\Omega-2)}{64\Omega^5}. \quad (4.86)$$

²Note, however, that with \bar{L} being a compact variable, we cannot, strictly speaking, expect a Gaussian.

In the large-volume limit we get

$$\langle \bar{L}^{2k} \rangle_V = \frac{(2k-1)!!}{(4\Omega)^k} = (2k-1)!! \langle \bar{L}^2 \rangle_V^k, \quad (4.87)$$

an identity typical for a Gaussian distribution. As a cross check, we calculate the Binder cumulant associated with p_V . From (4.84) and (4.85) we have

$$b_{4,V} \equiv \frac{\langle \bar{L}^4 \rangle_V}{\langle \bar{L}^2 \rangle_V^2} - 3 = -\frac{1}{\Omega}, \quad (4.88)$$

which obviously vanishes in the infinite-volume limit in accordance with (4.87). Summing up the moments (4.87), we obtain the large-volume partition function

$$Z_V(t) \simeq \exp(t^2/8\Omega), \quad (4.89)$$

which turns out to be Gaussian in t . Substituting $t = iu$, we have

$$Z_V(iu) = \int d\bar{L} \exp(-\Omega V[\bar{L}] + iu\bar{L}) \simeq \exp(-u^2/8\Omega). \quad (4.90)$$

To extract the mean-field distribution $p_V = \exp(-\Omega V)$ we take the Fourier transform with respect to u and find

$$p_V[\bar{L}] \simeq \sqrt{2\Omega/\pi} \exp(-2\Omega\bar{L}^2), \quad (4.91)$$

which is a perfect Gaussian distribution with variance

$$\sigma^2 \equiv 1/4\Omega = \langle \bar{L}^2 \rangle_V. \quad (4.92)$$

The fact that \bar{L} is compact does not really matter as in the large-volume limit assumed, the Gaussian is sharply localized at $\bar{L} = 0$. This is indeed seen from Fig. 4.6 which shows that a Gaussian fit to the distribution of \bar{L} ,

$$p_{V,\text{fit}}[\bar{L}] = \frac{1}{\sqrt{2\pi}\sigma} \exp(-\bar{L}^2/2\sigma^2), \quad (4.93)$$

works perfectly well.

This is corroborated by comparing the fit values for σ with the expectation values

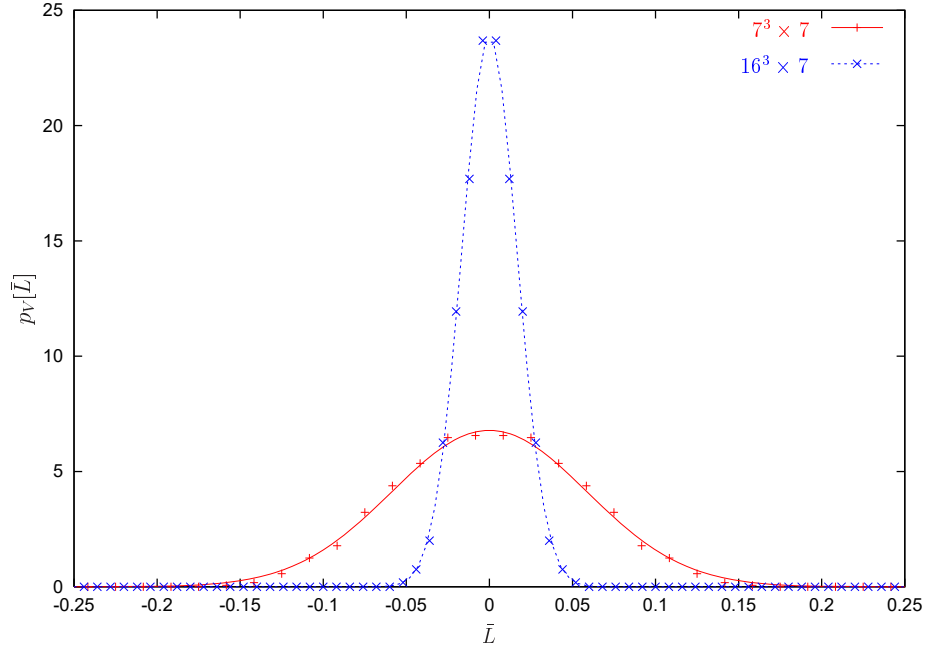


Figure 4.6.: Gaussian fits to the distribution $p_V[\bar{L}]$ obtained from simulating Yang–Mills on lattices of size $16^3 \times 7$ and $7^3 \times 7$. The values for the temporal extension N_t correspond to the symmetric phase.

calculated from Yang–Mills as displayed in Tab. 4.7 for different volumes and bin sizes.

The agreement between the fitted width and the expectation value $\langle \bar{L}^2 \rangle_V^{1/2}$ is quite impressive, in particular for large volumes, as expected. Due to the approximations made, however, we do not reproduce the absolute numbers given by (4.92). If we define

$$\gamma \equiv \frac{\sigma^2(\Omega_1)}{\sigma^2(\Omega_2)} = \frac{\Omega_2}{\Omega_1}, \quad (4.94)$$

we get for $\Omega_1 = 7^3$ and $\Omega_2 = 16^3$ the numerical value $\gamma = (16/7)^3 = 11.94$ while the results of Tab. 4.7 yield

$$\gamma = 11.1 \pm 0.4, \quad N_t = 6, \quad (4.95)$$

$$\gamma = 11.5 \pm 0.9, \quad N_t = 7, \quad (4.96)$$

where the error has been estimated by varying the bin sizes. Thus, at least for sufficiently low temperature (large N_t) we obtain the correct scaling of the width

$\Omega \times N_t$	config.s/bin	σ	$\langle \bar{L}^2 \rangle_V^{1/2}$
$7^3 \times 6$	120	0.0837	0.0773
$7^3 \times 6$	80	0.0845	0.0773
$7^3 \times 7$	120	0.0582	0.0549
$7^3 \times 7$	80	0.0588	0.0549
$16^3 \times 6$	250	0.0249	0.0252
$16^3 \times 7$	150	0.0167	0.0164
$16^3 \times 7$	250	0.0167	0.0164

Table 4.7.: Width σ of the Gaussian fit (4.93) compared to the expectation value $\langle \bar{L}^2 \rangle_V^{1/2}$ calculated from the $SU(2)$ Monte Carlo ensemble. The values for the temporal extension N_t correspond to the symmetric phase.

with the volume.

Things are different in the broken phase, $T > T_c$, where the single-site distribution is not flat. Thus, we cannot derive the generating functional and the distribution of the mean-field \bar{L} in an analogous way. However, in contrast to the symmetric phase where the maximum of $p_V[\bar{L}]$ is located at $\bar{L} = 0$, the broken phase apparently has to show two degenerate maxima at $\bar{L} = \pm b \neq 0$. It turns out that, as shown in Figs 4.7 and 4.8, a fit to a double-Gaussian

$$p_{V,\text{fit}}[\bar{L}] = \frac{1}{2\sqrt{2\pi}\sigma'} \left[\exp(-(\bar{L} - b)^2/2\sigma'^2) + \exp(-(\bar{L} + b)^2/2\sigma'^2) \right] \quad (4.97)$$

does the job in this case. σ' denotes the width of each of the two peaks, and it should be clear that a relation of the form (4.92) relating the width to the mean value $\langle \bar{L}^2 \rangle_V^{1/2}$ does not hold. By increasing the (spatial) volume or by decreasing the temperature (moving deeper into the broken phase) the curves become more and more sharply peaked in agreement with the scaling behavior (4.94). In the large volume limit one can therefore expect the value of $\langle \bar{L}^2 \rangle_V^{1/2}$ being close to b . This is indeed true as shown in Tab. 4.8. Furthermore, a comparison of Fig. 4.7 and Fig. 4.8 shows how tunneling between the degenerate minima of the potential (which are maxima of the distribution) gets suppressed with increasing spatial volume. The green curve ($N_t = 4$) is close to the critical temperature in the broken phase. However, for volume

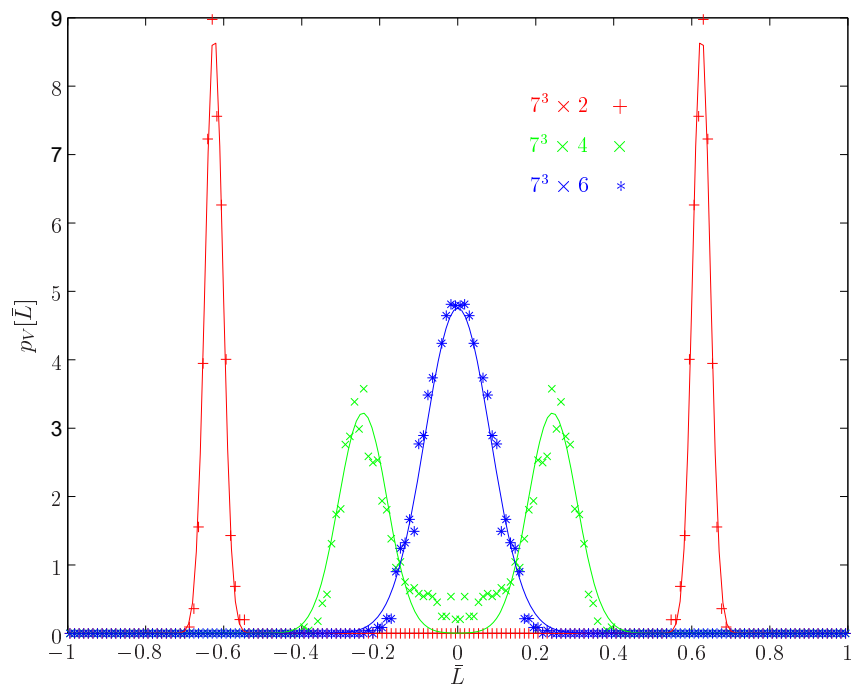


Figure 4.7.: Gaussian and double-Gaussian fits to the distribution $p_V[\bar{L}]$ obtained from simulating Yang–Mills on lattices of size $7^3 \times N_t$. $N_t = 6$ corresponds to the symmetric phase and $N_t = 2, 4$ to the broken phase.

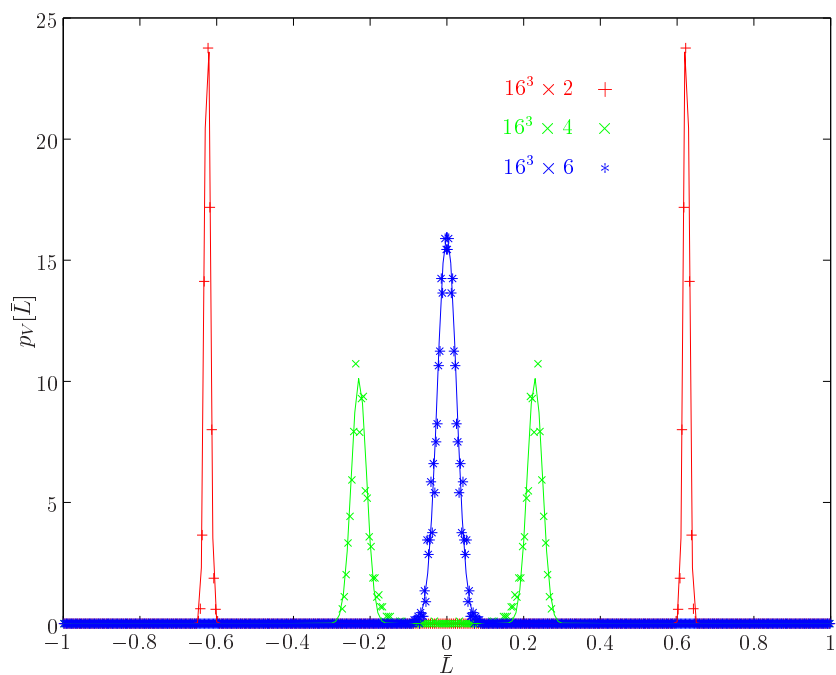


Figure 4.8.: Same as Fig 4.7 for lattices of size $16^3 \times N_t$.

$\Omega \times N_t$	σ'	b	$\langle \bar{L}^2 \rangle^{1/2}$
$7^3 \times 1$	0.0159(8)	0.8571(7)	0.8600
$7^3 \times 2$	0.0226(2)	0.6248(3)	0.6230
$7^3 \times 3$	0.0421(1)	0.4088(2)	0.4049
$7^3 \times 4$	0.0619(9)	0.2430(2)	0.2338
$16^3 \times 1$	0.0067(4)	0.8515(9)	0.8611
$16^3 \times 2$	0.0070(3)	0.6244(4)	0.6239
$16^3 \times 3$	0.0125(2)	0.4055(2)	0.4051
$16^3 \times 4$	0.0198(2)	0.2268(2)	0.2266

Table 4.8.: Width σ' and peak-separation b of the double-Gaussian fit (4.97) and the expectation value $\langle \bar{L}^2 \rangle^{1/2}$ calculated from the $SU(2)$ Monte Carlo ensemble. The values for the temporal extension N_t correspond to the broken phase.

$\Omega = 7^3$ the distribution shows an overlap among the peaks and, as expected, the double-Gaussian is a less good approximation. For a larger volume, $\Omega = 16^3$, the peaks are more narrow and well separated, indicating that tunneling is more strongly suppressed.

4.6. Reproducing the Two-Point Function

The procedure developed so far is based on the single-site distribution of the Polyakov loop which is under good (semianalytic) control. By construction, the effective action obtained in this way reproduces the Yang–Mills distribution quite well (recall Figs 4.4 and 4.5). At this point it is natural to ask how well we are reproducing correlators of the Polyakov loop. After all, these are intimately related to the confining potential ($T < T_c$) or the Debye mass ($T > T_c$), see e.g. [58]. In Figs 4.9 and 4.10 we compare the Yang–Mills two-point function with the one obtained from the Svetitsky–Yaffe effective action (4.2) using the couplings from Tab. 4.6. The figures suggest that we are doing quite well in the symmetric phase ($\beta = 2.20$, i.e. $T < T_c$). In the broken phase ($\beta = 2.40$, i.e. $T > T_c$), however, there is room for improvement both in the exponential decay and the value $\langle L \rangle^2$ of the plateau. To assess the (dis)agreement

quantitatively we fit all two-point functions according to

$$G_{x_0} \equiv \langle L_{\mathbf{x}} L_0 \rangle = a [\exp(-bx) + \exp(-b(N_s - x))] + c. \quad (4.98)$$

The values for the fit parameters are listed in Tab. 4.9 and corroborate the qualitative statements made above.

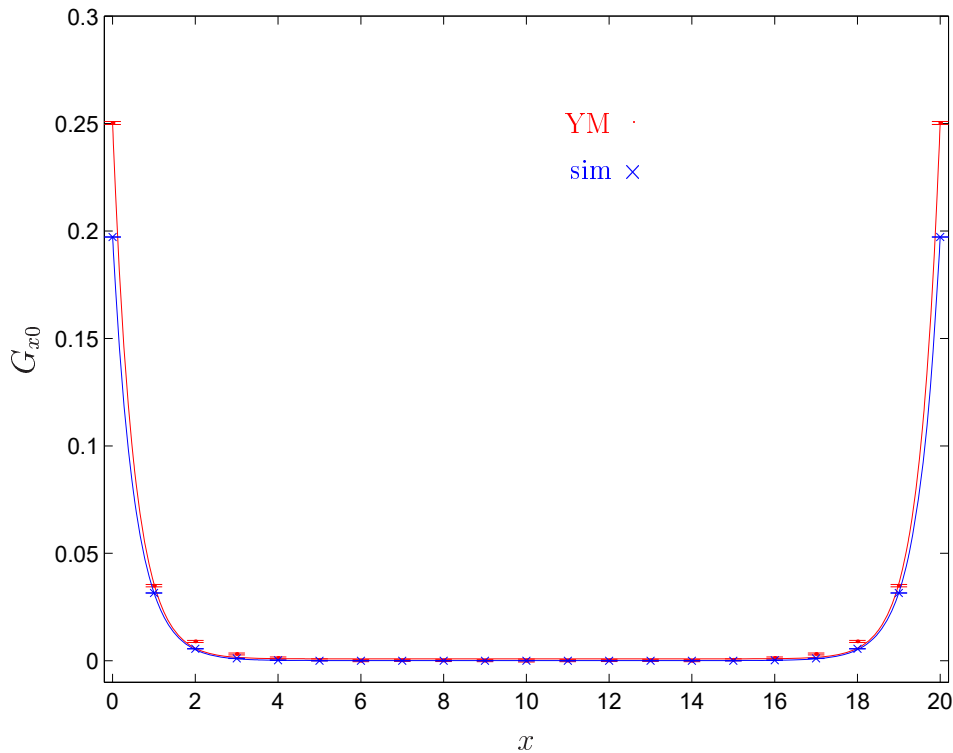


Figure 4.9.: The Yang–Mills two–point function (YM) compared to the one obtained from the Svetitsky–Yaffe effective action with four couplings (sim). Input: $\beta = 2.20$, $N_s = 20$.

In order to improve the matching between the effective theory and Yang–Mills we obviously have to include more operators. In previous applications this has mainly been done for Ising systems [122, 143, 144, 123, 145] or twodimensional nonlinear sigma models [146, 113]. In these cases, the set of operators is restricted as they square to unity. For the Polyakov loop, the situation is different, as arbitrary (ultralocal) powers as well as hopping terms associated with arbitrary powers are allowed, i.e. terms like $L_{\mathbf{x}_1}^{p_1} L_{\mathbf{x}_2}^{p_2} L_{\mathbf{x}_3}^{p_3} \dots$. It turns out that the IMC procedure tends to get destabilized upon including more and more monomials in $L_{\mathbf{x}}$. As a result, the values for the couplings

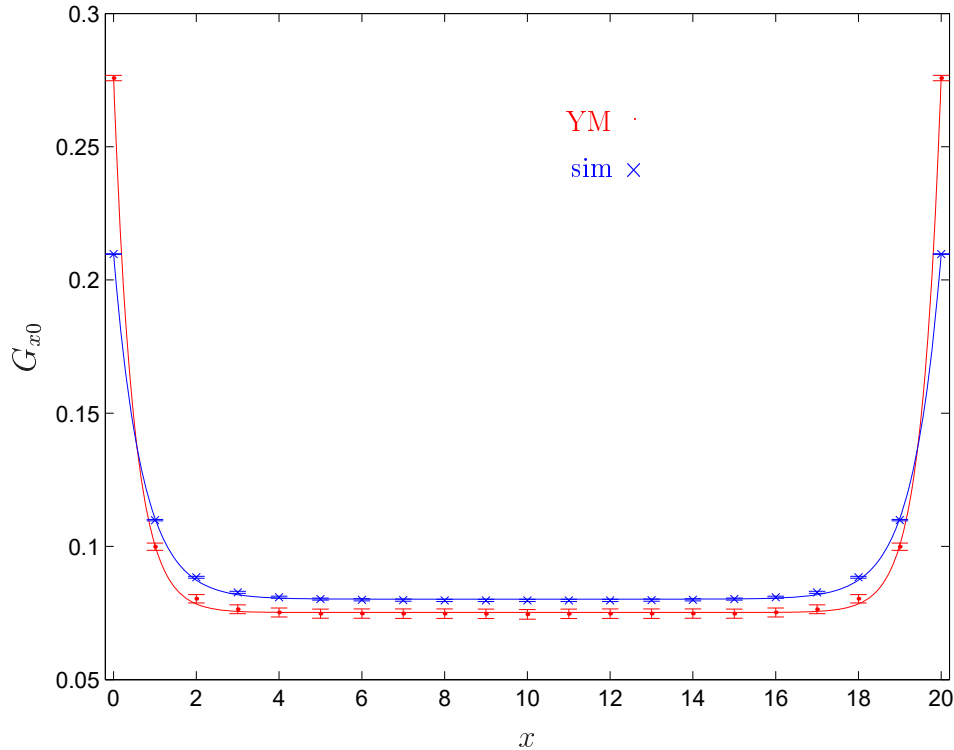


Figure 4.10.: The Yang–Mills two–point function (YM) compared to the one obtained from the Svetitsky–Yaffe effective action with four couplings (sim). Input: $\beta = 2.40$, $N_s = 20$.

β		a	b	c
2.20	YM	0.2493	1.9627	0.0009
	sim	0.1971	1.8309	0.0001
2.40	YM	0.2006	2.0715	0.0752
	sim	0.1295	1.4499	0.0802

Table 4.9.: Comparison of the fit parameters from (4.98) associated with Figs 4.9 and 4.10.

depend rather strongly on the number of operators present *and* of equations used in the overdetermined linear system. Inspired by the results from the high–temperature expansion on the lattice [124, 125] we have therefore changed our operator basis from the monomials to *characters*. Being orthogonal class functions these seem to be the natural candidates for an economic set of operators. At this point it should be noted

that for an effective action with a finite number of terms different choices for bases are not equivalent. As stated in Section 4.1, for $SU(2)$ the characters can be expressed as polynomials in the traced Polyakov loop, $L = \text{tr}\mathfrak{P}/2 = \cos\theta$, according to

$$\chi_j(L) \equiv \frac{\sin((2j+1)\theta)}{\sin\theta} = \sum_{p=0}^{[j]} (-1)^p \binom{2j+1}{2p+1} L^{2j-2p} (1-L^2)^p, \quad j = 0, \frac{1}{2}, 1, \dots \quad (4.99)$$

This formula allows to reobtain the L -representation from the characters. The first few relations are

$$\chi_{1/2} = 2L, \quad \chi_1 = 4L^2 - 1, \quad \chi_{3/2} = 8L^3 - 4L, \quad \dots \quad (4.100)$$

These are sufficient to obtain monomials up to terms of order L^6 . To streamline notation it is useful to define a basic link variable associated with lattice points \mathbf{x} and \mathbf{y} and $SU(2)$ ‘color spin’ j ,

$$X_{j; \mathbf{x}\mathbf{y}} \equiv \chi_j(L_{\mathbf{x}})\chi_j(L_{\mathbf{y}}), \quad (4.101)$$

which we represent graphically as

$$\bullet \text{---} \bullet \quad \equiv \quad X_{1/2; \mathbf{x}\mathbf{y}} = 4L_{\mathbf{x}}L_{\mathbf{y}}, \quad (4.102)$$

$$\bullet \text{---} \bullet \text{---} \bullet \quad \equiv \quad X_{1; \mathbf{x}\mathbf{y}} = 16L_{\mathbf{x}}^2L_{\mathbf{y}}^2 - 4L_{\mathbf{x}}^2 - 4L_{\mathbf{y}}^2 + 1, \quad (4.103)$$

$$\bullet \text{---} \bullet \text{---} \bullet \text{---} \bullet \quad \equiv \quad X_{3/2; \mathbf{x}\mathbf{y}} = 64L_{\mathbf{x}}^3L_{\mathbf{y}}^3 - 32L_{\mathbf{x}}L_{\mathbf{y}}^3 - 32L_{\mathbf{x}}^3L_{\mathbf{y}} + 16L_{\mathbf{x}}L_{\mathbf{y}}, \quad (4.104)$$

\vdots

A link with n ‘internal’ lines thus corresponds to the representation labelled by $j = n/2$. These links are the basic building blocks of our basis of effective operators. The leading order of the high-temperature expansion [124, 125] is then given by the expression

$$S_{\text{LO}} \equiv \sum_{\mathbf{x}, \mathbf{i}, j} \lambda_j X_{j; \mathbf{x}, \mathbf{x}+\mathbf{i}}, \quad (4.105)$$

with λ_j a known function of the temporal Wilson coupling β_t and extension N_t that decreases rapidly with ‘color spin’ j . If we denote the basic link as $X_{j; \mathbf{x}, \mathbf{x}+\mathbf{r}}$, we have two parameters controlling our basis, the representation number j and the effective range (link length) $r = |\mathbf{r}|$. Several test runs of the IMC routines confirm good



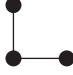
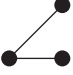
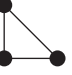

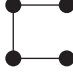
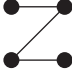


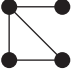



						
-0.11150	-0.02003	-0.00477	0.00257	0.00368	0.00191	-0.00052
-0.15908	-0.06020	-0.00614	0.00649	0.00535	0.00547	0.00003
						
0.00090	-0.00085	0.00070	-0.00004	0.00021	-0.00833	0.00008
0.00096	-0.00053	0.00052	-0.00055	0.00001	0.04305	-0.00061

Table 4.10.: Effective operators and couplings for $\beta = 2.20$ (upper entries) and $\beta = 2.40$ (lower entries), $N_s = 20$.

convergence in j so that we will restrict ourselves to the lowest representations. The maximum range we allow for is the plaquette diagonal, $r \leq \sqrt{2}$. To further restrict the number of operators, we limit ourselves to a maximum number of four links of type (4.101) that can be drawn within a single plaquette. A typical term, for instance, is thus given by

$$\begin{array}{c} \bullet \\ \diagup \quad \diagdown \\ \bullet \quad \bullet \\ \diagdown \quad \diagup \\ \bullet \end{array} \equiv X_{1/2; \mathbf{x}, \mathbf{x}+i} X_{1/2; \mathbf{x}, \mathbf{x}+j} X_{1/2; \mathbf{x}, \mathbf{x}+i+j} X_{1/2; \mathbf{x}+i, \mathbf{x}+j} . \quad (4.106)$$

Altogether we have 14 operators corresponding to 18 monomials in L . They are displayed in Tab. 4.10 together with the couplings associated with them.

Several comments are in order at this point. By allowing for all possible distances $x = 0, 1, \dots, 10$ in the Schwinger–Dyson equations (4.31), we obtain a maximum number of 140 equations for our 14 operators. The values of the couplings remain fairly stable if we vary the number of equations used in the IMC least–square routine (changes approximately 1% for the relevant couplings). The smallest χ^2 per degree of freedom is $5 \cdot 10^{-5}$ for the maximum number of 140 equations.

For the operators (4.102 – 4.104) we find rapid decrease with spin j . Similarly, if we increase the number of links within the elementary plaquette, the associated couplings tend to decrease. The leading order hopping term, $\bullet \text{---} \bullet$ ($r = 1$) dominates by one

order of magnitude compared to the terms with $r = \sqrt{2}$. This already indicates that the effective interactions are short-ranged in accordance with the Svetitsky–Yaffe conjecture.

If we denumerate the couplings by g_1, \dots, g_{14} from left to right, we may express the new effective action as

$$\tilde{S}_{\text{eff}} \equiv \sum_{a=1}^{14} g_a \tilde{S}_a , \quad (4.107)$$

Note that, according to (4.102 – 4.104), the old LO coupling λ_0 is given by a (rapidly convergent) series in j ,

$$\lambda_0 = 4 g_1 + 16 g_{14} + \text{terms with } j > 3/2 = \begin{cases} -0.445 & \text{for } \beta = 2.20 \\ -0.646 & \text{for } \beta = 2.40 \end{cases} . \quad (4.108)$$

These numerical values for λ_0 agree reasonably well with those of Table 4.6, where only four operators had been used. The benchmark test to be performed is the calculation of the two-point function G_{x_0} using the new effective couplings g_a . Figs 4.11 and 4.12 show that we have indeed improved the matching between Yang–Mills and the effective action.

This is quantitatively confirmed by repeating the fit of (4.98) and Tab. 4.9. The results displayed in Tab. 4.11 convincingly show the improvement in the effective action, in particular in the broken phase.

β		a	b	c
2.20	YM	0.2493	1.9627	0.0009
	sim	0.2509	1.9837	0.0001
2.40	YM	0.2006	2.0715	0.0752
	sim	0.2051	1.9257	0.0758

Table 4.11.: Comparison of the fit parameters from (4.98) associated with Figs 4.11 and 4.12.

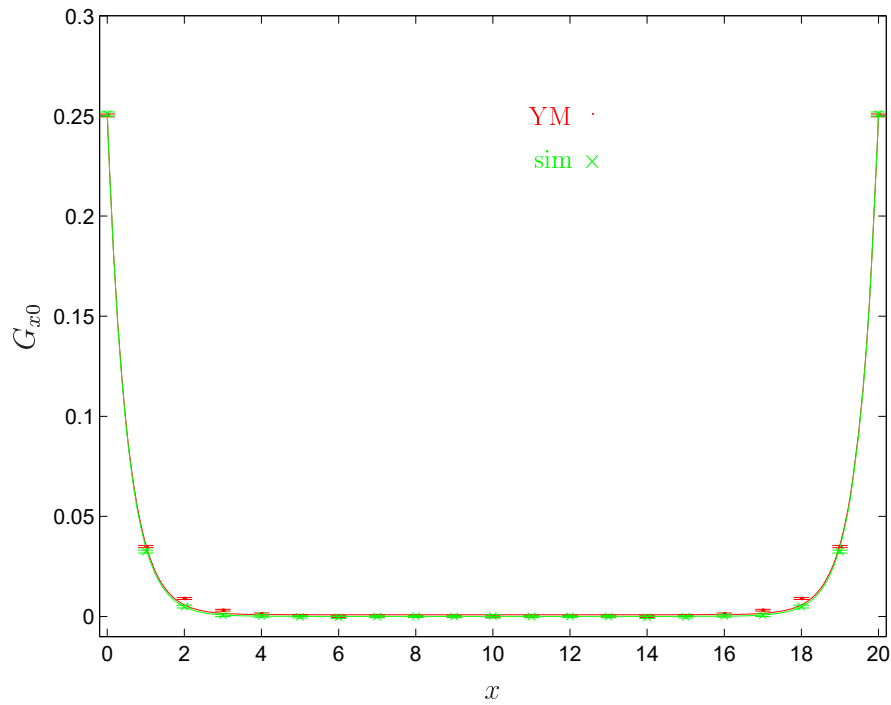


Figure 4.11.: The Yang–Mills two–point function (YM) compared to the one obtained from the character action with 14 couplings (sim). Input: $\beta = 2.20$, $N_s = 20$.

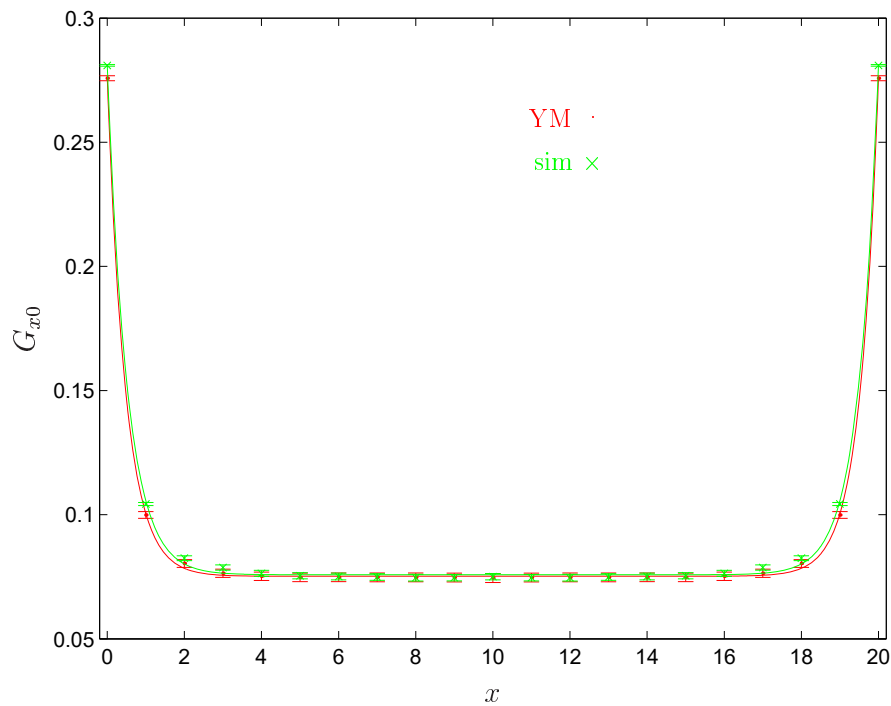


Figure 4.12.: Same as in Fig 4.11 for $\beta = 2.40$.

4.7. Remarks II

We have derived effective actions describing the dynamics of the (traced) Polyakov loop variable $L_{\mathbf{x}} \equiv \text{tr } \mathfrak{P}_{\mathbf{x}}/2$, and hence of the deconfinement phase transition. It has turned out useful, however, to regard the effective action as being derived from a more general theory depending on the untraced Polyakov loop $\mathfrak{P}_{\mathbf{x}}$ [126]. The corresponding symmetry $SU(2) \times SU(2)$ is not a symmetry of the effective action but nevertheless it is inherited in the Haar measure which implies novel Schwinger–Dyson equations for Polyakov loop correlators. It seems that a remnant of this symmetry shows up in the single–site distribution p_W of $L_{\mathbf{x}}$ which is flat below T_c meaning that $\mathfrak{P}_{\mathbf{x}}$ is distributed uniformly over the group manifold. It would be desirable to really *prove* this equipartition for which we have found convincing numerical evidence.

By definition, one cannot calculate correlations from single–site distributions. Vice versa, the matching of these distributions does not imply that the correlation functions match as well. A direct comparison shows that the two–point functions of the Yang–Mills and Svetitsky–Yaffe ensembles differ somewhat, in particular in the broken phase. To improve the matching we included more terms, in particular hopping terms ranging up to a distance of $\sqrt{2}$. Technically, this is a tricky task since, depending on the number of operators and Schwinger–Dyson equations used, the procedure becomes unstable. This may be a numerical problem as the determinants of the matrices to be inverted become as small as 10^{-40} . To overcome these difficulties we changed our operator basis from monomials in $L_{\mathbf{x}}$ to characters being orthogonal polynomials in $L_{\mathbf{x}}$. Doing so the inverse Monte Carlo procedure stabilized, even if the number of operators is large. Furthermore, the determinants are of order one or higher, which is advantageous for numerical reasons.

Further research should be devoted to the following issues. The predictions of the effective actions for the dynamics of the phase transition should be investigated in detail. This includes an analysis of the effective potential(s) near and beyond the transition point as well as calculations of critical exponents. The latter will yield a check whether the effective action $S_{\text{eff}}[L]$ is indeed in the universality class of the \mathbb{Z}_2 –Ising–model. In addition, it should be possible to generalize the methods developed in this thesis to higher $SU(N)$ gauge groups.

5. Summary

The present thesis is devoted to a long standing and yet unsolved problem in modern physics, color confinement. This phenomenon is one among a couple of interesting features occurring in QCD at low energies. In order to learn something about these effects it should be sufficient to restrict oneself to the relevant energy scale while degrees of freedom corresponding to large energies are absorbed into low-energy parameters. This method, known as the effective field theory approach, is adopted throughout this thesis. Furthermore, at low energies the running coupling is large and perturbation theory has no predictive power. For this reason we have to apply some nonperturbative technique. The method of choice is lattice gauge theory, presently being the most powerful nonperturbative approach.

In this thesis we tested and developed low-energy effective models for confining theories using inverse Monte Carlo (IMC) techniques based on Schwinger–Dyson relations and Ward identities which we derived analytically. As a result we have found strong evidence that the Faddeev–Niemi conjecture does not hold whereas our finite temperature calculations support the Svetitsky–Yaffe conjecture.

The first model studied is an effective action for a unit color vector \mathbf{n} proposed by Faddeev and Niemi (FN). They originally stated that low-energy $SU(2)$ Yang–Mills theory is equivalent to a Skyrme–type sigma model. More specifically, FN suggested that the knot solitons of their model might be related to the Yang–Mills glueball spectrum. We have performed a lattice test of this conjecture as follows.

Using standard Monte Carlo techniques, we have generated an ensemble of $SU(2)$ link fields from the Wilson action. This ensemble was used to extract an associated ensemble of \mathbf{n} , parametrizing the gauge invariant distance between the maximally–Abelian and lattice Landau gauge slices. As these gauges are close to each other, there is a preferred direction for the \mathbf{n} –field which corresponds to explicit symmetry

breaking. In this way we avoid the appearance of massless Goldstone bosons and thus generate a nonvanishing mass gap. A study of the exponential decay of correlators yields a mass gap close to 1 GeV. To find the effective action describing the Yang–Mills ensemble of \mathbf{n} -fields we have employed inverse Monte Carlo techniques. The relevant Schwinger–Dyson relations and Ward identities have been evaluated numerically for the Yang–Mills ensemble on the one hand, and for ensembles stemming from the effective FN action on the other hand. To allow for explicit symmetry breaking we have added a minimal symmetry breaking term to the effective action which is of leading order (LO) in the derivatives, in contrast to the FN term which is next to leading order (NLO). As a result, we have found strong evidence that the ensemble generated from Yang–Mills theory cannot be described by the FN action plus a minimal symmetry–breaking term to allow for a mass gap. This follows from a number of discrepancies between the two ensembles.

First, and most prominent, the sign of the coupling associated with the symmetry breaking term is positive, implying negative magnetization. The value from Yang–Mills theory, however, is positive. Second, the reduced two–point functions show just the opposite monotonic behavior compared to Yang–Mills. Third, the size of the gluonic mass gap is larger than for the Yang–Mills ensemble of \mathbf{n} -fields. A coincidence of both, however, cannot be expected due to the nonlocal relation between effective and Yang–Mills degrees of freedom. Comparing the disagreement for different scales separately, we have found indications that the Schwinger–Dyson relations of both theories agree much better for large distances, corresponding to energies of about 0.25 GeV or even less. This is far below the glueball spectrum, and addressing the question of the mass gap makes no sense at this scale. However, by adding more (symmetry–breaking) terms to the action, magnetization, mass gap and susceptibility probably can be rendered correctly. Since we have worked with only one choice of an \mathbf{n} -field, our results rule out the Faddeev–Niemi conjecture only for this particular example. But irrespective of this choice, the following statement holds. For finite temperature, the σ -model is in the universality class of the $4d$ Heisenberg model, while $SU(2)$ Yang–Mills theory is in the $3d$ Ising class if the Svetitsky–Yaffe conjecture is true (which is numerically supported). If the σ -model scale were below the critical temperature, the effective theory would be valid in the confined phase only. In this case the former is not capable of describing Yang–Mills theory close to the phase transition.

Inspired by recent work on finite temperature QCD we have extended our IMC pro-

cedure to another type of effective models. It was argued by Svetitsky and Yaffe that finite temperature $SU(N)$ Yang–Mills theory in d dimensions lies in the same universality class as a \mathbb{Z}_N spin model in $d - 1$ dimensions. To be closer to $SU(2)$ Yang–Mills theory, however, we have not chosen \mathbb{Z}_N Ising spins as effective variables but Polyakov loops. Since the expectation value of the traced Polyakov loop serves as an order parameter for the confinement-deconfinement phase transition, such an effective model should be capable of describing physics near the critical temperature.

From a general theory depending on the untraced Polyakov loop with symmetry $SU(2) \times SU(2) \sim SO(4)$ we have derived an effective action $S_{\text{eff}}[L]$ for the (traced) Polyakov loop variable L . The $SO(4)$ symmetry is not a symmetry of the effective action but inherited by the Haar measure. On this basis we have derived novel Schwinger–Dyson equations for Polyakov loop correlators. Computing the single-site distribution $p_W[L]$ this symmetry shows up as p_W is flat in the symmetric phase ($T < T_c$), which means that the untraced Polyakov loop is distributed uniformly over the group manifold. As the single-site distribution of L is exactly known in the confinement phase, we can give exact predictions for all moments $\langle L^{2k} \rangle$ and thus for the Binder cumulant, $b_4 = -1$. Above T_c , we have fitted the log-distribution $W \sim \log p_W$ by polynomials so that also in this case we have good quantitative control of the distribution. It turns out that $W[L]$ and $S_{\text{eff}}[L]$ are related in a manner that is simple enough to proceed by analytic means. Assuming that expectations taken in the effective action are unchanged if L is changed at a single site we have been able to express the effective couplings $S_{\text{eff}}[L]$ in terms of the fitted parameters of W and the coupling λ_0 of the hopping term. The latter has been determined by means of the Schwinger–Dyson equations. The single-site distributions resulting from the effective theory agree very well with those obtained directly from Yang–Mills. Furthermore, the effective action perfectly reproduces the Schwinger–Dyson equations based on the $SO(4)$ invariance of the Haar measure. We have also determined the (constraint) effective potential from the single-site distribution p_W by applying the Law of Large Numbers. As expected for the confined phase ($T < T_c$), we obtain a Gaussian distribution for the mean field \bar{L} if the volume is large and the temperature small enough. In the broken phase ($T > T_c$) we have found that the distribution can be fitted very well to a double-Gaussian. Doing so also shows that close to the critical temperature tunneling becomes suppressed by enlarging the volume.

Since correlation functions cannot be computed from single-site distributions, the

matching of the latter does not imply matching of the former. In order to improve the matching of the correlation functions we have extended our model by including more terms, in particular hopping terms corresponding to larger distances. To achieve progress in this direction we have replaced the operators (monomials in L) in the effective action by characters, which are orthogonal polynomials in L . Doing so, the IMC procedure turns out to be very stable, even for a large number of operators and Schwinger–Dyson equations. The couplings decrease rapidly with increasing characters so that we have restricted the ansatz to leading first three (nontrivial) representations. In this way we have obtained the effective couplings for a total number of 14 operators. The resulting effective theory has short–range interactions and reproduces the Yang–Mills two–point function very well. This is consistent with the conjecture of Svetitsky and Yaffe.

On the technical side we have clarified some details concerning the methods of singular value decomposition and least squares in the context of inverse Monte Carlo. We have demonstrated that missing operators in the ansatz to be fitted by the data show up as a systematically floating least square solution as the number of equations is varied. This effect is more serious the more important the neglected operator is. The use of different sizes of the system of equations is therefore crucial to obtain a reasonable solution, and also helps to improve the ansatz. Using the singular value decomposition one should be very careful in distinguishing the singular values. Whether a very small diagonal entry is treated as zero (and thus left out) depends on the particular problem. Is the smallness caused by almost linear dependent columns of the matrix the singular values have to be regarded as nonzero.

Bibliography

- [1] F. Halzen and A. D. Martin, *Quarks and Leptons: An Introductory Course in Modern Particle Physics*, New York, Wiley (1984) 396p.
- [2] S. L. Glashow, *Partial Symmetries of Weak Interactions*, *Nucl. Phys.* **22** (1961) 579–588.
- [3] J. Goldstone, A. Salam, and S. Weinberg, *Broken Symmetries*, *Phys. Rev.* **127** (1962) 965–970.
- [4] S. Weinberg, *A Model of Leptons*, *Phys. Rev. Lett.* **19** (1967) 1264–1266.
- [5] M. Gell-Mann, *A Schematic Model of Baryons and Mesons*, *Phys. Lett.* **8** (1964) 214–215.
- [6] G. Zweig, *An $SU(3)$ Model for Strong Interaction Symmetry and its Breaking. 2*, CERN-TH-412.
- [7] J. D. Bjorken, *Asymptotic Sum Rules at Infinite Momentum*, *Phys. Rev.* **179** (1969) 1547–1553.
- [8] J. D. Bjorken and E. A. Paschos, *Inelastic Electron Proton and Gamma Proton Scattering, and the Structure of the Nucleon*, *Phys. Rev.* **185** (1969) 1975–1982.
- [9] R. P. Feynman, *Very High-Energy Collisions of Hadrons*, *Phys. Rev. Lett.* **23** (1969) 1415–1417.
- [10] **Particle Data Group** Collaboration, K. Hagiwara, K. and others, O. Zenin, *Review of Particle Physics*, *Phys. Rev.* **D66** (2002) 010001+.
- [11] **LEPS** Collaboration, T. Nakano *et al.*, *Evidence for a narrow $S=+1$ Baryon Resonance in Photoproduction from the Neutron*, *Phys. Rev. Lett.* **91** (2003) 012002 [arXiv:hep-ex/0301020].
- [12] **DIANA** Collaboration, V. V. Barmin *et al.*, *Observation of a Baryon Resonance with Positive Strangeness in K^+ Collisions with Xe Nuclei*, *Phys. Atom. Nucl.* **66** (2003) 1715 [*Yad. Fiz.* **66** (2003) 1763] [arXiv:hep-ex/0304040].

- [13] **CLAS** Collaboration, S. Stepanyan *et al.*, *Observation of an Exotic $S = +1$ Baryon in Exclusive Photoproduction from the Deuteron*, arXiv:hep-ex/0307018.
- [14] **SAPHIR** Collaboration, J. Barth *et al.*, *Observation of the Positive-Strangeness Pentaquark Θ^+ in Photoproduction with the SAPHIR Detector at ELSA*, arXiv:hep-ex/0307083.
- [15] J. Greensite, *The Confinement Problem in Lattice Gauge Theory*, *Prog. Part. Nucl. Phys.* **51** (2003) 1, [hep-lat/0301023].
- [16] A. Smilga, *Lectures on Quantum Chromodynamics*, Singapore, Singapore: World Scientific (2001) 322p.
- [17] D. J. Gross and F. Wilczek, *Ultraviolet Behavior of Non-Abelian Gauge Theories*, *Phys. Rev. Lett.* **30** (1973) 1343–1346.
- [18] S. Weinberg, *Non-Abelian Gauge Theories of the Strong Interactions*, *Phys. Rev. Lett.* **31** (1973) 494–497.
- [19] H. Fritzsch, M. Gell-Mann, and H. Leutwyler, *Advantages of the Color Octet Gluon Picture*, *Phys. Lett.* **B47** (1973) 365–368.
- [20] T. P. Cheng and L. F. Li, *Gauge Theory of Elementary Particle Physics*, Oxford, UK: Clarendon (1984) 536P. (Oxford Science Publications).
- [21] P. de Forcrand and O. Philipsen, *Adjoint String Breaking in 4d $SU(2)$ Yang-Mills Theory*, *Phys. Lett.* **B475** (2000) 280–288, [hep-lat/9912050].
- [22] G. S. Bali, *The Mechanism of Quark Confinement*, hep-lat/9809351.
- [23] J. B. Kogut and L. Susskind, *Scale Invariant Parton Model*, *Phys. Rev.* **D9** (1974) 697–705.
- [24] J. Ambjorn, P. Olesen, and C. Peterson, *Stochastic Confinement and Dimensional Reduction. 2. Three-Dimensional $SU(2)$ Lattice Gauge Theory*, *Nucl. Phys.* **B240** (1984) 533.
- [25] G. S. Bali, *Casimir Scaling of $SU(3)$ Static Potentials*, *Phys. Rev.* **D62** (2000) 114503, [hep-lat/0006022].
- [26] B. Lucini and M. Teper, *Confining Strings in $SU(N)$ Gauge Theories*, *Phys. Rev.* **D64** (2001) 105019, [hep-lat/0107007].
- [27] M. J. Teper, *Lattice Field Theory and $SU(N)$ Gauge Theories*, <http://www-thphys.physics.ox.ac.uk/users/MikeTeper/erice.ps>.
- [28] A. Hanany, M. J. Strassler, and A. Zaffaroni, *Confinement and Strings in MQCD*, *Nucl. Phys.* **B513** (1998) 87–118, [hep-th/9707244].

- [29] K. Johnson and C. B. Thorn, *String-like Solutions of the Bag Model*, *Phys. Rev.* **D13** (1976) 1934.
- [30] M. J. Teper, *Glueball Masses and Other Physical Properties of $SU(N)$ Gauge Theories in $d = 3+1$: A Review of Lattice Results for Theorists*, hep-th/9812187.
- [31] C. Amsler and F. E. Close, *Evidence for a Scalar Glueball*, *Phys. Lett.* **B353** (1995) 385–390, [hep-ph/9505219].
- [32] F. E. Close and A. Kirk, *Scalar Glueball Q Anti- Q Mixing Above 1-GeV and Implications for Lattice QCD*, *Eur. Phys. J.* **C21** (2001) 531–543, [hep-ph/0103173].
- [33] M. G. Alford, *QCD at High Density / Temperature*, *Nucl. Phys. Proc. Suppl.* **117** (2003) 65–82, [hep-ph/0209287].
- [34] F. Csikor *et. al.*, *Lattice QCD at Non-Vanishing Density: Phase Diagram, Equation of State*, hep-lat/0301027.
- [35] S. Weinberg, *Phenomenological Lagrangians*, *Physica* **A96** (1979) 327.
- [36] A. S. Kronfeld, *Uses of Effective Field Theory in Lattice QCD*, hep-lat/0205021.
- [37] Y. Nambu and G. Jona-Lasinio, *Dynamical Model of Elementary Particles Based on an Analogy with Superconductivity. i*, *Phys. Rev.* **122** (1961) 345–358.
- [38] E. Eichten and B. Hill, *Static Effective Field Theory: $1/m$ Corrections*, *Phys. Lett.* **B243** (1990) 427–431.
- [39] E. Eichten and B. Hill, *An Effective Field Theory for the Calculation of Matrix Elements Involving Heavy Quarks*, *Phys. Lett.* **B234** (1990) 511.
- [40] W. E. Caswell and G. P. Lepage, *Effective Lagrangians for Bound State Problems in QED, QCD, and other Field Theories*, *Phys. Lett.* **B167** (1986) 437.
- [41] B. A. Thacker and G. P. Lepage, *Heavy Quark Bound States in Lattice QCD*, *Phys. Rev.* **D43** (1991) 196–208.
- [42] M. Baker, J. S. Ball, and F. Zachariasen, *Dual Long Distance QCD*, *Phys. Rev.* **D37** (1988) 1036. Erratum: *ibid.* 3785 (1988).
- [43] T. Suzuki, *A Ginzburg-Landau Type Theory of Quark Confinement*, *Prog. Theor. Phys.* **80** (1988) 929.
- [44] S. Maedan and T. Suzuki, *An Infrared Effective Theory of Quark*

- Confinement Based on Monopole Condensation*, *Prog. Theor. Phys.* **81** (1989) 229–240.
- [45] Y. Koma, H. Suganuma, and H. Toki, *Flux-Tube Ring and Glueball Properties in the Dual Ginzburg-Landau Theory*, *Phys. Rev.* **D60** (1999) 074024, [hep-ph/9902441].
- [46] D. Antonov, *String Representation and Nonperturbative Properties of Gauge Theories*, *Surveys High Energ. Phys.* **14** (2000) 265–355, [hep-th/9909209].
- [47] L. Faddeev and A. Niemi, *Partially Dual Variables in $SU(2)$ Yang-Mills Theory*, *Phys. Rev. Lett.* **82** (1999) 1624, [hep-th/9807069].
- [48] T. H. R. Skyrme, *A Nonlinear Field Theory*, *Proc. Roy. Soc. Lond.* **A260** (1961) 127–138.
- [49] L. Faddeev and A. Niemi, *Knots and Particles*, *Nature* **387** (1997) 58, [hep-th/9610193].
- [50] R. Battye and P. Sutcliffe, *Knots as Stable Soliton Solutions in a Three-Dimensional Classical Field Theory*, *Phys. Rev. Lett.* **81** (1998) 4798, [hep-th/9808129].
- [51] J. Gladikowski and M. Hellmund, *Static Solitons with Nonzero Hopf Number*, *Phys. Rev.* **D56** (1997) 5194, [hep-th/9609035].
- [52] A. M. Polyakov, *Thermal Properties of Gauge Fields and Quark Liberation*, *Phys. Lett.* **B72** (1978) 477.
- [53] L. Susskind, *Lattice Models of Quark Confinement at High Temperature*, *Phys. Rev.* **D20** (1979) 2610.
- [54] B. Svetitsky and L. Yaffe, *Critical Behavior at Finite-Temperature Confinement Transitions*, *Nucl. Phys.* **B210** (1982) 423.
- [55] L. G. Yaffe and B. Svetitsky, *First-Order Phase Transition in the $SU(3)$ Gauge Theory at Finite Temperature*, *Phys. Rev.* **D26** (1982) 963.
- [56] T. Banks and A. Ukawa, *Deconfining and Chiral Phase Transition in Quantum Chromodynamics at Finite Temperature*, *Nucl. Phys.* **B225** (1983) 145.
- [57] M. Ogilvie, *Effective-Spin Model for Finite-Temperature QCD*, *Phys. Rev. Lett.* **52** (1984) 1369.
- [58] B. Svetitsky, *Symmetry Aspects of Finite-Temperature Phase Transitions*, *Phys. Rept.* **132** (1986) 1.
- [59] K. G. Wilson, *Confinement of Quarks*, *Phys. Rev.* **D10** (1974) 2445–2459.

- [60] M. Creutz, *Quarks, Gluons and Lattices*. Cambridge Monographs on Mathematical Physics. Cambridge University Press, Cambridge, 1983.
- [61] J. B. Kogut, *A Review of the Lattice Gauge Theory Approach to Quantum Chromodynamics*, *Rev. Mod. Phys.* **55** (1983) 775.
- [62] I. Montvay and G. Münster, *Quantum Fields on a Lattice*. Cambridge University Press, Cambridge, 1994.
- [63] H. Rothe, *Lattice Gauge Theory*. World Scientific, Singapore, 1992. Ch. 14.
- [64] A. S. Kronfeld and P. B. Mackenzie, *Progress in QCD Using Lattice Gauge Theory*, *Ann. Rev. Nucl. Part. Sci.* **43** (1993) 793–828, [[hep-ph/9303305](#)].
- [65] S. Aoki, *Lattice Calculations and Hadron Physics*, *Int. J. Mod. Phys.* **A15S1** (2000) 657–683, [[hep-ph/9912288](#)].
- [66] G. Munster and M. Walzl, *Lattice Gauge Theory: A Short Primer*, [hep-lat/0012005](#).
- [67] T. DeGrand, *Lattice QCD and the CKM Matrix*, [hep-ph/0008234](#).
- [68] H. Hamber and G. Parisi, *Numerical Estimates of Hadronic Masses in a Pure SU(3) Gauge Theory*, *Phys. Rev. Lett.* **47** (1981) 1792.
- [69] E. Marinari, G. Parisi, and C. Rebbi, *Computer Estimates of Meson Masses in SU(2) Lattice Gauge Theory*, *Phys. Rev. Lett.* **47** (1981) 1795.
- [70] D. Weingarten, *Monte Carlo Evaluation of Hadron Masses in Lattice Gauge Theories with Fermions*, *Phys. Lett.* **B109** (1982) 57.
- [71] **CP-PACS** Collaboration, S. Aoki *et. al.*, *Quenched Light Hadron Spectrum*, *Phys. Rev. Lett.* **84** (2000) 238–241, [[hep-lat/9904012](#)].
- [72] J. Iizuka, *Systematics and Phenomenology of Meson Family*, *Prog. Theor. Phys. Suppl.* **37** (1966) 21–34.
- [73] S. Okubo, *Phi Meson and Unitary Symmetry Model*, *Phys. Lett.* **5** (1963) 165–168.
- [74] N. Metropolis, A. W. Rosenbluth, M. N. Rosenbluth, A. H. Teller, and E. Teller, *Equation of State Calculations by Fast Computing Machines*, *J. Chem. Phys.* **21** (1953) 1087–1092.
- [75] G. Bhanot, *The Metropolis Algorithm*, *Rept. Prog. Phys.* **51** (1988) 429.
- [76] M. Creutz, *Monte Carlo Study of Quantized SU(2) Gauge Theory*, *Phys. Rev.* **D21** (1980) 2308–2315.
- [77] N. Cabibbo and E. Marinari, *A New Method for Updating SU(N) Matrices*

- in Computer Simulations of Gauge Theories, Phys. Lett.* **B119** (1982) 387–390.
- [78] R. H. Swendsen and J.-S. Wang, *Nonuniversal Critical Dynamics in Monte Carlo Simulations, Phys. Rev. Lett.* **58** (1987) 86–88.
- [79] U. Wolff, *Collective Monte Carlo Updating for Spin Systems, Phys. Rev. Lett.* **62** (1989) 361.
- [80] S. L. Adler, *An Overrelaxation Method for the Monte Carlo Evaluation of the Partition Function for Multiquadratic Actions, Phys. Rev.* **D23** (1981) 2901.
- [81] F. R. Brown and T. J. Woch, *Overrelaxed Heat Bath and Metropolis Algorithms for Accelerating Pure Gauge Monte Carlo Calculations, Phys. Rev. Lett.* **58** (1987) 2394.
- [82] M. Creutz, *Overrelaxation and Monte Carlo Simulation, Phys. Rev.* **D36** (1987) 515.
- [83] A. Wightman, *Quantum Field Theory in Terms of Vacuum Expectation Values, Phys. Rev.* **101** (1956) 860.
- [84] S.-K. Ma, *Renormalization Group by Monte Carlo Methods, Phys. Rev. Lett.* **37** (1976) 461–464.
- [85] R. Swendsen, *Monte Carlo Renormalization Group, Phys. Rev. Lett.* **42** (1979) 859.
- [86] E. C. G. Stueckelberg and A. Petermann, *Normalization of Constants in the Quanta Theory, Helv. Phys. Acta* **26** (1953) 499–520.
- [87] M. Gell-Mann and F. E. Low, *Quantum Electrodynamics at Small Distances, Phys. Rev.* **95** (1954) 1300–1312.
- [88] A. Gonzalez-Arroyo and M. Okawa, *Renormalized Coupling Constants by Monte Carlo Methods, Phys. Rev.* **D 35** (1987) 672.
- [89] W. Press, S. Teukolsky, W. Vetterling, and B. Flannery, *Numerical Recipes in C*. Cambridge University Press, Cambridge, 1992.
- [90] K. Symanzik, *Continuum Limit and Improved Action in Lattice Theories. 2. $O(N)$ Nonlinear Sigma Model in Perturbation Theory, Nucl. Phys.* **B226** (1983) 205.
- [91] K. Symanzik, *Continuum Limit and Improved Action in Lattice Theories. 1. Principles and ϕ^4 Theory, Nucl. Phys.* **B226** (1983) 187.
- [92] M. Lüscher and P. Weisz, *On-Shell Improved Lattice Gauge Theories, Commun. Math. Phys.* **97** (1985) 59.

- [93] J. Hietarinta and P. Salo, *Faddeev-Hopf Knots: Dynamics of Linked Unknots*, *Phys. Lett.* **B451** (1999) 60, [[hep-th/9811053](#)].
- [94] P. van Baal and A. Wipf, *Classical Gauge Vacua as Knots*, *Phys. Lett.* **B515** (2001) 181–184, [[arXiv:hep-th/0105141](#)].
- [95] E. Langmann and A. Niemi, *Towards a sTring Representation of Infrared $SU(2)$ Yang-Mills Theory*, *Phys. Lett.* **B463** (1999) 252, [[hep-th/9905147](#)].
- [96] S. Shabanov, *An Effective Action for Monopoles and Knot Solitons in Yang-Mills Theory*, *Phys. Lett.* **B458** (1999) 322, [[hep-th/9903223](#)].
- [97] S. Shabanov, *Yang-Mills Theory as an Abelian Theory Without Gauge Fixing*, *Phys. Lett.* **B463** (1999) 263, [[hep-th/9907182](#)].
- [98] H. Gies, *Wilsonian Effective Action for $SU(2)$ Yang-Mills Theory with Cho-Faddeev-Niemi-Shabanov Decomposition*, *Phys. Rev.* **D63** (2001) 125023, [[hep-th/0102026](#)].
- [99] S. Shabanov, *Infrared Yang-Mills Theory as a Spin System: A Lattice Approach*, *Phys. Lett.* **B522** (2001) 201–209, [[hep-lat/0110065](#)].
- [100] F. Freire, *Abelian Projected $SU(2)$ Yang-Mills Action for Renormalisation Group Flows*, *Phys. Lett.* **B526** (2002) 405, [[hep-th/0110241](#)].
- [101] N. Manton, *The Force between 't Hooft-Polyakov Monopoles*, *Nucl. Phys.* **B126** (1977) 525.
- [102] Y. Cho, *Restricted Gauge Theory*, *Phys. Rev.* **D21** (1980) 1080.
- [103] L. D. Faddeev and A. J. Niemi, *Electric-Magnetic Duality in Infrared $SU(2)$ Yang-Mills Theory*, *Phys. Lett.* **B525** (2002) 195–200, [<http://arXiv.org/abs/hep-th/0101078>].
- [104] G. 't Hooft, *Gauge Theories with Unified Weak, Electromagnetic and Strong Interactions*, in: *High Energy Physics*, Proceedings of the EPS International Conference, Palermo 1975, A. Zichichi, ed., Editrice Compositori, Bologna 1976.
- [105] A. S. Kronfeld, M. L. Laursen, G. Schierholz, and U.-J. Wiese, *Monopole Condensation and Color Confinement*, *Phys. Lett* **B198** (1987) 516.
- [106] R. C. Brower, K. N. Orginos, and C.-I. Tan, *Magnetic Monopole Loop for Yang-Mills Instanton*, *Phys. Rev.* **D55** (1997) 6313, [[hep-th/9610101](#)].
- [107] T. Kovacs and E. Tomboulis, *On p-Vortices and the Gribov Problem*, *Phys. Lett.* **B463** (1999) 104–108, [[hep-lat/9905029](#)].
- [108] C. Davies, G. Batrouni, G. Katz, A. Kronfeld, G. Lepage, K. Wilson,

- P. Rossi, and B. Svetitsky, *Fourier Acceleration in Lattice Gauge Theories. 1. Landau Gauge Fixing*, *Phys. Rev.* **D37** (1988) 1581.
- [109] V. Gribov, *Quantization of Non-Abelian Gauge Theories*, *Nucl. Phys.* **B139** (1978) 1.
- [110] F. Bruckmann, T. Heinzl, T. Tok, and A. Wipf, *Instantons and Gribov Copies in the Maximally Abelian Gauge*, *Nucl. Phys.* **B584** (2000) 589, [[hep-th/0001175](#)].
- [111] F. Bruckmann, T. Heinzl, T. Vekua, and A. Wipf, *Magnetic Monopoles vs. Hopf Defects in the Laplacian (Abelian) Gauge*, *Nucl. Phys.* **B593** (2001) 545, [[hep-th/0007119](#)].
- [112] M. Falcioni, G. Martinelli, M. Paciello, G. Parisi, and B. Taglienti, *A New Proposal for the Determination of the Renormalization Group Trajectories by Monte Carlo Renormalization Group Method*, *Nucl. Phys.* **B265** (1986) 187.
- [113] A. Gottlob, M. Hasenbusch, and K. Pinn, *Iterating Block Spin Transformations of the $O(3)$ Non-Linear Sigma-Model*, *Phys. Rev.* **D54** (1996) 1736–1747, [[hep-lat/9601014](#)].
- [114] K. Yee, *Abelian Projection QCD: Action and Crossover*, *Phys. Lett.* **B347** (1995) 367–374, [[hep-lat/9503003](#)].
- [115] M. Ogilvie, *Theory of Abelian Projection*, *Phys. Rev.* **D59** (1999) 074505, [[hep-lat/9806018](#)].
- [116] M. Ogilvie, *Center Symmetry and Abelian Projection at Finite Temperature*, [hep-lat/0208072](#).
- [117] M. Caselle and M. Hasenbusch, *Deconfinement Transition and Dimensional Cross-Over in the 3d Gauge Ising Model*, *Nucl. Phys.* **B470** (1996) 435–453, [[hep-lat/9511015](#)].
- [118] F. Gliozzi and P. Provero, *The Svetitsky-Yaffe Conjecture for the Plaquette Operator*, *Phys. Rev.* **D56** (1997) 1131–1134, [[hep-lat/9701014](#)].
- [119] M. Pepe and P. de Forcrand, *Finite Size Scaling of Interface Free Energies in the 3-d Ising Model*, *Nucl. Phys. B (Proc. Suppl.)* **106** (2002) 914, [[hep-lat/0110119](#)].
- [120] P. de Forcrand and O. Jahn, *Deconfinement Transition in 2+1-Dimensional $SU(4)$ Lattice Gauge Theory*, [hep-lat/0309153](#).
- [121] J. Polonyi and K. Szlachanyi, *Phase Transition from Strong Coupling Expansion*, *Phys. Lett.* **B110** (1982) 395.

- [122] M. Okawa, *Universality of the Deconfining Phase Transition in (3+1)-Dimensional SU(2) Lattice Gauge Theory*, *Phys. Rev. Lett.* **60** (1988) 1805.
- [123] S. Fortunato, F. Karsch, P. Petreczky, and H. Satz, *Effective Z(2) Spin Models of Deconfinement and Percolation in SU(2) Gauge Theory*, *Phys. Lett.* **B503** (2001) 321, [[hep-lat/0011084](http://arXiv.org/abs/hep-lat/0011084)].
- [124] M. Caselle, *Recent Results in High-Temperature Lattice Gauge Theories*, <http://arXiv.org/abs/hep-lat/9601009>. in: *Selected Topics in Nonperturbative QCD*, A. Di Giacomo and D. Diakonov, eds., Proceedings International School of Physics “Enrico Fermi”, Course CXXX, Varenna, Italy, 1995, IOS Press, Amsterdam, 1996.
- [125] M. Billo, M. Caselle, A. D’Adda, and S. Panzeri, *Toward an Analytic Determination of the Deconfinement Temperature in SU(2) L.G.T*, *Nucl. Phys.* **B472** (1996) 163, [<http://arXiv.org/abs/hep-lat/9601020>].
- [126] R. Pisarski, *Quark-Gluon Plasma as a Condensate of Z(3) Wilson Lines*, *Phys. Rev.* **D62** (2000) 111501(R), [[hep-ph/0006205](http://arXiv.org/abs/hep-ph/0006205)].
- [127] P. Meisinger, T. Miller, and M. Ogilvie, *Phenomenological Equations of State for the Quark-Gluon Plasma*, *Phys. Rev.* **D65** (2002) 034009.
- [128] H. Reinhardt, *Resolution of Gauss’ Law in Yang-Mills Theory by Gauge Invariant Projection: Topology and Magnetic Monopoles*, *Nucl. Phys.* **B503** (1997) 505, [[hep-th/9702049](http://arXiv.org/abs/hep-th/9702049)].
- [129] C. Ford, U. G. Mitreuter, T. Tok, A. Wipf, and J. M. Pawłowski, *Monopoles, Polyakov Loops and Gauge Fixing on the Torus*, *Ann. Phys. (N.Y.)* **269** (1998) 26, [[hep-th/9802191](http://arXiv.org/abs/hep-th/9802191)].
- [130] O. Jahn and F. Lenz, *Structure and Dynamics of Monopoles in Axial Gauge QCD*, *Phys. Rev.* **D58** (1998) 085006, [[hep-th/9803177](http://arXiv.org/abs/hep-th/9803177)].
- [131] G. ’t Hooft, *Topology of the Gauge Condition and New Confinement Phases in Non-Abelian Gauge Theories*, *Nucl. Phys.* **B190** (1981) 455.
- [132] K. Binder, *Critical Properties from Monte Carlo Coarse Graining and Renormalization*, *Phys. Rev. Lett.* **47** (1981) 693.
- [133] J. Fingberg, U. M. Heller, and F. Karsch, *Scaling and Asymptotic Scaling in the SU(2) Gauge Theory*, *Nucl. Phys.* **B392** (1993) 493–517, [[hep-lat/9208012](http://arXiv.org/abs/hep-lat/9208012)].
- [134] M. Mathur, *Landau Ginzburg Model and Deconfinement Transition for Extended SU(2) Wilson Action*, [hep-lat/9501036](http://arXiv.org/abs/hep-lat/9501036).

- [135] H. Ursell, *The Evaluation of Gibbs' Phase Integral for Imperfect Gases*, *Proc. Cambridge Phil. Soc.* **23** (1927) 685.
- [136] J. Mayer, *The Statistical Mechanics of Condensing Systems. i*, *J. Chem. Phys.*, **5** (1937) 67.
- [137] F. Coester and R. Haag, *Representation of States in a Field Theory with Canonical Variables*, *Phys. Rev.* **117** (1960) 1137.
- [138] H. Römer and T. Filk, *Statistische Mechanik*. VCH, Weinheim, 1994. (in German).
- [139] L. O'Raifeartaigh, A. Wipf, and H. Yoneyama, *The Constraint Effective Potential*, *Nucl. Phys.* **B271** (1986) 653.
- [140] D. Gross, R. Pisarski, and L. Yaffe, *QCD and Instantons at Finite Temperature*, *Rev. Mod. Phys.* **53** (1981) 43.
- [141] N. Weiss, *Effective Potential for the Order Parameter of Gauge Theories at Finite Temperature*, *Phys. Rev.* **D24** (1981) 475.
- [142] Y. Fujimoto, H. Yoneyama, and A. Wipf, *Symmetry Restoration of Scalar Models at Finite Temperature*, *Phys. Rev.* **D38** (1988) 2625–2634.
- [143] M. Fukugita, M. Okawa, and A. Ukawa, *Order of the Deconfining Phase Transition in $SU(3)$ Lattice Gauge Theory*, *Phys. Rev. Lett.* **63** (1989) 1768.
- [144] B. Svetitsky and N. Weiss, *Ising Description of the Transition Region in $SU(3)$ Gauge Theory at Finite Temperature*, *Phys. Rev.* **D56** (1997) 5395.
- [145] F. Karsch, *Lattice QCD at High Temperature and Density*, in *Dense Matter*, Lect. Notes Phys. **583**, pp. 209–249, Springer, 2001. [hep-lat/0106019](#).
Lectures given at 40th Internationale Universitätswochen fuer Theoretische Physik (IUKT 40), Schladming, Styria, Austria, 3-10 Mar 2001.
- [146] P. Hasenfratz and F. Niedermayer, *Perfect Lattice Action for Asymptotically Free Theories*, *Nucl. Phys.* **B414** (1994) 785–814, [[hep-lat/9308004](#)].
- [147] M. Faber, J. Greensite, and S. Olejnik, *Remarks on the Gribov Problem in Direct Maximal Center Gauge*, *Phys. Rev.* **D64** (2001) 034511, [[hep-lat/0103030](#)].
- [148] A very illustrative introduction to Singular Value Decomposition can be found on Todd Will's page,
<http://www.davidson.edu/math/will/svd/svd/index.html>.

Publications

- [LRD1] L. Dittmann, T. Heinzl and A. Wipf, *A Lattice Study of the Faddeev-Niemi Effective Action*, *Nucl. Phys. Proc. Suppl.* **106** (2002) 649–651 [arXiv:hep-lat/0110026].
- [LRD2] L. Dittmann, T. Heinzl and A. Wipf, *Effective Sigma Models and Lattice Ward Identities*, *JHEP* **0212** (2002) 014 [arXiv:hep-lat/0210021].
- [LRD3] L. Dittmann, T. Heinzl and A. Wipf, *An Effective Lattice Theory for Polyakov Loops*, arXiv:hep-lat/0306032.

A. Conventions

Left and right lattice derivatives are defined as

$$\partial_\mu f_x \equiv f_{x+\mu} - f_x , \quad (\text{A.1})$$

$$\partial_\mu^\dagger f_x \equiv f_{x-\mu} - f_x . \quad (\text{A.2})$$

The ordinary lattice Laplacian $\Delta \equiv -\partial_\mu^\dagger \partial_\mu$ is a negative semi-definite operator. Its action on lattice functions f is given by

$$\Delta f_x \equiv - \sum_\mu (2f_x - f_{x+\mu} - f_{x-\mu}) . \quad (\text{A.3})$$

The *covariant* Laplacian $\Delta[U]$ in the adjoint representation acts as

$$\Delta^{ab}[U] f_x^b \equiv - \sum_\mu (2f_x^a - R_{x,\mu}^{ab} f_{x+\mu}^b - R_{x-\mu,\mu}^{ba} f_{x-\mu}^b) , \quad (\text{A.4})$$

where we have defined the *adjoint link*

$$R_{x,\mu}^{ab} \equiv \frac{1}{2} \text{tr}(\tau^a U_{x,\mu} \tau^b U_{x,\mu}^\dagger) . \quad (\text{A.5})$$

B. Relating LLG and MAG

From (3.9) it follows immediately that the LLG *minimizes* the functional [147]

$$\bar{F}_{\text{LLG}} \equiv \sum_l \text{tr}(\mathbb{1} - {}^\Omega U_l), \quad l \equiv (x, \mu), \quad (\text{B.1})$$

and thus tends to bring the links U_l close to $\mathbb{1}$. The MAG, on the other hand, minimizes

$$\bar{F}_{\text{MAG}} \equiv \sum_l (1 - {}^g R_l^{33}), \quad (\text{B.2})$$

and thus wants to bring the 33-entry of the adjoint link R_l^{ab} close to 1. From (A.5) it is obvious that, if U_l equals unity, the same will be true for R_l . This can be made more precise: if $U_l \simeq \mathbb{1} + iaA_l$, A_l hermitean, then it is an easy exercise to show that $R_l^{33} = 1 + O(a^2)$. In this sense, the LLG is close to the MAG.

C. Schwinger–Dyson Equations and Ward Identities

We begin with computing the infinitesimal rotations of the various contributions in (3.15) and (3.16) to the effective action. It turns out that, for all S_j , the action of the angular momentum can be written as

$$i\mathbf{L}_x S_j = \mathbf{n}_x \times \mathbf{K}_{jx} , \quad (\text{C.1})$$

(and analogous for the S'_k) with the vectors \mathbf{K}_{jx} and \mathbf{K}'_{kx} given by

$$\mathbf{K}_{1x} = 2\Delta \mathbf{n}_x \quad (\text{C.2})$$

$$\mathbf{K}_{2x} = 2\Delta^2 \mathbf{n}_x \quad (\text{C.3})$$

$$\mathbf{K}_{3x} = 2[\Delta \mathbf{n}_x (\mathbf{n}_x \cdot \Delta \mathbf{n}_x) + \Delta (\mathbf{n}_x (\mathbf{n}_x \cdot \Delta \mathbf{n}_x))] \quad (\text{C.4})$$

$$\mathbf{K}_{4x} = 2[\partial_\mu^\dagger \partial_\nu \mathbf{n}_x (\mathbf{n}_x \cdot \partial_\mu^\dagger \partial_\nu \mathbf{n}_x) + \partial_\mu^\dagger \partial_\nu (\mathbf{n}_x (\mathbf{n}_x \cdot \partial_\mu^\dagger \partial_\nu \mathbf{n}_x))] \quad (\text{C.5})$$

$$\mathbf{K}'_{1x} = \mathbf{h} \quad (\text{C.6})$$

$$\mathbf{K}'_{2x} = 2\mathbf{h} (\mathbf{n}_x \cdot \mathbf{h}) \quad (\text{C.7})$$

$$\mathbf{K}'_{3x} = \mathbf{h} (\mathbf{n}_x \cdot \Delta \mathbf{n}_x) + \Delta \mathbf{n}_x (\mathbf{n}_x \cdot \mathbf{h}) + \Delta (\mathbf{n}_x (\mathbf{n}_x \cdot \mathbf{h})) . \quad (\text{C.8})$$

Choosing the F 's in (3.26) as n_x^a , $n_x^a n_y^b$ and $n_x^a n_y^b n_z^c$, respectively, results in the Ward identities

$$G_{xy}^{ii} \lambda'_1 + 2G_{\underline{xy}}^{3ii} \lambda'_2 + G_{\underline{xy}}^{\Delta ii} \lambda'_3 = -2G_y^3 , \quad (\text{C.9})$$

$$G_{\underline{xyz}}^{ii3} \lambda'_1 + 2G_{\underline{xyz}}^{3ii3} \lambda'_2 + G_{\underline{xyz}}^{\Delta ii3} \lambda'_3 = -2G_{yz}^{33} + G_{yz}^{ii} , \quad (\text{C.10})$$

$$G_{\underline{xyz}z'}^{iii3} \lambda'_1 + 2G_{\underline{xyz}z'}^{3iii3} \lambda'_2 + G_{\underline{xyz}z'}^{\Delta iii3} \lambda'_3 = -2G_{yz}^{333} + 2G_{yz}^{i(i3)} . \quad (\text{C.11})$$

Here, the superscript ($i3$) denotes symmetrization in $i, 3$, and we have introduced the shorthand notations

$$G_{xyz\dots}^{abc\dots} \equiv \langle n_x^a n_y^b n_z^c \dots \rangle, \quad (\text{C.12})$$

$$G_{\underline{xy}\dots}^{ii\dots} \equiv \sum_x G_{xy\dots}^{ii\dots}, \quad (\text{C.13})$$

$$G_{\underline{xy}\dots}^{3ii\dots} \equiv \sum_x \langle n_x^3 n_x^i n_y^i \dots \rangle, \quad (\text{C.14})$$

$$G_{\underline{xy}\dots}^{\Delta ii\dots} \equiv \sum_x \langle (n_x^a \Delta n_x^a) n_x^i n_y^i \dots \rangle, \quad (\text{C.15})$$

with \underline{x} denoting summation over all lattice sites x . In particular, one has

$$G_y^3 \equiv \mathfrak{M}, \quad G_{\underline{xy}}^{ii} \equiv 2\chi^\perp, \quad G_{xy}^{ii} \equiv 2G_{xy}^\perp, \quad G_{xy}^{33} \equiv G_{xy}^\parallel. \quad (\text{C.16})$$

It seems that a particular recurrence pattern arises in (C.9–C.11) that could be used to derive a Ward identity for an insertion of an arbitrary number of \mathbf{n} 's. For the NLO derivative expansion, however, the three identities are sufficient to determine the symmetry–breaking couplings λ' .

For the particular case that F in (3.23) equals n , $F_x^a = n_x^a$, we can give the general Schwinger–Dyson equation in closed form,

$$\sum_j \lambda_j H_{j,xy} + \sum_k \lambda'_k H'_{k,xy} = -\mathfrak{M} \delta_{xy}, \quad (\text{C.17})$$

where we have introduced the two–point function

$$H_{j,xy} \equiv \langle n_x^i n_y^{[i} K_{jy}^{3]} \rangle, \quad (\text{C.18})$$

and, completely analogous, $H'_{k,xy}$. The FN terms are (C.4) minus (C.5), so that the relevant two–point function becomes

$$H_{xy}^{\text{FN}} \equiv H_{3,xy} - H_{4,xy}, \quad (\text{C.19})$$

which has been used in (3.43).

D. Histograms and Bins

Given a probability density $p_W[L]$ one defines the associated (cumulative) distribution function

$$P_W[L] \equiv \int_{-1}^L dL' \sqrt{1-L'^2} p_W[L'] . \quad (\text{D.1})$$

Density p_W and distribution P_W are related to our histograms as follows. We have a total number N of ‘events’ or ‘measurements’ saying that a Polyakov loop at site \mathbf{x} belonging to an arbitrary configuration takes its value in some prescribed interval (‘bin’). Accordingly, N is a fairly large number,

$$N = N_s^3 \times N_{\text{config}} = 20^3 \times 400 = 3.2 \times 10^6 . \quad (\text{D.2})$$

The number of bins (labeled by integers i) is denoted by I , the number of events in bin i by C_i . This number represents the height of the i th column in the histogram counting the absolute numbers of events with values in $[L_{i-1}, L_i]$. The relative counting *rate* is obtained by normalization,

$$c_i \equiv C_i/N = P_W[L_i] - P_W[L_{i-1}] = p_W[\bar{L}_i] \sqrt{1-\bar{L}_i^2} \Delta L_i , \quad (\text{D.3})$$

where $\Delta L_i \equiv L_i - L_{i-1}$ and $\bar{L}_i \in [L_{i-1}, L_i]$ chosen appropriately. The situation is depicted in Fig. D.1.

Good statistics is achieved if the counting rate c_i is approximately constant because then all bins will be equally ‘populated’. This can be achieved by suitably choosing the bin sizes ΔL_i which, however, is somewhat tricky because of the nontrivial measure in (D.1). If we ignore this for the moment and choose an *equidistant* partition,

$$\Delta L_i = \Delta L = 2/I , \quad (\text{D.4})$$

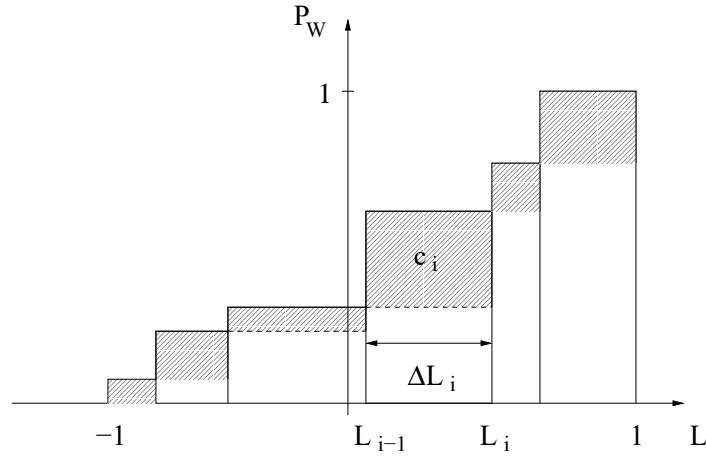


Figure D.1.: General histogram for distribution function $P_W[L]$.

the total count in bin i becomes

$$C_i = \frac{2N}{I} p_W[\bar{L}_i] \sqrt{1 - \bar{L}_i^2}. \quad (\text{D.5})$$

This yields rather bad statistics near the boundaries $L = \pm 1$, in particular for $T > T_c$, due to the suppression by the measure. For instance, choosing $\beta = 2.4$, $I = 100$, i.e. $\Delta L = 1/50$, one typically finds $C_1 \simeq 14000$ data points in the first bin (near $L = -1$), while the population of the bins near $L = 0$ is larger by a factor of five, $C_{50} \simeq 73000$. The suppression by the geometry thus ‘wins’ against the density which is peaked near $L = \pm 1$. In the quantity of interest, the probability density,

$$p_W[\bar{L}_i] = \frac{C_i}{\sqrt{1 - \bar{L}_i^2}} \frac{I}{2N}, \quad (\text{D.6})$$

one divides by the measure factor which tends to zero near $L = \pm 1$. This yields the peaks near $L = \pm 1$ but at the same time further enhances the statistical error close to the boundaries. For $T < T_c$, this is not much of a problem as we have equipartition, $p_W[L] = \text{const} = p_W^- = 2/\pi$, and the density is known anyhow. For $T > T_c$, however, (D.6) implies that the bulk of the density is located where the statistical error is largest. On the other hand, the behavior of p_W in this regime determines the higher order couplings κ_{2k} . The lesson to be learned is that the partition should be modified such as to correctly incorporate the effect of the measure. To this end, we demand

that the counting rate be constant, $c_i = c$, for $T < T_c$, hence, from (D.3),

$$c = p_{\bar{W}} \sqrt{1 - \bar{L}_i^2} \Delta L_i = 1/I . \quad (\text{D.7})$$

Thus, in order to properly take into account the measure, the bin size ΔL_i has to be chosen such that

$$\sqrt{1 - \bar{L}_i^2} \Delta L_i = \text{const} = c/w_- = \frac{1}{I p_{\bar{W}}} . \quad (\text{D.8})$$

This can be achieved by going over to continuum notation,

$$c/p_{\bar{W}} = \int_{L_{i-1}}^{L_i} dL \sqrt{1 - L^2} \equiv P_W[L_i] - P_W[L_{i-1}] , \quad (\text{D.9})$$

and solving this recursion for L_i numerically with $P_W(L)$ given by

$$P_W[L] = \frac{1}{2} \left[L \sqrt{1 - L^2} + \arcsin(L) \right] . \quad (\text{D.10})$$

Alternatively, one may produce an ordered list of all data points for L , and partition this list in such a way that all bins contain the same number C of ‘events’. The sampling points L_i are then given by the smallest (or largest, depending on the counting convention) value of L in bin i .

For $T > T_c$, the density p_W is then given by

$$p_W[\bar{L}_i] = \frac{I p_{\bar{W}}}{N} C_i . \quad (\text{D.11})$$

This has been displayed in Fig. 4.1. Obviously, measure effects are now absent and the difference between C_i and C represents the deviation from equipartition.

E. Least Squares, Singular Value Decomposition and IMC

E.1. Least-Square Method and SVD

Given an overdetermined system of m equations for $n < m$ unknowns $\lambda_i, i = 1, \dots, n$,

$$A\lambda = b, \quad (\text{E.1})$$

the least square solution is given by

$$\lambda = (A^T A)^{-1} A^T b \quad (\text{E.2})$$

which minimizes

$$\chi^2 = |A\lambda - b|^2. \quad (\text{E.3})$$

Implementing this procedure numerically runs into problems in case the matrix $A^T A$ is ill-conditioned, i.e. $\det(A^T A)$ is very small (numerically zero). Here, the singular value decomposition (SVD) comes into play which decomposes the $m \times n$ matrix A as

$$A = (u_1 | \dots | u_n) \text{diag}(w_1, \dots, w_n) \begin{pmatrix} v_1 \\ \text{---} \\ \vdots \\ \text{---} \\ v_n \end{pmatrix} \equiv U W V^T \quad (\text{E.4})$$

with column-orthogonal $m \times n$ -matrix U , $n \times n$ semi-positive diagonal matrix W and $n \times n$ orthogonal matrix V . Such a decomposition is always possible and unique up to permutation of columns in the three matrices or forming linear combinations of those columns of U and V where corresponding elements of W are equal [89]. The decomposition is based on an orthonormal basis $\{v_i, i = 1, \dots, n\}$ of \mathbb{R}^n via the definitions

$$w_i = \|Av_i\|, \quad u_i = \begin{cases} 0 & \text{if } w_i = 0 \\ (Av_i)/w_i & \text{if } w_i \neq 0 \end{cases}. \quad (\text{E.5})$$

The basis $\{v_i\}$ can always be chosen such that $Av_i \cdot Av_j = 0, \forall i \neq j$ [148]. In this case, the vectors $u_i, i = 1, \dots, n$ are pairwise perpendicular and $\{u_i \neq 0, i = 1, \dots, k \leq n\}$ is an orthonormal basis of a k -dimensional subspace of \mathbb{R}^m . With $\{u_i, i = k+1, \dots, m\}$ being an orthonormal basis for the $(m-k)$ -dimensional subspace perpendicular to $span\{u_1, \dots, u_k\}$ one can extend (E.4) to

$$A = (u_1 | \dots | u_k | u_{k+1} | \dots | u_m) \left(\begin{array}{ccc|c} w_1 & & 0 & 0 \\ & \ddots & & \\ 0 & & w_k & 0 \\ \hline & & & 0 \end{array} \right) \begin{pmatrix} v_1 \\ \hline \vdots \\ \hline v_n \end{pmatrix} \quad (\text{E.6})$$

where left and right hand side agree on the basis $\{v_i\}$. The least square solution of (E.1) is then given by

$$\lambda = (v_1 | \dots | v_k) \text{diag}(1/w_1, \dots, 1/w_k) \begin{pmatrix} u_1 \\ \hline \vdots \\ \hline u_k \end{pmatrix} b \equiv A^+ b = \sum_{i=1}^k \frac{u_i \cdot b}{w_i} v_i \quad (\text{E.7})$$

where A^+ is called pseudo-inverse of A . Starting from (E.7), there are further least square solutions which differ by linear combinations of vectors from the null-space of

A ,

$$\lambda = A^+b + \alpha_{k+1}v_{k+1} + \cdots + \alpha_nv_n .$$

The SVD even solves homogeneous equations where $b = 0$. Since those v_i with corresponding $w_i = 0$ form an orthonormal basis of the null-space of A , any column v_i of V is a solution of the homogeneous system.

Note that in the solution (E.7) the singular values $w_j = 0$ have been left out. This is crucial in the case that they are identically zero. In real numerics w_j may be very small but finite. Whether such a w_j is treated as zero depends on the particular problem. Reordering the singular values $w_1 \leq w_2 \leq \cdots \leq w_n$ one defines a condition number w_1/w_n being large if there is a singular value very small compared to the others. A matrix with a large condition number is called ill-conditioned and often displays extreme sensitivity, even to small changes of the right hand side b .

However, experience teaches to use all information one can get and not to throw away anything. In particular, if there are small singular values due to columns of A that are almost (!) linear dependent, increasing the number of digits to achieve higher accuracy has turned out to be the better choice compared to throwing away the entries corresponding to small singular values.

E.2. Avoiding Trouble with IMC

Here we want to give a technical remark which may be important for people having trouble in solving (over)determined systems in IMC. Based on the Schwinger-Dyson relations we want to provide an optimized system including the most relevant operators in the ansatz 4.1. The best choice is to take *first of all* the set of operators appearing in the equations of motion, i.e. S_a differentiated with respect to the basic fields. This yields as many equations as there are unknowns and one has to invert a symmetric matrix. The χ^2 tells how good the solution is. However, there is a way to learn something more. Successively enlarging the number of equations and observing the behavior of the (least-square-)solution we have found a systematic flow in case there is an operator missing in our ansatz. The flow is larger the more important the neglected term is. Furthermore, the calculated couplings are far off the correct

ones. Playing around with a toy model we have checked all these features, and also that couplings corresponding to dispensable terms in the action come out as zero (see Tab. E.1). The action is

$$\begin{aligned}
S &= \sum_a \lambda_a S_a \\
&= \lambda_1 \sum_{\langle \mathbf{x}\mathbf{y}\rangle_1} L_{\mathbf{x}} L_{\mathbf{y}} + \sum_{\mathbf{x}} [\lambda_2 L_{\mathbf{x}}^2 + \lambda_3 L_{\mathbf{x}}^4 + \lambda_4 L_{\mathbf{x}}^6] + \lambda_5 \sum_{\langle \mathbf{x}\mathbf{y}\rangle_{\sqrt{2}}} L_{\mathbf{x}} L_{\mathbf{y}} + \lambda_6 \sum_{\langle \mathbf{x}\mathbf{y}\rangle_{\sqrt{3}}} L_{\mathbf{x}} L_{\mathbf{y}} \quad (\text{E.8})
\end{aligned}$$

with $\langle \mathbf{x}\mathbf{y}\rangle_r$ denoting all neighbors \mathbf{x} and \mathbf{y} of distance $|\mathbf{x} - \mathbf{y}| = r$. In the first row of Tab. E.1 the input data are given. The simulated action includes a hopping term S_1 and a potential of orders 2, 4 and 6 in the variable, S_2, S_3, S_4 . Below we see how this is reproduced using different ansätze for the action. In the first case we have checked that we reproduce the input couplings by testing the simulated action. Second, we have added some more terms to the action to see whether they come out as zero. Both tests work very well, and do not depend on the number of equations (minimal set up to fifteen) used. Dropping the leading potential term, S_2 , however, there is no stable solution. As seen in the lowest row the couplings start to float systematically by increasing the number of equations, here shown for 3, 8, 12 and 15 equations. In particular, the resulting potential couplings differ drastically from the input.

	λ_1	λ_2	λ_3	λ_4	λ_5	λ_6	χ^2/dof
input	-0.7600	1.9572	-1.0215	0.6976	0	0	—
output	-0.7602	1.9602	-1.0222	0.6914	—	—	$3.2 \cdot 10^{-12}$
	-0.7604	1.9605	-1.0221	0.6904	0.00010	-0.00009	$3.5 \cdot 10^{-9}$
	-0.7343	—	7.6591	-7.7944	—	—	$5.2 \cdot 10^{-7}$
	-0.7296	—	7.0143	-6.7781	—	—	$1.0 \cdot 10^{-7}$
	-0.7274	—	6.7289	-6.3344	—	—	$3.9 \cdot 10^{-6}$
	-0.7259	—	6.5349	-6.0351	—	—	$1.7 \cdot 10^{-6}$

Table E.1.: Testing IMC with a toy model. The output data are given for different ansätze. Included terms are those where a numerical value of the coupling is given.

Zusammenfassung

Die vorliegende Arbeit befaßt sich mit dem niederenergetischen Bereich der Quantenchromodynamik (QCD). Dort gibt es einige äußerst interessante, aber noch nicht zur vollsten Zufriedenheit verstandene Phänomene, wie zum Beispiel das ‘color confinement’, das besagt, daß es keine freien farbgeladenen Teilchen gibt. Theoretische Untersuchungen zeigen, daß sich diese Tatsache auch schon in der reinen Yang–Mills–Theorie (ohne Quark–Felder) in einem mit dem Abstand linear anwachsenden Quark–Potential widerspiegelt. Um das zu untersuchen, liegt es daher nahe, sich auf die ohnehin schon nichttriviale Yang–Mills–Theorie beschränken, und die Ursache für ein solches Verhalten in deren nicht–Abelscher Struktur zu suchen.

Der theoretische Zugang zu dieser Theorie wird dabei noch zusätzlich durch die laufende Kopplung erschwert, die im Bereich kleiner Energien groß ist und eine störungstheoretische Behandlung ausschließt. Da die für uns interessante Problemstellung offensichtlich von der Energieskala abhängt, scheint es sinnvoll, nur den dafür relevanten Bereich zu betrachten und Effekte von außerhalb dieser Skala geeignet in Koeffizienten oder Parameter zu absorbieren. Durch diese Abintegration der Hochenergiefreiheitsgrade sollte sich eine einfacher zu handhabende Theorie ergeben, die aber im zugehörigen Energiebereich dieselben Effekte aufweist wie die volle Theorie. Erstere trägt den Namen ‘Effektive Theorie’. Wie bereits angedeutet, ist desweiteren die Benutzung nicht–störungstheoretischer Behandlungsweisen unerlässlich, um den Bereich niedriger Energien zu erschließen. Eine der leistungsfähigsten Methoden dieser Art ist die numerische Simulation (Monte–Carlo) von Gittereichtheorien. Diese wird in der vorliegenden Arbeit benutzt, um Kandidaten für effektive Theorien für den Niederenergiebereich der $SU(2)$ Yang–Mills–Theorie zu testen und zu erweitern bzw. deren Kopplungskonstanten zu berechnen. Die dazu benutzte (numerische) Methode ist inverses Monte–Carlo (IMC), das auf Schwinger–Dyson–Gleichungen und

Ward-Identitäten aufbaut. Diese werden analytisch aus den Symmetrieeigenschaften der betrachteten Theorie hergeleitet.

Das erste hier behandelte Modell geht auf Faddeev und Niemi zurück, die einen Ansatz für eine effektive Wirkung vorschlugen, die nicht nur die Gluon-Dynamik bei niedrigen Energien beschreiben sondern auch alle im Infraroten wichtigen Terme beinhalten sollte. Dieser mögliche Zusammenhang mit Yang-Mills sollte in einem ersten Schritt näher untersucht werden. Ausgehend von mittels Monte-Carlo-Simulation generierten Yang-Mills-Konfigurationen wurden aus den Eichfeldern die effektiven Felder extrahiert. In diesem Fall geschah das über die Fixierung der Landau-Eichung, die noch eine globale $SU(2)$ übrig läßt, welche in einem zweiten Schritt durch die Maximal-Abelsche Eichung zu einer globalen $U(1)$ gebrochen wurde. Das effektive Einheitsvektorfeld \mathbf{n} kann daher als Maß für den eichinvarianten Abstand dieser beiden Eichungen angesehen werden. Da beide Eichungen nicht weit voneinander entfernt sind, ergibt sich eine Vorzugsrichtung für \mathbf{n} , was einer expliziten Symmetriebrechung entspricht, durch welche masselose Goldstone-Bosonen vermieden werden und ein Massengap erzeugt wird.

Die für niedrige Energien sinnvolle Gradientenentwicklung erlaubt zunächst einen minimalen Ansatz (führende Ordnung) für die Wirkung eines σ -Modells, der ein zusätzlicher symmetriebrechender Term hinzugefügt wurde. Über die zugehörigen Schwinger-Dyson-Gleichungen lassen sich die in diesem Modell noch freien Kopplungen bestimmen. Es zeigt sich jedoch, daß die Schwinger-Dyson Gleichungen, geometrisch veranschaulicht als eine Gerade, nicht mit den Daten aus Yang-Mills zusammenpassen. Im IMC-Verfahren zeigt sich das in einem systematischen Laufen der berechneten Kopplungen bei Variation der Bestimmungsgleichungen im überbestimmten System. Weitere signifikante Diskrepanzen ergeben sich in der Ward-Identität, der Suszeptibilität und der Magnetisierung. All das ist ein deutlicher Hinweis darauf, daß das minimale Modell nicht in der Lage ist, die Yang-Mills-Theorie zu repräsentieren.

Um eine Verbesserung zu erzielen, wurde daraufhin das Modell um einen Term nächsthöherer Ordnung, den Faddeev-Niemi-Term, erweitert. Die Berechnung der nunmehr drei Kopplungen gestaltet sich wesentlich stabiler. Der FN-Term hat jedoch zur Folge, daß sich das Vorzeichen des Symmetriebrechungsterms umkehrt, was einer negativen Magnetisierung entsprechen würde. Das steht jedoch im Widerspruch zu der Beobachtung aus Yang-Mills. Die Simulation dieses erweiterten Modells zeigt eine

sehr gute (numerische) Genauigkeit der Schwinger–Dyson–Gleichungen, und auch die oben angesprochene negative Magnetisierung wird reproduziert, so daß die Theorie in sich konsistent ist. Das (erweiterte) FN–Modell ist aufgrund dieser Tatsachen (zumindest mit unserer Wahl des Feldes \mathbf{n}) nicht geeignet, die Yang–Mills–Theorie zu beschreiben. Wir fanden jedoch Indizien dafür, daß die Erweiterung des Modells auf noch mehr (symmetriebrechende) Terme (höherer Ordnung) und insbesondere die Beschränkung auf große Abstände (kleinere Energien) zu einer besseren Übereinstimmung mit Yang–Mills führt. Das deutet darauf hin, daß dieses Modell höchstens sehr weit unterhalb der Glueball–Massenskala eine effektive Beschreibung liefern könnte. Daher sollte es auch nicht verwundern, daß das erhaltene Massengap von ungefähr 1.2 GeV nicht dem Yang–Mills–Wert von ca. 1.7 GeV entspricht.

In einem zweiten Schwerpunkt wurden die im Kontext der FN–Modelle entwickelten IMC–Methoden auf eine Klasse von effektiven Theorien angewandt, die ihren Ursprung in der Beschreibung des confinement–deconfinement Phasenübergangs haben. Die Freiheitsgrade in der effektiven Theorie werden dabei durch den (gespurten) Polyakovloop repräsentiert. Ausgehend von der $SO(4)$ –Symmetrie des Integrationsmaßes wurden zunächst Schwinger–Dyson–Gleichungen sowohl für den ungespurten als auch den gespurten Polyakovloop hergeleitet, um im IMC–Verfahren zur Bestimmung der Wirkung Verwendung zu finden. Angeregt durch die Tatsache, daß der Erwartungswert des Polyakovloops als Ordnungsparameter für den Phasenübergang dient, wurde zunächst dessen Wahrscheinlichkeitsdichte bestimmt. Unterhalb der kritischen Temperatur ergibt sich ein flaches Histogramm, was einer Gleichverteilung des gespurten Polyakovloops entspricht. Oberhalb der kritischen Temperatur hingegen werden die Zentrumselemente bevorzugt. Die flache Verteilung ermöglichte in der symmetrischen Phase die exakte analytische Berechnung der Erwartungswerte sämtlicher Potenzen des Polyakovloops, der zugehörigen erzeugenden Funktion und somit auch die Bestimmung der Binderkumulante, $b_4 = -1$. In der gebrochenen Phase konnte die Verteilung polynomiell gefittet werden. Um diese Verteilungen mit Hilfe einer effektiven Theorie zu reproduzieren, wurde zunächst versucht, soweit wie möglich in analytischer Vorgehensweise fortzufahren. Ein Ginzburg–Landau–artiger Ansatz bestehend aus einem Wechselwirkungsterm und Potentialtermen erwies sich dafür gerade noch als einfach genug. Damit gelang es, alle Potentialkopplungen λ_{2k} durch die Wechselwirkungskopplung λ_0 und numerisch zu bestimmende höhere Momente des Nächste–Nachbar–Feldes auszudrücken. Durch die abgeleit-

eten Schwinger–Dyson–Gleichungen wurden mittels IMC λ_0 und somit alle λ_{2k} bestimmt. Eine Simulation dieser so bestimmten effektiven Theorie zeigt sowohl in der gebrochenen als auch in der symmetrischen Phase ein sehr gutes Übereinstimmen der Wahrscheinlichkeitsverteilungen mit den Yang–Mills–Daten, das durch Hinzunahme weiterer Potentialterme sogar noch verbessert werden kann. Aufbauend darauf wurde das effektive Potential berechnet, das die Verteilung des mittleren Feldes \bar{L} bestimmt. Im Grenzfall großen Volumens und unter Benutzung des Gesetzes der großen Zahlen erhält man eine um $\bar{L} = 0$ lokalisierte Gaußverteilung mit einer Varianz, die dem Erwartungswert des quadrierten mittleren Feldes entspricht. Ein Fit der Yang–Mills–Daten zeigt eine sehr gute Übereinstimmung mit diesem Ergebnis, insbesondere für große Volumen. Auch das vorausgesagte Skalenverhalten der Halbwertsbreiten in Abhängigkeit vom Volumen wird sehr gut reproduziert. Oberhalb der kritischen Temperatur, also in der gebrochenen Phase, erwartet man zwei Maxima der Verteilung, jedoch ist eine analytische Herleitung aufgrund der nichtflachen Wahrscheinlichkeitsdichte nicht möglich. Ein Fit der Daten an eine doppelte Gaußkurve zeigt aber auch in diesem Fall eine sehr gute Übereinstimmung. Insbesondere zeigt sich beim Phasenübergang ein Verschmelzen der beiden Kurven zu der oben genannten Gaußverteilung in der symmetrischen Phase. Bezüglich der Volumenabhängigkeit zeigt sich das erwartete Verhalten; das Tunneln ist mit wachsendem Volumen unterdrückt und die Halbwertsbreiten werden schmaler.

Da es sich bei diesen Betrachtungen um einen semianalytischen Zugang handelt, der auf der Verteilung des einzelnen Polyakovloops aufbaut, kann im allgemeinen nicht erwartet werden, daß Korrelationsfunktionen richtig reproduziert werden. Um die effektive Theorie dahingehend zu verbessern wurden noch weitere Terme zur Wirkung hinzugezogen, insbesondere Hoppingterme, die höhere Abstände beinhalten. Für Ising–Modelle ist diese Vorgehensweise bekannt, jedoch quadriert dort das Feld zu eins, im Unterschied zu unserem Modell. Hier sind im Prinzip alle ultralokalen Potenzen des Polyakovloops als auch Hoppingterme mit beliebigen solchen Potenzen erlaubt. Die Schwierigkeit besteht also darin, einen möglichst kleinen Satz solcher Terme zu finden, der sowohl das IMC–Verfahren stabilisiert als auch die Korrelationsfunktion gut reproduziert. Das gelang durch den Wechsel von Monomen im Polyakovloop zu deren Linearkombinationen, den Charakteren der Gruppe. Beide Darstellungsweisen können ineinander umgerechnet werden. Dadurch war es möglich, auch Wechselwirkungsterme mit Abständen bis $r = \sqrt{2}a$ zu berücksichtigen. Die

Berechnungen zeigen ein schnelles Abfallen der Kopplungen hin zu höheren Charakteren, was eine Beschränkung auf die ersten drei rechtfertigt. Desweiteren wurden zu den drei Nächste-Nachbar-Termen aus Konsistenzgründen insgesamt elf weitere Terme zu höheren Abständen hinzugezogen. Mit dieser Wahl ist das IMC sehr stabil, und die so erhaltene Theorie zeigt kurzreichweitige Wechselwirkung, im Einklang mit der Vorhersage von Svetitsky und Yaffe. Die Simulation der effektiven Theorie mit den so berechneten Kopplungen zeigt eine wesentliche Verbesserung der Zweipunkt-funktion, die jetzt sowohl in der symmetrischen als auch in der gebrochenen Phase gut mit der aus Yang-Mills übereinstimmt.

Vom technischen Standpunkt her wurde der Zusammenhang von Singular-Value-Decomposition und Least-Square-Methode zur Lösung überbestimmter Gleichungssysteme innerhalb der inversen Monte-Carlo-Methode näher untersucht. Es wurde gezeigt, in welcher Weise sich das Fehlen relevanter Operatoren im Ansatz des zu bestimmenden Funktionales auf das Verhalten der Least-Square-Lösung niederschlägt. Demzufolge ist ein systematisches Laufen des Lösungsvektors unter Erhöhung der Anzahl Gleichungen ein deutliches Anzeichen dafür, daß der gewählte Ansatz nicht ausreicht, um die zugrunde gelegten Erwartungswerte im Gleichungssystem zu beschreiben. Die Stärke des Laufens ist proportional zur Wichtigkeit des fehlenden Operators. Daher ist es bei der Least-Square-Methode nicht ausreichend, nur einen möglichen Satz von Gleichungen zu untersuchen, zumal die so erhaltene (instabile) Lösung auch weit entfernt ist von der richtigen. Weiterhin ergab sich, daß bei Verwendung der Singular-Value-Decomposition die sehr kleinen Diagonaleinträge nur mit äußerster Vorsicht auszusortieren sind. Es kommt hier auf die Ursache der Kleinheit an. Ist sie dadurch begründet, daß Zeilen oder Spalten in der Koeffizientenmatrix fast linear abhängig sind, führt ein Weglassen der zugehörigen Komponenten (und damit der enthaltenen Information) zu einer vergleichsweise schlechten Lösung. Sinnvoller ist es in diesem Fall, auch die kleinen Beiträge beizubehalten und im Gegenzug die Anzahl mitgenommener Digits zu erhöhen. Als Orientierungsmaß dient dabei die Größe der Determinante der zu invertierenden Matrix.

Ehrenwörtliche Erklärung

Ich erkläre hiermit ehrenwörtlich, daß ich die vorliegende Arbeit selbständig, ohne unzulässige Hilfe Dritter und ohne Benutzung anderer als der angegebenen Hilfsmittel und Literatur angefertigt habe. Die aus anderen Quellen direkt oder indirekt übernommenen Daten und Konzepte sind unter Angabe der Quelle gekennzeichnet. Niemand hat von mir unmittelbar oder mittelbar geldwerte Leistungen für Arbeiten erhalten, die im Zusammenhang mit dem Inhalt der vorgelegten Dissertation stehen. Insbesondere habe ich hierfür nicht die entgeltliche Hilfe von Vermittlungs- bzw. Beratungsdiensten in Anspruch genommen.

Die Arbeit wurde bisher weder im In- noch im Ausland in gleicher oder ähnlicher Form einer anderen Prüfungsbehörde vorgelegt.

Die geltende Promotionsordnung der Physikalisch-Astronomischen Fakultät ist mir bekannt.

Ich versichere ehrenwörtlich, daß ich nach bestem Wissen und Gewissen die reine Wahrheit gesagt und nichts verschwiegen habe.

Jena, 3. November 2003

Leander Dittmann

Danksagung

Zu sehr vielem Dank verpflichtet bin ich Prof. Andreas Wipf, der mir nicht nur die Möglichkeit eröffnete, hier am TPI zu arbeiten und zu forschen, sondern mir auch in jeglicher Hinsicht die denkbar beste Betreuung und umfangreiche Unterstützung zuteil werden ließ. Ganz spezieller Dank gebührt Dr. Thomas Heinzl, dessen uneigennützig und aufopferungsvolle Hilfsbereitschaft wesentlich zum Gelingen dieser Arbeit beitrug.

Für ungezählte Diskussionen und Gespräche, auch außerphysikalische Fragestellungen beinhaltend, sei Dank kundgetan allen weiteren Mitstreitern unserer Arbeitsgruppe mit denen ich während meines hiesigen Aufenthaltes viele gemeinsame angenehme Stunden erleben durfte,¹ Dr. Falk Bruckmann, Dörte Hansen, Dr. Laur Järv, Andreas Kirchberg, Dr. Alexei Kotov, Jean Dominique Länge, Christoph Mayer, Dr. Thomas Mohaupt, Frank Saueressig, Dr. Thomas Strobl, Prof. Mikhail Volkov, Dr. Erik Wöhnert. Selbiges gilt uneingeschränkt auch für Michael Brüggemann, sowie für die technische Leitung unter Frau Ritter, Frau Wagner und Dr. Martin Weiß.

Nicht minder Dank sei gerichtet an Prof. Michael Müller–Preußker und Dr. Gunnar Bali, die, als Experten auf diesem Gebiet, sich die Zeit nahmen, mir mit ihrem Wissen und Entgegenkommen den Einstieg in die Monte–Carlo–Simulation zu erleichtern.

Für wertvolle und lehrreiche Anregungen fachlicherseits danke ich an dieser Stelle auch Dr. Philippe de Forcrand und Dr. Sergei Shabanov.

Ein herzlicher Dank geht an die Juristin und Physikerin Michaela Rau.

Besonderer Dank richtet sich nicht zuletzt auch an meine Eltern und Geschwister, die mich immer vorbehaltlos unterstützten.

Dem Land Thüringen wird für die finanzielle Unterstützung gedankt.

¹Reihenfolge alphabetisch nach Nachnamen.

Lebenslauf

Name	Leander Dittmann
geboren	3. November 1974 in Weida
Nationalität	deutsch
Familienstand	ledig

Schule

09/1981 - 08/1991	Polytechnische Oberschule 'Erich Weinert' in Frießnitz
09/1991 - 06/1994	BBS Metall in Gera
06/1994:	Abitur

Studium

10/1994 - 09/1999	Physikstudium, Friedrich-Schiller-Universität Jena
09/1999	Diplom, Thema: Dualitätstransformationen in (Quanten)- Feldtheorien Betreuer: Prof. Dr. A. Wipf
seit 10/1999	Doktorand am Theoretisch-Physikalisches Institut der Friedrich-Schiller-Universität Jena Betreuer: Prof. Dr. A. Wipf